ROLES OF AXIAL LIGANDS IN CATALYTIC OXIDATIONS BY HEME ENZYMES

Akihiro Takahashi

DOCTOR OF PHILOSOPHY

Department of Functional Molecular Science
School of Physical Sciences
The Graduate University for Advanced Studies

2009

CONTENTS

PART I.

GENERAL INTRODUCTION

Metal ions are common natural constituents of proteins and play crucial roles in life processes. Iron ions are the metal ions of choice for many biological processes because of their abundance in the geosphere, there inherent electronic properties, and their accessible redox potentials.[1] The active site structures of iron proteins can be classified as either heme proteins or nonheme iron proteins. In heme proteins, the iron ion is bound to a porphyrin, which consists of a tetrapyrrole macrocycle, and is linked to a protein backbone via an amino acid residue (axial ligand).[2] On the other hand, nonheme iron proteins generally form a mono-nuclear or multi-nuclear iron center with direct coordinations of amino acid residues.[3] The functions of iron proteins are controlled by the structures of metal active sites which includes geometry and nature of the ligands attached to the iron ions, and the environment of the active site – the polarity and steric constraints of proteins in the immediate vicinity of the iron ions. The elucidation of the structural and functional relationships of iron proteins is a long-standing theme in bioinorganic chemistry.

Heme proteins display a diversity of biological functions. These functions include simple electron transfer reactions, such as those catalyzed by b- and c-type cytochromes, oxygen transport and storage via hemoglobin and myoglobin, oxygen reduction to the level of water by cytochrome oxidase, oxygenations of organic substrates as facilitated by cytochromes P450, and the reduction of peroxides by catalases and peroxidases.[1] Heme proteins that perform a catalytic function are called heme enzymes: cytochromes P450, peroxidases, and catalases. The diversity of functions for the heme proteins results entirely from the influence of the axial ligand and protein environment around heme, since these heme proteins share a common the same iron protoporphyrin IX prosthetic group.

Scheme 1.1. Schematic catalytic cycle of peroxidases.

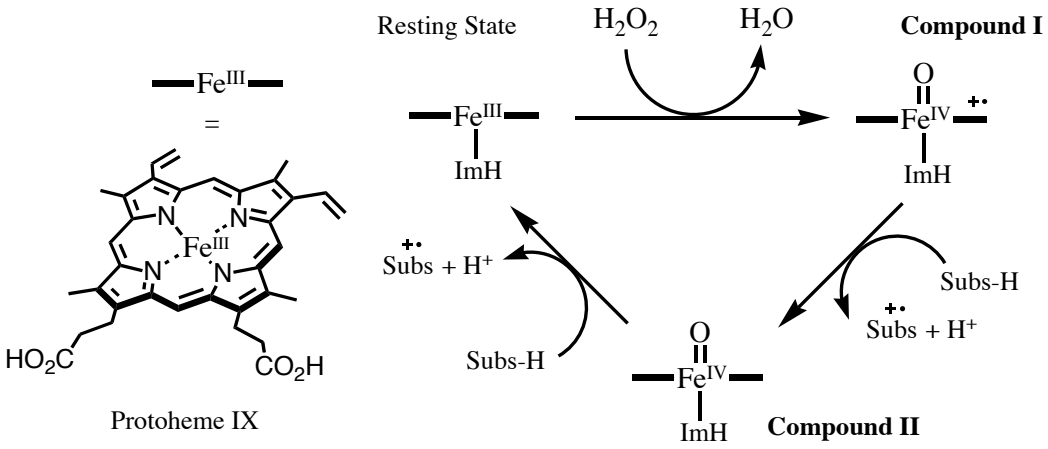

In heme enzymes, peroxidases are a ubiquitous class of enzymes that catalyze the oxidation of a wide variety of organic and inorganic substrate molecules with hydrogen peroxide.[4] Most peroxidases contain an iron protoporphyrin IX (protoheme IX) as their prosthetic group and share common reaction intermediates, compound I and II, as described above.[4,5] The initial step in the catalytic mechanism is heterolysis of the O-O bond of hydrogen peroxide, resulting in the two-electron deficient compound I (Fe^{4+}=O, R•) and water, where R is the organic moiety of the heme or an amino acid residue. Then, compound I is reduced to the resting state by sequential one-electron oxidation of two substrates, SH, via the intermediate compound II (Fe^{4+}=O). Interestingly, compound I is also believed to be the common intermediate in the catalytic cycles of cytochrome P450, chloroperoxidase (CPO), and catalase.[2,5-8] Although these enzymes share a common reactive intermediate, the reactivity of compound I differs from enzyme to enzyme. Compound I in cytochrome P450 directly transfers a single oxygen atom to a variety of substrates, while those in peroxidase and catalase carry out one-electron oxidation of organic substrates, such as

amines and phenols, and oxidation of hydrogen peroxide to water and oxygen gas, respectively.[2a,4-7] It is generally accepted that the diverse functions of compound I are controlled by heme environmental structures. One significant structural difference in these heme enzymes is the heme axial ligand.[4-7,9] As shown in Figure 1, histidine and tyrosine residues (imidazole and phenolate) are coordinated to the heme iron as axial ligands in peroxidases other than CPO and catalases, respectively. In cytochrome P450 and CPO, a cysteine residue (thiolate) is the heme axial ligand. The amino acids that serve as the axial ligands are highly conserved in these heme enzymes, which suggestes a functional role.

Table 1.1. Reactions of heme-containing enzymes.

Enzyme	Reaction
Horseradish peroxidase	$A\text{-}H_2 + H_2O_2 \rightarrow A + 2H_2O$
Cytochrome *c* peroxidase	$ROOH + 2H^+ + 2e^- \rightarrow ROH + H_2O$
Chloroperoxidase	$A\text{-}H_2 + X^- + 2H^+ + H_2O_2 \rightarrow A\text{-}X + 2H_2O$
Catalase	$2H_2O_2 \rightarrow 2H_2O + O_2$
Cytochrome P450	$R\text{-}H + O_2 + 2H^+ + 2e^- \rightarrow ROH + H_2O$

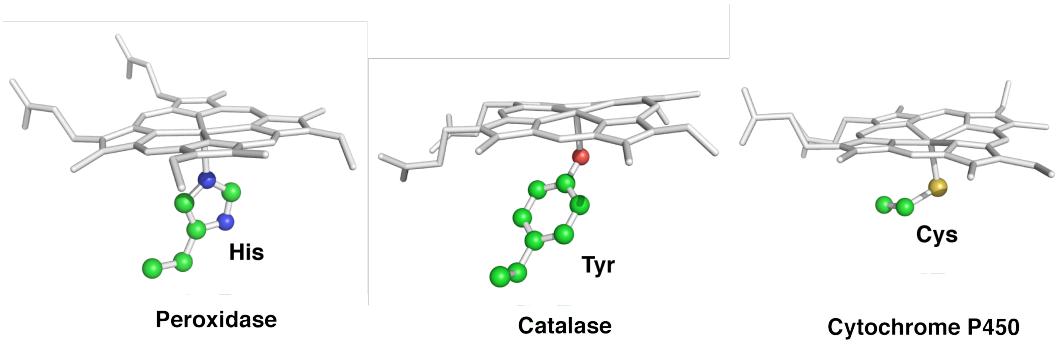

Figure 1.1. Active site structures of peroxidase, catalase, and cytochrome P450.

Scheme 1.2.

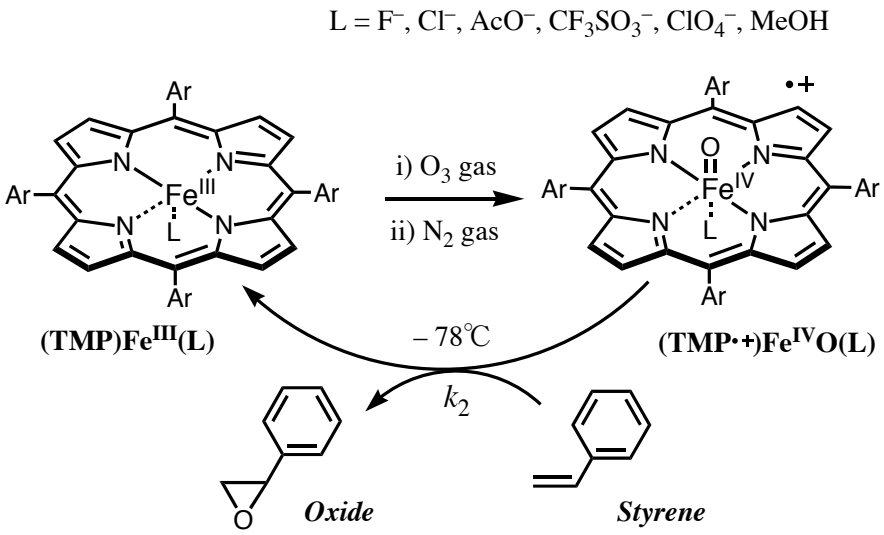

Many synthetic model studies have been performed to investigate the functional role of the axial ligand in the reactivity of compound I.[10-15] Catalytic oxygenation reactions with synthetic iron and manganese porphyrin complexes have demonstrated a significant axial ligand effect on their catalytic activity, yield, and selectivity.[10-13] However, these studies have not directly shown the axial ligand effect on the electronic structure and reactivity of compound I because these catalytic reactions contain many simple reaction steps that are affected by the axial ligand.[13a-d,16,17] The axial ligand effect on compound I has recently been studied on compound I model complexes and theoretical calculations based on density functional theory.[18-21] For example, Gross et al. reported a pronounced axial ligand effect on the reaction rate for the epoxidation of styrene with $Fe^{IV}O(TMP^{+\bullet})(L)$, where TMP = tetramesitylporphyrin and L = F^-, Cl^-, AcO^-, $CF_3SO_3^-$, ClO_4^-, and CH_3OH (see Scheme 1.2).[14] While the rates of styrene epoxidation by $Fe^{IV}O(TMP^{+\bullet})(L)$ complexes were increased in the order of F^- >> CH_3OH > Cl^- > AcO^- >> $CF_3SO_3^-$, a cogent explanation could not be given. While,

numerous attempts have been directed at elucidating the axial ligand effect on the electronic structure and reactivity of compound I, the answer to that question has been remained open to further study.[14d,15a,19] In particular, the following two questions are unresolved: (1) the difference between enzyme axial ligands, such as imidazole, phenolate, thiolate, and other inorganic anion ligands, such as F^-, Cl^-, and AcO^-: and, (2) how the axial ligand regulates the reactivity of compound I.

The objective of this thesis is to answer the above-mentioned questions using synthetic compound I model complexes. Part II focuses on the effect of axial ligand on the reactivity of compound I. In chapter 1, the author attempted to synthesize compound I model complexes with imidazole and phenolate axial ligands, which were the first legitimate model complexes of compound I for peroxidases and catalases, respectively. In chapters 2 and 3, the author investigated the thermodynamic stability of compound I model complexes, as well as ferric heme complexes, to reveal how the axial ligand regulates the reactivity of compound I. Part III deals with the chemoselectivity and the electronic structure of compound I model complexes to reveal the axial ligand effect on the electronic structure and reactivity of compound I.

References

(1) See, for example: Lippard, S. J.; Berg. J. M. In *Principles of Bioinorganic Chemistry*; University Science Books: California, 1994.

(2) (a) Sono, M.; Roach, M. P.; Coulter, E. D.; Dawson, J. H. *Chem. Rev*. **1996,** *96*, 2841-2887. (b) Dawson, J. H.; Sono, M. *Chem. Rev*. **1987,** *87*, 1255-1276.

(3) (a) Que, L., Jr.; Ho, R. Y. N. *Chem. Rev*. **1996,** *96*, 2607-2624. (b) Costas, M.; Mehn, M, P.; Jensen, M, P.; Que, L., Jr. *Chem. Rev*. **2004,** *104*, 939-986.

(4) (a) Dunford, H. B. *Heme Peroxidases*, Wiley-VCH: New York, 1999. (b) Dunford, H. B.; Stillman, J. S. *Coord. Chem*. **1976,** *19,* 187-251.

(5) Schonbaum, G. R.; Chance, B. In *The Enzymes*; Boyer, P. D., Ed.; Academic Press: New York, 1976; Vol. 13, pp 363-408.

(6) Watanabe, Y.; Groves, J. T. In *The Enzymes*; Sigman, D. S., Ed.; Academic Press: New York, 1992; Vol. 20, pp 405-452.

(7) Oritz de Montellano, P. R. In *Cytochrome P450: Structure, Mechanism, and Biochemistry*, 2nd ed.; Plenum Publishing Corporation: New York, 1995.

(8) Dawson, J. H. *Science* **1988,** *240*, 433-438.

(9) Poulos, T. L. *J. Biol. Inorg. Chem*. **1996,** *1*, 356-359.

(10) (a) Robert, A.; Loock, B.; Momenteau, M.; Meunier, B. *Inorg. Chem*. **1991**, *30*, 706-711. (b) Meunier, B. *Chem. Rev*. **1992,** *92*, 1411-1456.

(11) Battioni, P.; Renaud, J. P.; Bartoli, J. F.; Reina-Artiles, M.; Fort, M.; Mansuy, D. *J. Am. Chem. Soc*. **1988**, *110*, 8462-8470.

(12) (a) Higuchi, T.; Uzu, S.; Hirobe, M. *J. Am. Chem. Soc*. **1990**, *112*, 7051-7052. (b) Suzuki, N.; Higuchi, T.; Urano, Y.; Kikuchi, K.; Uekusa, H. Ohashi, Y.; Uchida, T.; Kitagawa, T.; Nagano, T. *J. Am. Chem. Soc*. **1999**, *121*, 11571-11572. (c) Urano, Y.; Higuchi, T.; Hirobe, M.; Nagano, T. *J. Am. Chem. Soc*. **1997**, *119*,

12008-12009. (d) Ohno, T.; Suzuki, N.; Dokoh, T.; Urano, Y.; Kikuchi, K.; Hirobe, M.; Higuchi, T.; Nagano, T. *J. Inorg. Biochem.* **2000**, *82*, 123-125.

(13) (a) Song, W. J.; Ryu, Y. O.; Song, R.; Nam, W. *J. Biolog. Inorg. Chem.* **2005,** *10,* 294-394. (b) Nam, W.; Lim, M. H.; Oh, S.-Y.; Lee, J. H.; Lee, H.J.; Woo, S.K.; Kim, C.; Shin, W. *Angew. Chem., Int. Ed.* **2000,** *39,* 3646-3649. (c) Nam, W.; Lim, M. H.; Oh, S.-Y. *Inorg. Chem.* **2000**, *39*, 5572-5575. (d) Nam, W.; Jin, S. K.; Lim, M. H.; Ryu, J. Y.; Kim, C. *Inorg. Chem.* **2002**, *41*, 3647-3652. (e) Nam, W.; Lim, M. H.; Moon, S. K.; Kim, C. *J. Am. Chem. Soc.* **2000**, *122*, 10805-10809.

(14) (a) Gross, Z.; Nimri, S. *Inorg. Chem.* **1994**, *33*, 1731-1732. (b) Gross, Z.; Nimri, S. *J. Am. Chem. Soc.* **1995**, *117*, 8021-8022. (c) Gross, Z. *J. Biol. Inorg. Chem.* **1996**,1, 368-371. (d) Gross, Z.; Nimri, S.; Barzilay, C. M.; Simkhovich, L. *J. Biol. Inorg. Chem.* **1997**, *2*, 492-506.

(15) (a) Czarnecki, K.; Nimri, S.; Gross, Z.; Proniewicz, L. M.; Kincaid, J. R. *J. Am. Chem. Soc.* **1996**, *182*, 2929-2935. (b) Czarnecki, K.; Kincaid, J. R.; Fujii, H. *J. Am. Chem. Soc.* **1999**, *121*, 7953-7954.

(16) Collman, J. P.; Chien, A. S.; Eberspacher, T. A.; Brauman, J. I. *J. Am. Chem. Soc.* **2000**, *122*, 11098-11000.

(17) Vaz, A. D N.; Mcginnity, D. F.; Coon, A. M. *Proc. Natl. Acad. Sci. USA.* **1998,** *95,* 3555-3560.

(18) For a review, see: (a) Shaik, S.; Kumar, D.; de Visser, S. P.; Altun, A.; Thiel, W. *Chem. Rev.* **2005**, *105*, 2279-2328.

(19) Kamachi, T.; Kouno, T.; Nam, W.; Yoshizawa, K. *J. Inorg. Biochem.* **2006**, *100*, 751-754.

(20) Wang, R.; de Visser, S. P. *J. Inorg. Biochem.* **2007**, *101*, 1464-1472.

(21) (a) Green, M. T. *J. Am. Chem. Soc.* **1999**, *121*, 7939-7940. (b) Green, M. T. *J. Am. Chem. Soc.* **2000**, *122* 9495-9499.

PART II.

ROLES OF THE AXIAL LIGANDS IN OXIDATION REACTIONS BY COMPOUND I

Chapter 1. Effect of Imidazole and Phenolate Axial Ligands on the Electronic Structure and Reactivity of Oxoiron(IV) Porphyrin π-Cation Radical Complexes: Drastic Increase in Oxo-Transfer and Hydrogen Abstraction Reactivities

Chapter 2. Thermodynamic Factor Determining the Reactivity of Oxoiron(IV) Porphyrin π-Cation Radical Complexes Bearing Various Anionic Axial Ligands: Linear Relationship between Reaction Rate and Free Energy of Reaction

Chapter 3. Functional Role of Neutral Axial Ligand on the Reactivity of Oxoiron(IV) Porphyrin π-Cation Radical Complexes: Comparison Between Anionic and Neutral Axial Ligand Effects

---

Chapter 1.

Effect of Imidazole and Phenolate Axial Ligands on the Electronic Structure and Reactivity of Oxoiron(IV) Porphyrin π-Cation Radical Complexes: Drastic Increase in Oxo-Transfer and Hydrogen Abstraction Reactivities

Inorganic Chemistry in press

Akihiro Takahashi, Takuya Kurahashi, and Hiroshi Fujii

Abstract

To study the effect of axial ligands on the electronic structure and reactivity of compound I of peroxidases and catalases, oxoiron(IV) porphyrin π-cation radical complexes with imidazole, 2-methylimidazole, 5-methylimidazole, and 3-fluoro-4-nitrophenolate as the axial ligands were prepared by ozone oxidation of iron(III) complexes of 5, 10, 15, 20-tetramesitylporphyrin (TMP) and 2, 7, 12, 17-tetra-methyl-3, 8, 13, 18-tetramesitylporphyrin (TMTMP). These complexes were fully characterized by absorption, ^{1}H, ^{2}H, and ^{19}F NMR, EPR, and ESI-MS spectroscopy. The characteristic absorption peak of compound I at approximately 650 nm was found to be a good marker for estimation of the electron donor effect from the axial ligand. The axial ligand effect did not change the porphyrin π-cation radical state, the a_{2u} state of the TMP complexes, or the a_{1u} radical state of both the TMTMP complexes and compound I. The ferryl iron and porphyrin π-cation radical spins were effectively transferred into the axial ligands for the a_{2u} complexes, but not for the a_{1u} complexes. Most importantly, the reactivity of the oxoiron(IV) porphyrin π-cation radical complex was drastically increased by the imidazole and phenolate axial ligands. The reaction rate for cyclooctene epoxidation was increased 100 ~ 400-fold with axial coordination of imidazoles and phenolate. A similar increase was also observed for oxidation of 1,4-cyclohexadiene, *N*,*N*-dimethyl-*p*-nitroaniline, and hydrogen peroxide. These results suggest extreme enhancement of the reactivity of compound I by the axial ligand in heme enzymes. The functional role of axial ligands on the compound I in heme enzymes is discussed.

Abbreviation

TMP : 5, 10, 15, 20-tetramesitylporphyrin

TMTMP : 2, 7, 12, 17-tetramethyl-3, 8, 13, 18-tetramesitylporphyrin

Im : imidazole

2-MeIm : 2-methylimidazole

5-MeIm : 5-methylimidazole

1,2-DiMeIm : 1,2-dimethylimidazole

1,5-DiMeIm : 1,5-dimethylimidazole

4-NO_2-PhO : 4-nitrophenolate

3-F-4-NO_2-PhO : 3-fluoro-4-nitrophenolate

HRP : horseradish peroxidase

ASP: ascorbate peroxidase

LiP : lignin peroxidase

MnP : manganese peroxidase

CIP : *Coprinus cinereus* peroxidase

CPO : chloroperoxidase

BL-CAT : bovine liver catalase

Eo-CAT : *Exiguobacterium oxidotolerans* catalase

Pm-CAT : *Proteus mirabilis* catalase

Ml-CAT : *Micrococcus luteus* catalase

compound I : oxoiron(IV) porphyrin π-cation radical

Introduction

Oxoiron(IV) porphyrin π-cation radical species in peroxidases and catalases, called compound I, is known as a reactive intermediate of these enzymes.[1,2] It is also believed that compound I is formed as a reactive intermediate in the catalytic cycles of cytochromes P450.[3] Although these enzymes share a common reactive intermediate, the reactivity of compound I differs from enzyme to enzyme. The compound I in cytochromes P450 directly transfers a single oxygen atom to a variety of substrates, while those in peroxidases and catalases carry out one-electron oxidation of organic substrates, such as amines and phenols, and oxidation of hydrogen peroxide to water and oxygen gas, respectively.[1-3] It is generally accepted that the diverse functions of compound I are controlled by heme environmental structures, such as porphyrin peripheral structures, heme axial ligands, and protein structures around heme.

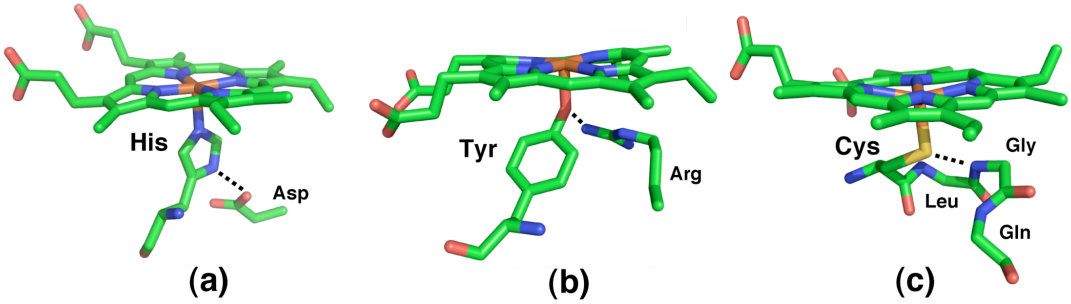

Figure 2.1.1. Active site structures of (a) peroxidase (HRP, PDB file 1DZ9), (b) catalase (*BL*-CAT, PDB file 2A9E), and (c) cytochrome P450 (Cytochrome $P450_{cam}$, PDB file 1HCH).

One significant structural difference in these heme enzymes is the heme axial ligand.[1-3] As shown in Figure 2.1.1, histidine and tyrosine residues (imidazole and phenolate) are coordinated to the heme iron as axial ligands in peroxidases other than CPO and catalases, respectively. In cytochromes P450 and CPO, a cysteine residue

(thiolate) is the heme axial ligand. The amino acids that serve as the axial ligands are highly conserved in these heme enzymes, suggesting some functional roles in these enzyme functions. In the reaction cycles of these enzymes, the axial ligand can affect both the formation of compound I and the reaction of compound I with the substrate. The effect of the axial ligand on the rate of compound I formation has been studied by mutation of the aspartic acids that interact with the proximal histidine residues in peroxidases; the mutations weakened the electron donor effect of the proximal histidines, drastically decreasing in the rates of compound I formation.[1,4] A similar axial ligand effect was also observed for synthetic heme enzyme model complexes. The rate of heterolytic cleavage of the O-O bond of iron bound *m*-chloroperbenzoate, which leads to formation of the compound I model complex, increased as the electron donor effect of the axial imidazole ligand increased.[5] These mutation and synthetic enzyme model studies demonstrate that an increase in the electron donor effect of the axial ligand enhances the rate of compound I formation.

The axial ligand effect also affects the electronic structure and reactivity of compound I. The EPR spectra of compound I in peroxidases and catalases indicated a change in intramolecular spin coupling between the ferryl ion and radical spins, probably due to differences in the axial ligand effect.[6-11] Catalytic oxidation reactions with synthetic iron porphyrin complexes having imidazoles, phenolates, and thiolates as axial ligands revealed significant effect of the axial ligand on product yield and selectivity.[12-17] For example, the imidazole and chloride axial ligands had greater product yields than the thiolate axial ligand in catalytic competitive oxidation of cyclooctane/cyclooctene. However, the thiolate axial ligand favored hydroxylation, whereas the imidazole and chloride axial ligands preferentially yielded epoxidation.[17] Moreover, the axial ligand effect on styrene epoxidation was reported using compound I

model complexes with chloride, fluoride, trifluoromethylsulfonate, methanol, and perchlorate axial ligands.[18] More recently, the axial ligand effect was also studied in detail with other synthetic iron porphyrin systems and DFT calculations.[19,20] Although these results clearly show the axial ligand effect on the electronic structure and reactivity of compound I, it is still unknown how the enzyme axial ligands (imidazole, phenolate, and thiolate) change the electronic state and reactivity of compound I. This is due to the difficulty of direct comparison of the reactivity of compound I in heme enzymes because of different protein structures, and due to the absence of stable compound I model complexes with imidazole, phenolate, and thiolate axial ligands because of rapid reduction of compound I model complexes by these axial ligands.

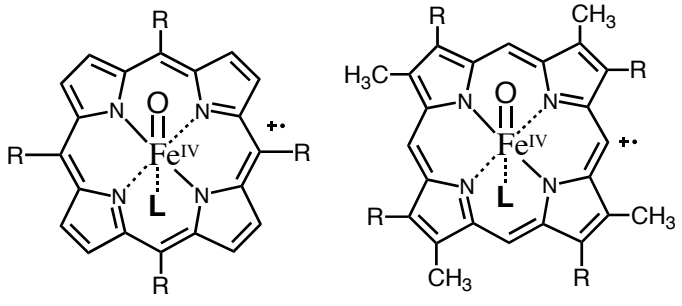

Figure 2.1.2. Structures of compound I model complexes prepared in this study.

In previous studies, we reported the first preparation of oxoiron(IV) porphyrin π-cation radical complexes with imidazole and 4-nitrophenolate as models for compound I of peroxidases and catalases.[21,22] Although the imidazole complex could be characterized with absorption, ^{1}H NMR, and resonance Raman spectroscopy, the

4-nitrophenolate complex was too unstable to characterize, except for its absorption spectrum. To fully characterize and compare reactivities, we comprehensively prepared oxoiron(IV) porphyrin π-cation radical complexes with imidazole, 2-methylimidazole, 5-methylimidazole, and 3-fluoro-4-nitrophenolate as axial ligands by ozone oxidation of iron(III) complexes of 5, 10, 15, 20-tetramesitylporphyrin (TMP) and 2, 7, 12, 17-tetramethyl-3, 8, 13, 18-tetramesitylporphyrin (TMTMP), as shown in Figure 2.1.2. A stable catalase compound I model complex was synthesized with the 3-fluoro-4-nitrophenolate axial ligand. These imidazole and phenolate complexes were fully characterized using UV-visible absorption, ^{1}H, ^{2}H, and ^{19}F NMR, EPR, and ESI-MS spectroscopy. Because of the structural similarity between TMTMP and protoporphyrin IX in heme enzymes, the TMTMP complexes more closely mimic the spectroscopic properties of compound I in peroxidases and catalases than the TMP complexes. The most important findings in this study were: 1) that the porphyrin π-cation radical spin was significantly transferred in the axial imidazole (phenolate) and oxo ligands for the a_{2u} radical complex, but not for the a_{1u} radical complex, and 2) that the oxidation reactivity of oxoiron(IV) porphyrin π-cation radical complex was drastically increased, more than 400 times in the most significant case, with the coordination of imidazole and phenolate axial ligands, suggesting extremely reactive compound I in heme enzymes. Based on the present spectroscopic and kinetic studies, the functional roles of axial ligands on compound I in heme enzymes and catalytic oxidation reactions are discussed in the final section.

Experimental Section

Instrumentation. UV-visible absorption spectra were recorded on an Agilent 8453 (Agilent Technologies) equipped with a USP-203 low-temperature chamber (UNISOKU). ^{1}H, ^{2}H, ^{13}C and ^{19}F NMR were measured on a Lambda-500 spectrometer (JEOL). ^{1}H, ^{2}H, and ^{13}C NMR Chemical shifts were reported versus tetramethylsilane (TMS) and referenced to residual solvent peaks (dichloromethane: 5.32 ppm). ^{19}F chemical shift values were referenced to external hexafluorobenzene (C_6F_6) at 0 ppm. The concentrations of NMR samples were ~5 mM. EPR spectra were recorded at 4 K on Bruker E500 X-band spectrometer with an Oxford Instruments EPR910 helium-flow cryostat (Bruker). The concentrations of EPR samples were 1–3 mM. ESI-MS spectra were obtained with a LCT time-of–flight mass spectrometer equipped with an elecrospray ionization interface (Micromass). For oxoiron(IV) porphyrin π-cation radical complexes, desolvation and nebulizer gases were cooled with liquid nitrogen. The ESI-MS samples were prepared by oxidation with ozone in acetonitrile or dichloromethane at 233 K, followed by dilution with the same solvent, and injected into the ESI-MS with a gastight syringe cooled with dry ice. The sample solution was then transferred to the inlet of the mass spectrometer through pre-cooled capillary tube. Gas chromatography-mass spectroscopy (GC-MS) analysis was performed on a QP-5000 GC-MS system (Shimadzu) equipped with a capillary gas chromatograph (GC-17A, CBP5-M25-025 capillary column). Ozone gas was generated by UV irradiation of oxygen gas (99.9%) with an ozone generator PR-1300 (Clear Water) and used without further purification.

Materials. Imidazole-d_4 (98 atom % D) was purchased from Aldrich. 2-Methylimidazole-d_6 (98.1 atom % D) was purchased from CDN ISOTOPES (Canada). 4-Methylimidazole-d_6 was prepared from 4-methylimidazole by activated 10% Pd/C in D_2O, according to the literature.[43] Deuterium incorporation into 4-methylimidazole, as analyzed by ^1H and ^{13}C NMR, was 2-H (95%), 5-H (95%) and 4-methyl group (50%). Dichloromethane was purchased from a commercial company as the anhydrous solvent and was stored in the presence of 4A molecular sieves. Other chemicals were purchased from commercial companies, and used without further purification. *meso*-Tetramesitylporphyrin ($TMPH_2$) and 2,7,12,17-teramethyl-3,8,13,18-tetramesityl-porphyrin ($TMTMPH_2$) were prepared according to the literature.[44] (TMP)$Fe^{III}Cl$ and (TMTMP)$Fe^{III}Cl$ were prepared by the insertion of iron into $TMPH_2$ and $TMTMPH_2$ with $FeCl_2$ and sodium acetate in acetic acid, respectively, and purified by silica gel column using CH_2Cl_2/CH_3OH as an eluent. (TMP)$Fe^{III}OH$ and (TMTMP)$Fe^{III}OH$ were obtained from (TMP)$Fe^{III}Cl$ and (TMTMP)$Fe^{III}Cl$, respectively, by passing through a basic alumina (10% water) column with dichloromethane as an eluent.[45] (TMP)$Fe^{III}ClO_4$ and (TMTMP)$Fe^{III}ClO_4$ were prepared by the reaction of (TMP)$Fe^{III}Cl$ and (TMTMP)$Fe^{III}Cl$, respectively, with silver(I) perchlorate in dichloromethane solution, and purified by re-crystallization from dichloromethane/*n*-hexane.[46] (TMP)$Fe^{III}NO_3$ and (TMTMP)$Fe^{III}NO_3$ were obtained by mixing (TMP)$Fe^{III}OH$ and (TMTMP)$Fe^{III}OH$ in toluene with 1 M nitric acid, and purified by re-crystallization from ether/*n*-hexane.[47] (TMP)$Fe^{III}(NO_3)$; ^1H NMR (CD_2Cl_2, 25°C), 4.0 and 6.2 (*ortho*-Me), 15.3 and 16.5 (*meta*-H), 4.3 (*para*-Me), 74.0 (pyrrole-H). UV-vis. (CH_2Cl_2, 25°C), 412, 514, 580, 647, and 691 nm. (TMTMP)$Fe^{III}(NO_3)$; ^1H NMR (CD_2Cl_2, 25°C), –49.6 (meso-H), 5.1 and 8.4 (*ortho*-Me), 12.9 and 13.3 (*meta*-H), 6.3 (*para*-Me), 58.7 (pyrrole-Me). UV-vis. (CH_2Cl_2, 25°C), 388, 506, 532, and 637 nm.

Synthesis. Iron(III) phenolate complexes. Iron(III) phenolate complexes were prepared by the published method.[48] (TMP)Fe^{III}OH and (TMTMP)Fe^{III}OH were dissolved in toluene and 1 equiv of phenol derivative (4-nitrophenol, pentafluorophenol, 3,4,5-trifluorophenol, or 3-fluoro-4-nitrophenol) was added with stirring. The green or red solution changed to brown as the phenol dissolved. The solution was evaporated to dryness and the residue was purified by crystallization from ether/hexane. Microcrystals of the iron(III) phenol complex were collected by filtration. (TMP)Fe^{III}(4-NO_2-PhO) ; ^{1}H NMR (CD_2Cl_2, 25°C), 3.0 and 5.2 (*ortho*-Me), 12.5 and 13.5 (*meta*-H), 3.7 (*para*-Me), 79.1 (pyrrole-H), –91.4 (phenol *ortho*-H), 83.0 (phenol *meta*-H). UV-vis. (CH_2Cl_2, 25°C), 420, 497, 559, 635 and 667 nm. (TMP)Fe^{III}(F_5-PhO) ; ^{1}H NMR (CD_2Cl_2, 25°C), 2.9 and 5.2 (*ortho*-Me), 12.7 and 13.6 (*meta*-H), 3.8 (*para*-Me), 78.7 (pyrrole-H). UV-vis. (CH_2Cl_2, 298K), 415, 500, 566, 642 and 673nm. (TMP)Fe^{III}(3,4,5-F_3-PhO) ; ^{1}H NMR (CD_2Cl_2, 25°C), 3.0 and 5.1 (*ortho*-Me), 12.3 and 13.3 (*meta*-H), 3.7 (*para*-Me), 79.8 (pyrrole-H), –101.0 (phenol *ortho*-H). UV-vis. (CH_2Cl_2, 25°C), 420, 490, 557, 620 and 666 nm. (TMP)Fe^{III}(3-F-4-NO_2-PhO) ; ^{1}H NMR (CD_2Cl_2, 25°C), 3.1 and 5.2 (*ortho*-Me), 12.7 and 13.7 (*meta*-H), 3.8 (*para*-Me), 78.9 (pyrrole-H), –85.1 and –81.5 (phenol *ortho*-H), 72.4 (phenol *meta*-H). ^{19}F NMR (CD_2Cl_2, 25°C), 58.4 (*meta*-F). UV-vis. (CH_2Cl_2, 25°C), 419, 500, 560, 640 and 668 nm. (TMTMP)Fe^{III}(4-NO_2-PhO) ; ^{1}H NMR (CD_2Cl_2, 25°C), –40.5 (meso-H), 4.8 and 7.4 (*ortho*-Me), 11.9 and 12.0 (*meta*-H), 6.0 (*para*-Me), 47.7 (pyrrole-Me), –83.1 and –79.9 (phenol *ortho*-H), 67.9 (phenol *meta*-H). UV-vis. (CH_2Cl_2, 25°C), 371, 398, 498, 526 and 619 nm. (TMTMP)Fe^{III}(3-F-4-NO_2-PhO) ; ^{1}H NMR (CD_2Cl_2, 25°C), –47.0 (meso-H), 4.5 and 7.3 (*ortho*-Me), 11.9 and 12.0 (*meta*-H), 5.0 (*para*-Me), 47.0 (pyrrole-Me), –83.1 and –79.9 (phenol *ortho*-H), 67.9 (phenol *meta*-H). ^{19}F NMR (CD_2Cl_2, 25°C), 58.3 (*meta*-F).

UV-vis. (CH_2Cl_2, 25°C), 370, 401, 496, 524 and 619 nm.

Iron(III) mono-imidazole complexes. Iron(III) porphyrin mono-imidazole complex was generated in situ by adding 1.0 equiv of imidazole, 2-methylimidazole, or 4-methylimidazole to perchlorate iron(III) porphyrin in dichloromethane.[49] $[(TMP)Fe^{III}(Im)]ClO_4$; ^1H NMR (CD_2Cl_2, 25°C), 3.1 and 5.3 (*ortho*-Me), 12.6 and 13.4 (*meta*-H), 4.3 (*para*-Me), 19.9 (pyrrole-H), –15.5 (Im 2-H), 30.1 (Im 4-H), 85.1 (Im 5-H), 100.4 (Im N-H). UV-vis. (CH_2Cl_2, 25°C), 412, 510, 575 and 690 nm. $[(TMP)Fe^{III}(2\text{-}MeIm)]ClO_4$; ^1H NMR (CD_2Cl_2, 298K), 2.7 and 5.7 (*ortho*-Me), 12.7 and 13.1 (*meta*-H), 4.1 (*para*-Me), 34.9 (pyrrole-H), 16.6 (2-MeIm 2-Me), 31.8 (2-MeIm 4-H), 65.8 (2-MeIm 5-H), 109.0 (2-MeIm N-H). UV-vis. (CH_2Cl_2, 25°C), 412, 511, 572 and 692 nm. $[(TMP)Fe^{III}(5\text{-}MeIm)]ClO_4$; ^1H NMR (CD_2Cl_2, 25°C), 13.0 and 13.9 (*meta*-H), 4.4 (*para*-Me), 31.7 (pyrrole-H), –18.6 (5-MeIm 2-Me), 31.7 (5-MeIm 4-H), 22.0 (5-MeIm 5-Me), 100.8 (5-MeIm N-H). UV-vis. (CH_2Cl_2, 25°C), 412, 510, 572 and 692 nm. $[(TMTMP)Fe^{III}(Im)]ClO_4$; ^1H NMR (CD_2Cl_2, 25°C), –16.6 (meso-H), 4.8 and 8.0 (*ortho*-Me), 13.5 and 14.4 (*meta*-H), 5.5 (*para*-Me), 69.2 (pyrrole-Me), –16.1 (Im 2-H), 31.2 (Hm 4-H), 82.6 (Im 5-H), 98.5 (Im N-H). UV-vis. (CH_2Cl_2, 25°C), 385, 503 and 626 nm. $[(TMTMP)Fe^{III}(2\text{-}MeIm)]ClO_4$; ^1H NMR (CD_2Cl_2, 25°C), –31.9 (meso-H), 5.1 and 8.8 (*ortho*-Me), 13.8 and 14.5 (*meta*-H), 6.2 (*para*-Me), 70.0 (pyrrole-Me), 17.5 (2-MeIm 2-Me), 35.9 (2-MeIm 4-H), 66.6 (2-MeIm 5-H), 110.0 (2-MeIm N-H). UV-vis. (CH_2Cl_2, 298K), 385, 503 and 626 nm. $[(TMTMP)Fe^{III}(5\text{-}MeIm)]ClO_4$; ^1H NMR (CD_2Cl_2, 298K), -20.1 (meso-H), 5.0 and 8.2 (*ortho*-Me), 13.7 and 14.5 (*meta*-H), 5.8 (*para*-Me), 70.3 (pyrrole-Me), -15.4 (5-MeIm 2-H), 32.6 (5-MeIm 4-H), 20.7 (5-MeIm 5-H), 99.5 (5-MeIm N-H). UV-vis. (CH_2Cl_2, 25°C), 385, 503 and 626 nm.

Oxoiron(IV) porphyrin complexes. Oxoiron(IV) porphyrin complexes were prepared as previously described.[45] (TMP)$Fe^{III}(ClO_4)_2$ or (TMTMP)$Fe^{III}(ClO_4)_2$, which was prepared from the oxidation of (TMP)Fe^{III}OH or (TMTMP)Fe^{III}OH with solid ferric perchlorate, in dichloromethane-d_2 was transferred through a short basic alumina (20% water) column (0.5 × 1 cm) at ambient temperature, directly into a NMR tube in dry ice-acetone bath. 1 equiv of 1-MeIm or 1,2-DiMeIm in dichloromethane-d_2 was slowly added to the cooled solution in the NMR tube.

Ozone oxidation of iron(III) porphyrin. For NMR or EPR measurement, iron(III) porphyrin complexes were dissolved in dichloromethane and placed in NMR or EPR cell. The solution was cooled by a dry-ice acetone bath. Ozone gas was slowly bubbled in the solution with a gastight syringe. With the formation of oxoiron(IV) porphyrin π-cation radical complexes, the brown solution changed to green. The oxidations were monitored by ^{1}H NMR or EPR spectra. For UV-visible absorption spectra, the oxidation was carried out in a 1 cm quartz cuvette in a low-temperature chamber set with a UV-visible absorption spectrometer and monitored by absorption spectral change. Finally, excess ozone gas was removed by bubbling argon gas with a gastight syringe.

Kinetics and product analysis. Oxoiron(IV) porphyrin π-cation radical (100 μM) in dichloromethane was prepared in a 1 cm quartz cuvette in a low-temperature chamber set with a UV-visible absorption spectrometer, as described above. An excess of cyclooctene (20–1000 equiv) was then added to the solution with vigorous stirring, and the reactions were monitored by the absorption spectral change at constant time intervals. After confirming the completion of the reactions, 10 equiv of

tetrabutylammonium iodide (nBu$_4$N$^+$I$^-$) was added to the solution at the same temperature. After warming to room temperature, quantitative product analyses were subsequently performed with GC-MS using undecane as an internal standard. The reaction rate constants were determined by computer simulation of absorption versus time for the reactions.

Scheme 1

X = ClO_4^-, NO_3^-

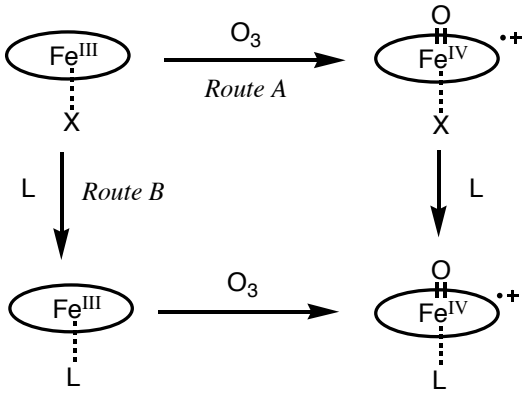

Results

Synthesis of Compound I Models. The oxoiron(IV) porphyrin π-cation radical complexes with imidazole and phenolate derivatives as axial ligands were prepared using two alternative routes, as shown in Scheme 2.1.1. [(TMP$^{+\bullet}$)Fe^{IV}O(L)](ClO$_4$) and [(TMTMP$^{+\bullet}$)Fe^{IV}O(L)](ClO$_4$), where L is Im, 2-MeIm, and 5-MeIm, were prepared from (TMP)Fe^{III}(ClO$_4$) and (TMTMP)Fe^{III}(ClO$_4$) using route B, respectively. [(TMTMP$^{+\bullet}$)-Fe^{IV}O(L)](ClO$_4$) also was prepared from (TMTMP)Fe^{III}(ClO$_4$) using route A. However, pure [(TMP$^{+\bullet}$)Fe^{IV}O(L)](ClO$_4$) could not be prepared using route A, because oxidation of (TMP)Fe^{III}(ClO$_4$) with ozone did not produce pure (TMP$^{+\bullet}$)Fe^{IV}O(ClO$_4$). To explore the effects of counter anions, we examined the preparation from nitrate iron(III) porphyrin complexes. In contrast to the perchlorate complexes, [(TMP$^{+\bullet}$)Fe^{IV}O(L)]-

(NO_3) and [(TMTMP$^{+\bullet}$)$Fe^{IV}O$(L)](NO_3) were prepared from (TMP)Fe^{III}(NO_3) and (TMTMP)Fe^{III}(NO_3) using route A, respectively. On the other hand, route B was not effective, except for the case of TMTMPFe^{III}(NO_3) and 2-methylimidazole, because the addition of 1 equiv of the imidazole derivative to the nitrate complex did not afford its mono-adduct complex, but rather a mixture of the parent and bis-adduct complexes. The oxoiron(IV) porphyrin π-cation radical complexes with imidazole derivatives, prepared from nitrate complexes using route A, were as stable as those prepared from perchlorate complexes at temperatures below 233 K in dichloromethane.

The preparation of oxoiron(IV) porphyrin π-cation radical complexes with phenolate derivatives (4-nitrophenolate, pentafluorophenolate, 3,4,5-trifluorophenolate, and 3-fluoro-4-nitrophenolate) as axial ligands was examined using route B for TMP and TMTMP complexes. The oxoiron(IV) porphyrin π-cation radical complexes with 4-nitrophenolate, 3,4,5-trifluorophenolate, and pentafluorophenolate were very unstable even at 183 K and quickly reduced to iron(III) porphyrin complexes with dissociation and decomposition of the axial phenol. However, the oxoiron(IV) porphyrin π-cation radical complex with 3-fluoro-4-nitrophenolate was stable enough for spectroscopic characterization at temperatures below 213 K in dichloromethane. In route A, the addition of 1 equiv of phenol derivatives to oxoiron(IV) porphyrin π-cation radical complex resulted in rapid reduction of the complex.

Characterization of Peroxidase Compound I Models. Figure 2.1.3, shows UV-visible absorption spectral changes for the formation of oxoiron(IV) porphyrin π-cation radical complexes with imidazole from the route A in dichloromethane at –80°C. Oxidation of (TMP)Fe^{III}(NO_3) with ozone at –80 °C yielded (TMP$^{+\bullet}$)Fe^{IV}O-(NO_3), which showed a Soret band with decreased intensity at 401 nm and an

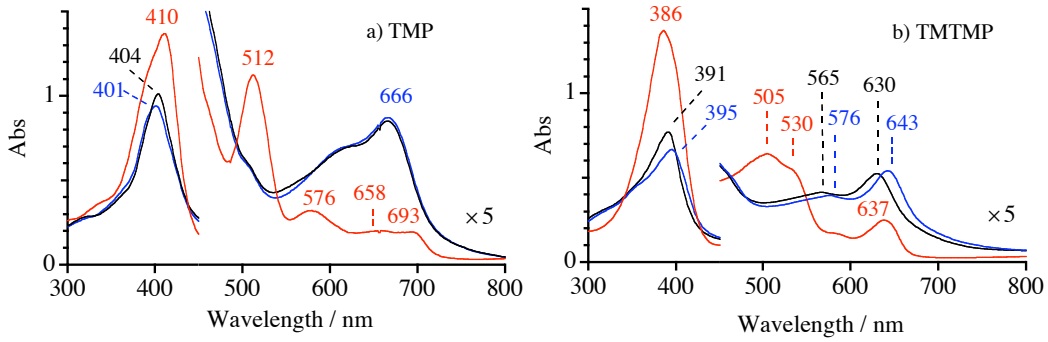

Figure 2.1.3. UV-visible absorption spectra of oxoiron(IV) porphyrin π-cation radical complexes (10 mM) with imidazole in dichloromethane at –80 °C. Red lines : $(P)Fe^{III}(NO_3)$, black lines : $(P^{+\bullet})Fe^{IV}O(NO_3)$, blue lines : $[(P^{+\bullet})Fe^{IV}O(Im)](NO_3)$. (a) P = TMP, (b) P = TMTMP.

absorption peak near 666 nm, as shown in Figure 2.1.3 a). The careful addition of 1 equiv of imidazole to $(TMP^{+\bullet})Fe^{IV}O(NO_3)$ showed a small but significant spectral change, indicating the formation of $[(TMP^{+\bullet})Fe^{IV}O(Im)](NO_3)$ without reduction of the porphyrin π-cation radical. Similarly, Figure 2.1.3 b) shows the formation of $[(TMTMP^{+\bullet})Fe^{IV}O(Im)](NO_3)$ using route A. With the coordination of imidazole, the intensity of the Soret band decreased and the absorption at 630 nm shifted to 643 nm. The absorption spectra of oxoiron(IV) porphyrin π-cation radical complexes having 2-methylimidazole and 5-methylimidazole were also measured, and the results are summarized in Table 2.1.1. The axial coordination of 2-methylimidazole and 5-methylimidazole did not change the peak positions for the TMP complexes, but did change them for the TMTMP complexes. The absorption spectral features of $[(TMTMP^{+\bullet})Fe^{IV}O(Im)](NO_3)$ more closely resembled those of compound I of peroxidases than those of $[(TMP^{+\bullet})Fe^{IV}O(Im)](NO_3)$ (Table 2.1.2).[23-28] Similar complexes with perchlorate anions were also prepared, and the peak positions were the same as those observed with nitrate anions.

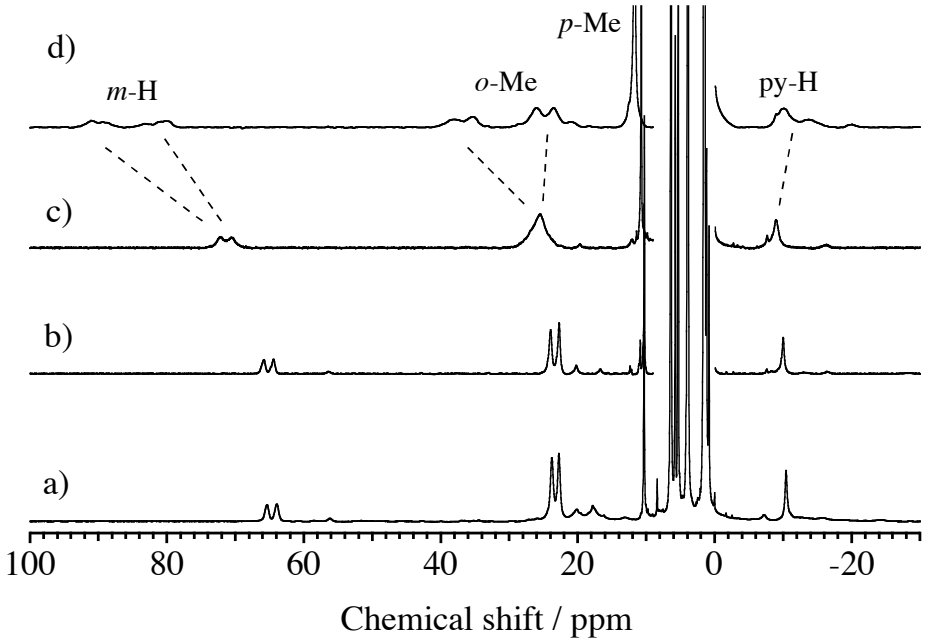

Figure 2.1.4. ^{1}H NMR spectra of [(TMP$^{+\bullet}$)Fe^{IV}O(L)](ClO$_4$) in dichloromethane-d_2 at –60 ˚C. a) L = Im, b) L = 5-MeIm, c) L = 2-MeIm, d) L = 2-MeIm at –90 ˚C

Figure 2.1.4 shows ^{1}H NMR spectra of [(TMP$^{+\bullet}$)Fe^{IV}O(L)](ClO$_4$) and [(TMTMP$^{+\bullet}$)Fe^{IV}O(L)](ClO$_4$), where L is either Im, 2-MeIm, or 5-MeIm, in dichloromethane-d_2. The ^{1}H NMR signals were assigned by deuterium-labeled compounds, signal intensities, and comparison with those of previously characterized (TMP$^{+\bullet}$)Fe^{IV}O(ClO$_4$).[29] The ^{1}H NMR shifts of [(TMP$^{+\bullet}$)Fe^{IV}O(L)](ClO$_4$) are summarized in Table 2.1.3. [(TMP$^{+\bullet}$)Fe^{IV}O(Im)](ClO$_4$) exhibits the pyrrole proton signal at –10.4 ppm, the *m*-protons of the meso mesityl group at 63.9 and 65.4 ppm, the *o*-methyl protons at 22.8 and 23.8 ppm, and the *p*-methyl protons at 10.3 ppm. The separation of the *o*-methyl and *m*-proton signals was reasonable for the coordination of two different axial ligands, oxo and imidazole. The large downfield shifts of the meso mesityl protons indicate an unpaired electron in the a_{2u} porphyrin π-orbital, a_{2u} porphyrin π-cation radical state. As shown in Figure 2.1.4, the ^{1}H NMR shifts of

[(TMP$^{+\bullet}$)Fe^{IV}O(5-MeIm)](ClO$_4$) were almost identical to those of [(TMP$^{+\bullet}$)Fe^{IV}O-(Im)](ClO$_4$). The ^{1}H NMR shifts of [(TMP$^{+\bullet}$)Fe^{IV}O(2-MeIm)](ClO$_4$) were similar to those of [(TMP$^{+\bullet}$)Fe^{IV}O(Im)](ClO$_4$) and [(TMP$^{+\bullet}$)Fe^{IV}O(5-MeIm)](ClO$_4$), but the ^{1}H NMR signals of [(TMP$^{+\bullet}$)Fe^{IV}O(2-MeIm)](ClO$_4$) were broader. When the temperature was lowered further, the ^{1}H NMR signals of [(TMP$^{+\bullet}$)Fe^{IV}O(2-MeIm)](ClO$_4$) became much broader and split at –90 ˚C as shown in Figure 2.1.4 d). This was because the rotation of the axially bound 2-methylimidazole along the Fe-N(2-MeIm) axis was hindered by a steric interaction between the 2-methyl group of 2-methylimidazole and the *o*-methyl group of the meso mesityl group. The ^{1}H NMR spectra of [(TMP$^{+\bullet}$)Fe^{IV}O(L)](NO$_3$) were identical to those of [(TMP$^{+\bullet}$)Fe^{IV}O(L)](ClO$_4$).

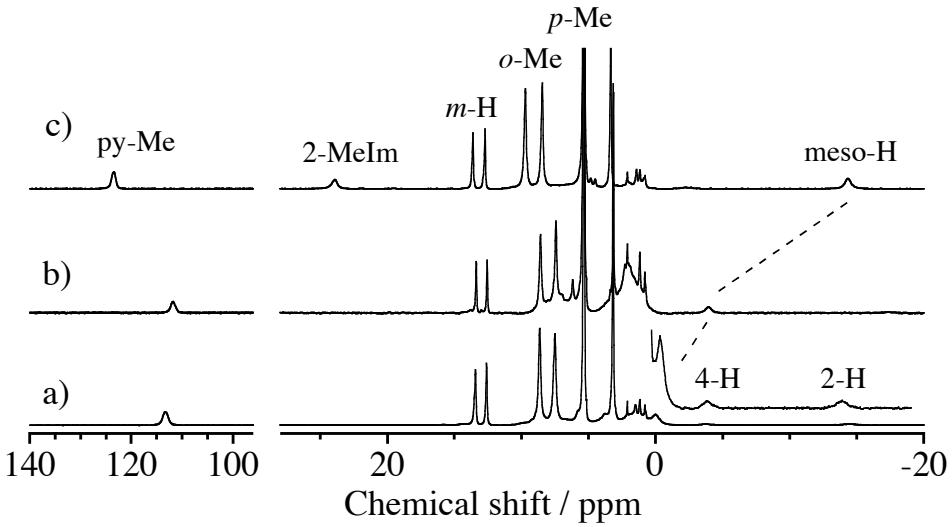

Figure 2.1.5. ^{1}H NMR spectra of [(TMTMP$^{+\bullet}$)Fe^{IV}O(L)](ClO$_4$) in dichloromethane -d_2 at –80 °C. a) L = Im, b) L = 5-MeIm, c) L = 2-MeIm.

Figure 2.1.5 shows the ^{1}H NMR spectra of [(TMTMP$^{+\bullet}$)Fe^{IV}O(L)](ClO$_4$), where L is either Im, 2-MeIm, or 5-MeIm, in dichloromethane-d_2 at –80 ˚C. The ^{1}H NMR signals of [(TMTMP$^{+\bullet}$)Fe^{IV}O(L)](ClO$_4$) were also assigned using deuterium labeled

compounds, signal intensities, and comparison with those of previously characterized $(TMTMP^{+\bullet})Fe^{IV}O(ClO_4)$.[21,29] The ^1H NMR shifts of $[(TMTMP^{+\bullet})Fe^{IV}O(L)](ClO_4)$ are summarized in Table 2.1.4. As reported, $[(TMTMP^{+\bullet})Fe^{IV}O(Im)](ClO_4)$ showed a large downfield shift of the pyrrole methyl signal at 113.2 ppm and small shift of the meso proton signal at 0.0 ppm.[21] The ^1H NMR spectra of $[(TMTMP^{+\bullet})Fe^{IV}O$-$(5\text{-MeIm})](ClO_4)$ and $[(TMTMP^{+\bullet})Fe^{IV}O(2\text{-MeIm})](ClO_4)$ were similar to that of $[(TMTMP^{+\bullet})Fe^{IV}O(Im)](ClO_4)$, but paramagnetic shifts of $[(TMTMP^{+\bullet})Fe^{IV}O(2\text{-MeIm})]$-$(ClO_4)$ were larger than those of the other two. The small paramagnetic shifts of the meso proton signals for $[(TMTMP^{+\bullet})Fe^{IV}O(L)](ClO_4)$ clearly indicate an unpaired electron in the a_{1u} porphyrin π-orbital, a_{1u} porphyrin π-cation radical state. Unlike $[(TMP^{+\bullet})Fe^{IV}O(2\text{-MeIm})](ClO_4)$, the rotation of the 2-MeIm in $[(TMTMP^{+\bullet})Fe^{IV}O$-$(2\text{-MeIm})](ClO_4)$ was not hindered. In fact, even at –90 ˚C, only a single pyrrole methyl signal was observed. This is because the *o*-methyl group of the pyrrole β-mesityl group in TMTMP is farther from the iron center than that of the meso mesityl group in TMP, resulting in a smaller steric effect on the rotation of 2-methylimidazole in TMTMP. The ^1H NMR spectra of $[(TMTMP^{+\bullet})Fe^{IV}O(L)](NO_3)$ were similar to those of $[(TMTMP^{+\bullet})Fe^{IV}O(L)](ClO_4)$. The temperature dependence of ^1H NMR signals for $[(TMP^{+\bullet})Fe^{IV}O(L)](ClO_4)$ and $[(TMTMP^{+\bullet})Fe^{IV}O(L)](ClO_4)$ showed normal Curie's law behavior.

Direct evidence for the coordination of imidazole derivatives to oxoiron(IV) porphyrin π-cation radical complexes was obtained by ^2H NMR spectra of iron-bound deuterium-labeled imidazole derivatives (Figure 2.1.6). The ^2H NMR shifts are summarized in Table 2.1.5, together with the NMR shifts of iron-bound imidazole signals of oxoiron(IV) and iron(III) porphyrin complexes. The ^2H NMR signals were assigned by their relative intensity and by substitution of each imidazole position with a

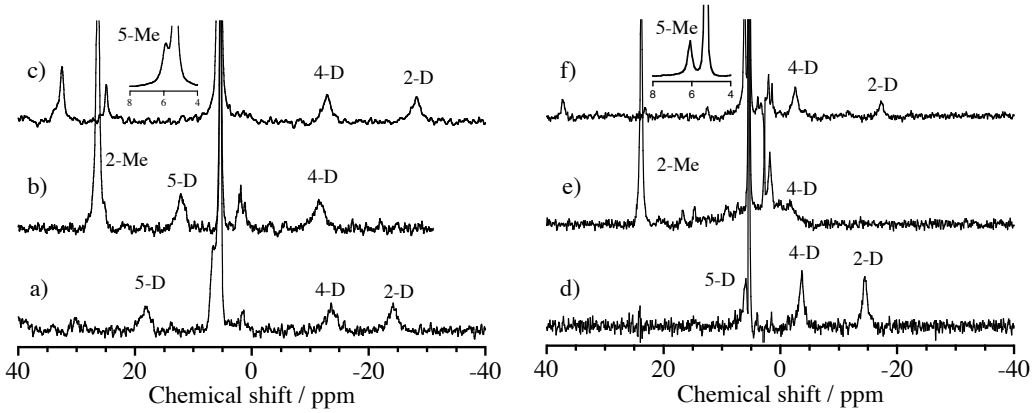

Figure 2.1.6. ^{2}H NMR spectra of a) [(TMP$^{+\bullet}$)Fe^{IV}O(Im-d_4)](ClO$_4$), b) [(TMP$^{+\bullet}$)Fe^{IV}O(2-MeIm-d_6)](ClO$_4$), c) [(TMP$^{+\bullet}$)Fe^{IV}O(5-MeIm-d_6)](ClO$_4$), d) [(TMTMP$^{+\bullet}$)Fe^{IV}O(Im-d_4)](ClO$_4$), e) [(TMTMP$^{+\bullet}$)Fe^{IV}O(2-MeIm-d_6)](ClO$_4$), and f) [(TMTMP$^{+\bullet}$)Fe^{IV}O(5-MeIm-d_6)](ClO$_4$) in dichloromethane. Temperature; a) – c) at –60 ˚C and d) – f) at –80 ˚C.

methyl group, which resulted in the disappearance of the signal for the substituted position and the appearance of a new signal for the introduced methyl group. The paramagnetic shifts of the ^{2}H NMR signals of the deuterium-labeled imidazole derivatives clearly showed their coordination to the ferryl iron site as axial ligands. The temperature dependence of these ^{2}H NMR signals showed normal Curie's law behavior. The ^{2}H NMR signals for the 2- and 4-positions of the iron-bound imidazole derivative showed upfield shifts, while those for the 5-position showed downfield shifts. With substitutions of the 2-positions with methyl groups, the ^{2}H NMR signals of the methyl groups were observed downfield. The ^{2}H NMR paramagnetic shifts of iron-bound imidazole signals for [(TMP$^{+\bullet}$)Fe^{IV}O(L)](ClO$_4$) were larger than those of [(TMTMP$^{+\bullet}$)Fe^{IV}O(L)](ClO$_4$).

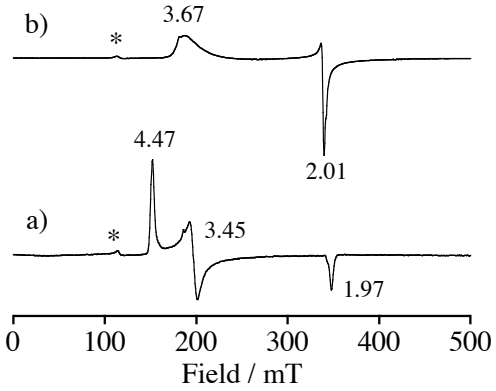

Figure 2.1.7. EPR spectra of (a) $[(P^{+\bullet})Fe^{IV}O(2\text{-MeIm})](ClO_4)$ at 4K. (a) P = TMP, in dichloromethane-toluene (5:1), (b) P = TMTMP, in dichloromethane-propionitrile (5:1). Signals denoted by asterisks are due to $[(TMP)Fe^{III}(2\text{-MeIm})](ClO_4)$ and $[(TMTMP)Fe^{III}(2\text{-MeIm})](ClO_4)$.

Figure 2.1.7 shows the EPR spectra of $[(TMP^{+\bullet})Fe^{IV}O(2\text{-MeIm})](ClO_4)$ and $[(TMTMP^{+\bullet})Fe^{IV}O(2\text{-MeIm})](ClO_4)$ at 4 K. $[(TMP^{+\bullet})Fe^{IV}O(2\text{-MeIm})](ClO_4)$ showed the EPR signals at g = 4.47, 3.45, and 1.97, which were similar to those of $(TMP^{+\bullet})Fe^{IV}O(ClO_4)$.[30] The EPR spectra of $[(TMP^{+\bullet})Fe^{IV}O(2\text{-MeIm})](ClO_4)$ were typical of those of S = 3/2 systems, indicating strong ferromagnetic interactions between ferryl iron (S = 1) and the porphyrin π-cation radical (S = 1/2). The EPR spectra of $[(TMP^{+\bullet})Fe^{IV}O(Im)](ClO_4)$ and $[(TMP^{+\bullet})Fe^{IV}O(5\text{-MeIm})](ClO_4)$ were very close to that of $[(TMP^{+\bullet})Fe^{IV}O(2\text{-MeIm})](ClO_4)$, suggesting similar spin interactions (Table 2.1.3). The g values for the TMP complexes were hardly changed by the axial ligand effect. As shown in Figure 2.1.7 b), the EPR spectrum of $[(TMTMP^{+\bullet})Fe^{IV}O(2\text{-MeIm})](ClO_4)$ differed from that of $[(TMP^{+\bullet})Fe^{IV}O(2\text{-MeIm})]$-$(ClO_4)$, but was similar to that of $[(TMTMP^{+\bullet})Fe^{IV}O(MeOH)](ClO_4)$ reported previously.[30] As observed for $[(TMTMP^{+\bullet})Fe^{IV}O(MeOH)](ClO_4)$,[30] the EPR spectrum of $[(TMTMP^{+\bullet})Fe^{IV}O(2\text{-MeIm})](ClO_4)$ was interpreted as a weak ferromagnetic interaction between ferryl iron (S = 1) and the porphyrin p-cation radical (S = 1/2).

The EPR spectra of [(TMTMP$^{+\bullet}$)Fe^{IV}O(Im)](ClO$_4$) and [(TMTMP$^{+\bullet}$)Fe^{IV}O(5-MeIm)]-(ClO$_4$) were similar to that of [(TMTMP$^{+\bullet}$)Fe^{IV}O(2-MeIm)](ClO$_4$), but the $g_\perp$ values were changed by the axial imidazole ligand (Table 2.1.4). This result suggests that the spin interaction was altered by the axial imidazole for the TMTMP complex. The EPR spectra of [(TMP$^{+\bullet}$)Fe^{IV}O(L)](NO$_3$) and [(TMTMP$^{+\bullet}$)Fe^{IV}O(L)](NO$_3$) were almost identical to those of [(TMP$^{+\bullet}$)Fe^{IV}O(L)](ClO$_4$) and [(TMTMP$^{+\bullet}$)Fe^{IV}O(L)](ClO$_4$), respectively.

The structural characterization of oxoiron(IV) porphyrin π-cation radical complexes having imidazole derivatives was examined using ESI-MS spectroscopy. ESI-MS peaks corresponding to [(TMP$^{+\bullet}$)Fe^{IV}O(L)]$^+$ and [(TMTMP$^{+\bullet}$)Fe^{IV}O(L)]$^+$ cations, where L = Im, 2-MeIm, and 5-MeIm, were detected (Table 2.1.6). The isotope distribution patterns of the observed ESI-MS peaks were almost identical to those calculated from [(TMP$^{+\bullet}$)Fe^{IV}O(L)]$^+$ and [(TMTMP$^{+\bullet}$)Fe^{IV}O(L)]$^+$ structures. All of the ESI-MS data supported the binding of imidazole derivatives as an axial ligand.

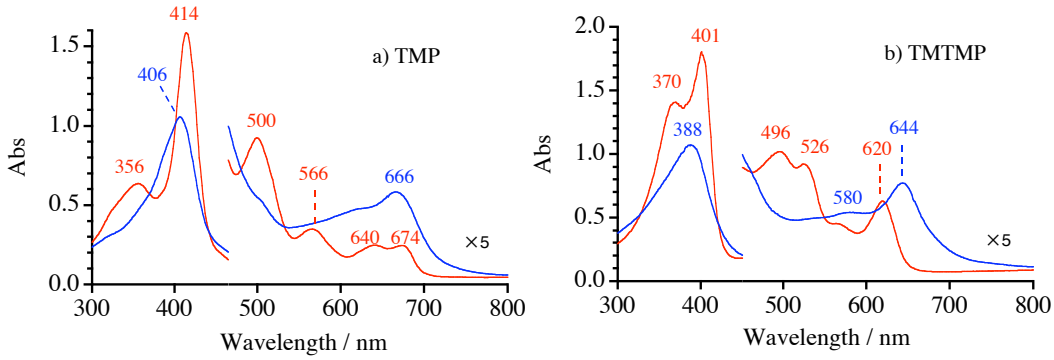

Figure 2.1.8. UV-visible absorption spectra of (P)Fe^{III}(3-F-4-NO$_2$-PhO) and (P$^{+\bullet}$)Fe^{IV}O(3-F-4-NO$_2$-PhO) in dichloromethane (concentration 1.0 × 10^{-5} M, 1cm path length cell) at –80°C: a) P = TMP, b) P = TMTMP.

Characterization of Catalase Compound I Models. Figure 2.1.8 shows UV-visible absorption spectra of (TMP$^{+\bullet}$)Fe^{IV}O(3-F-4-NO_2-PhO) and (TMTMP$^{+\bullet}$)Fe^{IV}O-(3-F-4-NO_2-PhO) prepared from route B. The absorption maxima of the spectra are listed in Table 2.1.1. The absorption spectra of (TMP$^{+\bullet}$)Fe^{IV}O(3-F-4-NO_2-PhO) and (TMTMP$^{+\bullet}$)Fe^{IV}O(3-F-4-NO_2-PhO) were very close to those of [(TMP$^{+\bullet}$)Fe^{IV}O(Im)]-(NO_3) and [(TMTMP$^{+\bullet}$)Fe^{IV}O(Im)](NO_3), respectively, shown in Figure 2.1.3. The binding of the phenolate anion did not affect their absorption spectral features. The absorption spectral features of (TMTMP$^{+\bullet}$)Fe^{IV}O(3-F-4-NO_2-PhO) were close to those of compound I of catalases.[10,31,32] While (TMP$^{+\bullet}$)Fe^{IV}O(3-F-4-NO_2-PhO) slowly decomposed to (TMP)Fe^{III}(3-F-4-NO_2-PhO) in dichloromethane at –80 °C (k_{decomp} = 3.3 × 10^{-4} s^{-1}), (TMTMP$^{+\bullet}$)Fe^{IV}O(3-F-4-NO_2-PhO) was stable for a few hours under the same conditions.

Figure 2.1.9 shows ^{1}H NMR spectra of (TMP$^{+\bullet}$)Fe^{IV}O(3-F-4-NO_2-PhO) and (TMTMP$^{+\bullet}$)Fe^{IV}O(3-F-4-NO_2-PhO) in dichloromethane-d_2 at –80 °C. The ^{1}H NMR signals were assigned with deuterium-labeled compounds, signal intensities, and comparison with those of previously characterized oxoiron(IV) porphyrin π-cation radical complexes.[29] The NMR shifts are summarized in Table 2.1.3 and 2.1.4. The ^{1}H NMR shifts of (TMP$^{+\bullet}$)Fe^{IV}O(3-F-4-NO_2-PhO) and (TMTMP$^{+\bullet}$)Fe^{IV}O-(3-F-4-NO_2-PhO) were close to those of (TMP$^{+\bullet}$)Fe^{IV}O(Im) and (TMTMP$^{+\bullet}$)Fe^{IV}O(Im), respectively. Coordination of the phenolate axial ligand did not drastically change their electronic structure. Direct evidence for the phenolate binding to oxoiron(IV) porphyrin π-cation radical complexes was obtained from their ^{19}F NMR spectroscopy. ^{19}F NMR spectra of (TMP$^{+\bullet}$)Fe^{IV}O(3-F-4-NO_2-PhO) and (TMTMP$^{+\bullet}$)Fe^{IV}O-(3-F-4-NO_2-PhO) exhibited ^{19}F NMR signals of the 3-F signals in the axial 3-F-4-NO_2-PhO at 48.4 and 70.6 ppm from C_6F_6, respectively. Compared with the ^{19}F

NMR shifts of (TMP)Fe^{III}(3-F-4-NO_2-PhO) and (TMTMP)Fe^{III}(3-F-4-NO_2-PhO), the ^{19}F NMR signals of (TMP$^{+\bullet}$)Fe^{IV}O(3-F-4-NO_2-PhO) and (TMTMP$^{+\bullet}$)Fe^{IV}O-(3-F-4-NO_2-PhO) showed upfield and downfield shifts, respectively. The ^{19}F NMR signals for the 3-F signals of (TMP$^{+\bullet}$)Fe^{IV}O(3-F-4-NO_2-PhO) and (TMTMP$^{+\bullet}$)Fe^{IV}O-(3-F-4-NO_2-PhO) showed normal Curie law behavior and had intercepts at $1/T = 0$ near 55.8 and 42.0 ppm, respectively, which were close to that of 3-fluoro-4-nitrophenol (49.7 ppm).

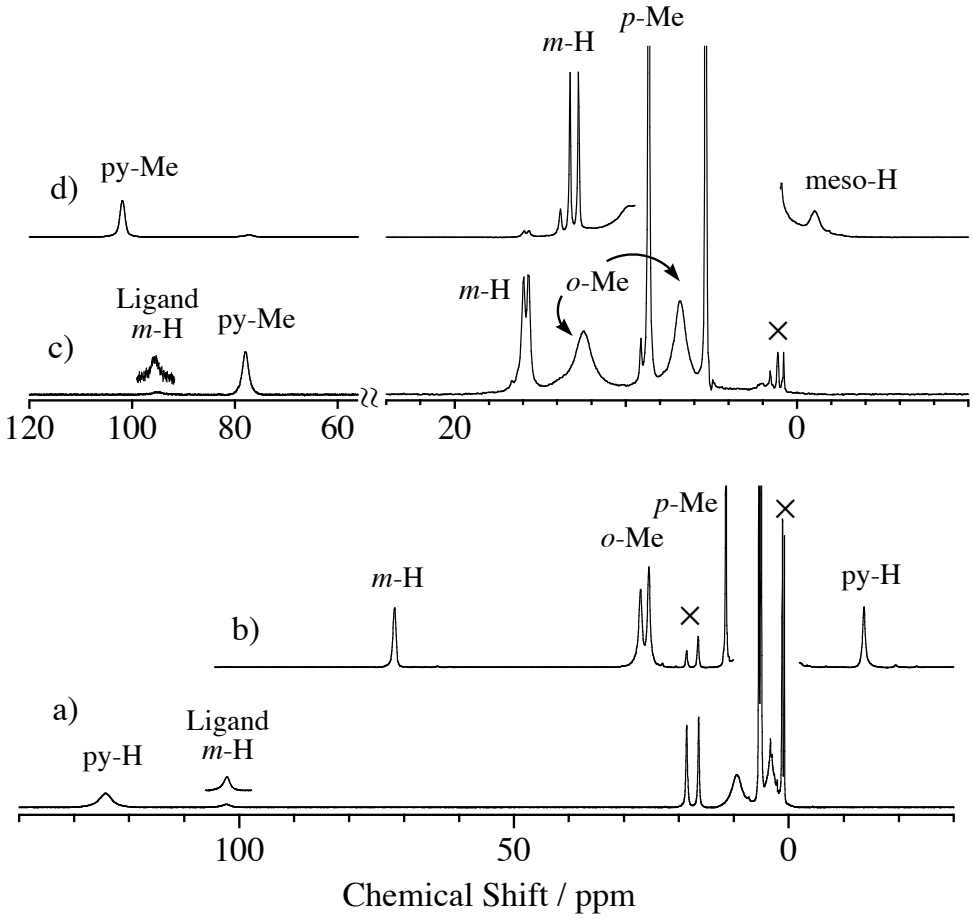

Figure 2.1.9. ^{1}H NMR spectra of iron porphyrin phenolate complexes in dichloromethane-d_2 at –80°C: a) (TMP)Fe^{III}(3-F-4-NO_2-PhO), b) (TMP$^{+\bullet}$)Fe^{IV}O-(3-F-4-NO_2-PhO), c) (TMTMP)Fe^{III}(3-F-4-NO_2-PhO), d) (TMTMP$^{+\bullet}$)Fe^{IV}O-(3-F-4-NO_2-PhO).

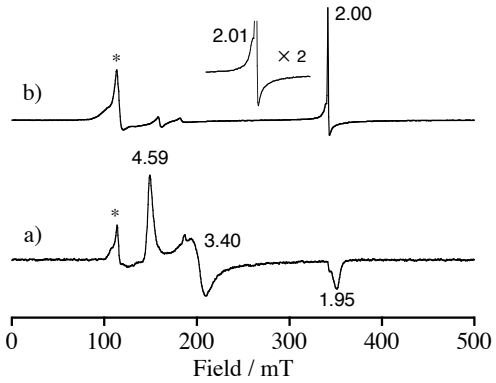

Figure 2.1.10. EPR spectra of a) $(TMP^{+\bullet})Fe^{IV}O$(3-F-4-NO_2-PhO) and b) $(TMTMP^{+\bullet})Fe^{IV}O$(3-F-4-$NO_2$-PhO) in dichloromethane-toluene (5:1) at 4 K. The signals denoted by asterisks exhibit signals for $(TMP)Fe^{III}$(3-F-4-NO_2-PhO) and $(TMTMP)Fe^{III}$(3-F-4-NO_2-PhO).

Figure 2.1.10 shows the EPR spectra of $(TMP^{+\bullet})Fe^{IV}O$(3-F-4-NO_2-PhO) and $(TMTMP^{+\bullet})Fe^{IV}O$(3-F-4-$NO_2$-PhO) in dichloromethane-toluene (5:1) at 4 K. The EPR spectrum of $(TMP^{+\bullet})Fe^{IV}O$(3-F-4-NO_2-PhO) was close to that of $[(TMP^{+\bullet})Fe^{IV}O$-(Im)$](ClO_4)$ and exhibited EPR signals at g = 4.59, 3.40, and 1.95, which were typical for S = 3/2 systems resulting from the ferromagnetic interaction, as observed for $[(TMP^{+\bullet})Fe^{IV}O(Im)]^+$. The *E/D* value (0.100) of $(TMP^{+\bullet})Fe^{IV}O$(3-F-4-NO_2-PhO) was larger than that (0.065) of $[(TMP^{+\bullet})Fe^{IV}O(Im)]^+$. On the other hand, the EPR spectrum of $(TMTMP^{+\bullet})Fe^{IV}O$(3-F-4-$NO_2$-PhO) was different from that of $[(TMTMP^{+\bullet})Fe^{IV}O(Im)]^+$ and exhibited an EPR signal at around g ~ 2.0. The EPR spectrum of $(TMTMP^{+\bullet})Fe^{IV}O$(3-F-4-$NO_2$-PhO) was close to that of compound I of *Pm*-CAT,[10] which was attributed to very weak magnetic interaction between iron(IV) and porphyrin radical spins. This indicates that the magnetic interaction between ferryl iron and the porphyrin π-radical became much weaker for TMTMP when the axial ligand was changed from imidazole to phenolate.

The structural characterization of ($TMP^{+\bullet}$)$Fe^{IV}O$(3-F-4-NO_2-PhO) and ($TMTMP^{+\bullet}$)-$Fe^{IV}O$(3-F-4-NO_2-PhO) was further examined using ESI-MS spectroscopy. However, ESI-MS spectrometry at low temperature did not give any ion peaks corresponding to ($TMP^{+\bullet}$)$Fe^{IV}O$(3-F-4-NO_2-PhO) and ($TMTMP^{+\bullet}$)$Fe^{IV}O$(3-F-4-NO_2-PhO) because of their neutral character.

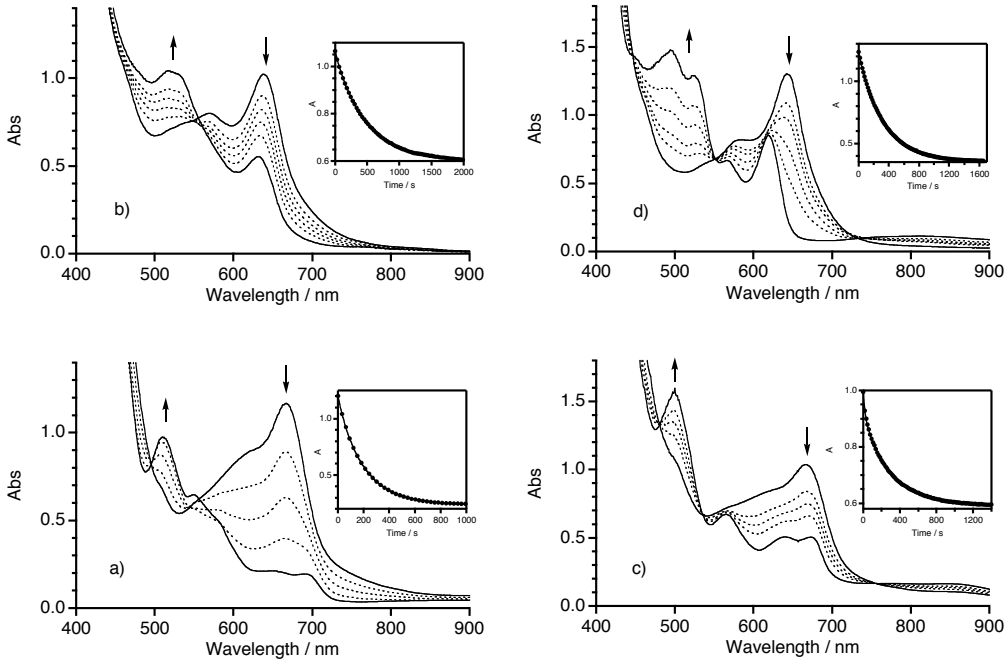

Figure 2.1.11. UV-visible absorption spectral change for the reactions of a) [($TMP^{+\bullet}$)$Fe^{IV}O$(Im)](NO_3), b) [($TMTMP^{+\bullet}$)$Fe^{IV}O$(Im)](NO_3), c) ($TMP^{+\bullet}$)$Fe^{IV}O$-(3-F-4-NO_2-PhO) and d) ($TMTMP^{+\bullet}$)$Fe^{IV}O$(3-F-4-NO_2-PhO) with cyclooctene (2.5×10^{-2} M) in dichloromethane at –80°C. Sample concentration = 1.0×10^{-4} M in 1cm path length cell. Insets; time dependence of the absorptions at (a) 667 nm, (b) 639 nm, (c) 667 nm and (d) 643 nm.

Reactivity of Compound I Models. To study the effect of axial ligands on reactivity, we examined reactions of oxoiron(IV) porphyrin π-cation radical complexes having various axial ligands with cyclooctene. Figure 2.1.11 a) and b) shows the absorption spectral changes for the epoxidation reactions of [($TMP^{+\bullet}$)$Fe^{IV}O$(Im)](NO_3)

and [(TMTMP$^{+\bullet}$)Fe^{IV}O(Im)](NO$_3$) with cyclohexene at –80 ˚C, respectively. Upon the addition of cyclooctene, the absorption spectra of [(TMP$^{+\bullet}$)Fe^{IV}O(Im)](NO$_3$) and [(TMTMP$^{+\bullet}$)Fe^{IV}O(Im)](NO$_3$) changed to those of (TMP)Fe^{III}(NO$_3$) and (TMTMP)Fe^{III}(NO$_3$) containing 1.0 equiv of imidazole, respectively. ^{1}H NMR measurements of the final reaction solutions clearly showed that the final product was a 1:1 mixture of nitrate and bis-imidazole iron(III) porphyrin complexes. The absorption spectral changes for the reactions showed a slight shift in isosbestic points because the reaction product changed from the mono-imidazole complex to a mixture of nitrate and bis-imidazole complexes, as the reaction product increased (Scheme 2.1.2). Similar absorption spectral changes were observed for cyclooctene epoxidation reactions when 2-methylimidazole and 5-methylimidazole were used as axial ligands. In spite of a slight shift in the isosbestic points, the time courses of the absorptions for the epoxidation reactions in the presence of large excess of cyclooctene could be fitted well with a single exponential function.[33] The apparent rate constants linearly depend on the concentration of cyclooctene, giving the second-order rate constants for cyclooctene epoxidation reactions (Table 2.1.7). To confirm the formation of the epoxidation product, GC-MS analysis was applied to each reaction solution used in these kinetic experiments, which showed the formation of cyclooctene oxide in more than 80% yield (see Table 2.1.7).

Scheme 2.1.2

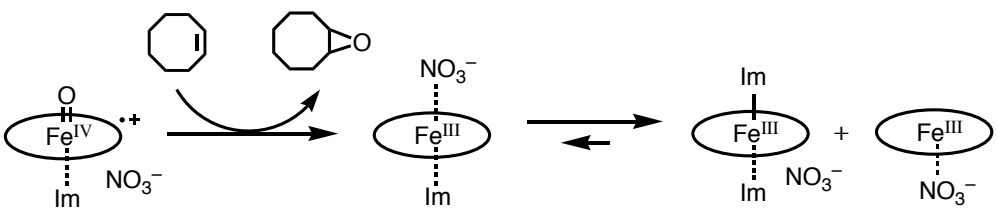

We further examined the reactions of oxoiron(IV) porphyrin π-cation radical complexes with 3-fluoro4-nitrophenolate as an axial ligand. Figure 2.1.11 c) and d) show absorption spectral changes for the reactions of $(TMP^{+\bullet})Fe^{IV}O(3\text{-F-4-}NO_2\text{-PhO})$ and $(TMTMP^{+\bullet})Fe^{IV}O(3\text{-F-4-}NO_2\text{-PhO})$, respectively, with cyclooctene at 193 K. Upon the addition of cyclooctene, the absorption spectra of $(TMP^{+\bullet})Fe^{IV}O(3\text{-F-4-}NO_2\text{-PhO})$ and $(TMTMP^{+\bullet})Fe^{IV}O(3\text{-F-4-}NO_2\text{-PhO})$ changed to those of $(TMP)Fe^{III}(3\text{-F-4-}NO_2\text{-PhO})$ and $(TMTMP)Fe^{III}(3\text{-F-4-}NO_2\text{-PhO})$ with clear isosbestic points. The formation of $(TMP)Fe^{III}(3\text{-F-4-}NO_2\text{-PhO})$ and $(TMTMP)Fe^{III}(3\text{-F-4-}NO_2\text{-PhO})$ was further confirmed by ^1H NMR measurements. Kinetic analysis showed the second-order rate constants at 0.126 $M^{-1}s^{-1}$ and 0.134 $M^{-1}s^{-1}$ for the cyclooctene epoxidation with $(TMP^{+\bullet})Fe^{IV}O(3\text{-F-4-}NO_2\text{-PhO})$ and $(TMTMP^{+\bullet})Fe^{IV}O(3\text{-F-4-}NO_2\text{-PhO})$, respectively. Analysis of the product using GC-MS showed that only cyclooctene oxide was detected, in 32 and 80 % yield for $(TMP^{+\bullet})Fe^{IV}O(3\text{-F-4-}NO_2\text{-PhO})$ and $(TMTMP^{+\bullet})Fe^{IV}O(3\text{-F-4-}NO_2\text{-PhO})$, respectively. The low yield of cyclooctene oxide for $(TMP^{+\bullet})Fe^{IV}O(3\text{-F-4-}NO_2\text{-PhO})$ may be due to its instability, as described in the section above.

The reaction rates of oxoiron(IV) porphyrin π-cation radical complexes with nitrate and chloride axial anions were also determined at 193 K. The second-order rate constants and the yields of cyclooctene oxide are summarized in Table 2.1.7. The reaction of $(TMTMP^{+\bullet})Fe^{IV}O(Cl)$ could not be examined because the ozone oxidation of $(TMTMP)Fe^{III}Cl$ at –80˚C did not form $(TMTMP^{+\bullet})Fe^{IV}O(Cl)$. The reaction rate constants and reaction yields for imidazole and phenolate complexes were much larger than those for nitrate and chloride. In the most extreme case, the reaction rate was ~400 times larger with the coordination of 2-mehtylimidazole to $(TMTMP^{+\bullet})Fe^{IV}O(NO_3)$.

To study the axial ligand effect on oxidation reactions other than epoxidation, we examined the reactions of oxoiron(IV) porphyrin π-cation radical complexes with *N*,*N*-dimethyl-*p*-nitroaniline and 1,4-cyclohexadiene (Table 2.1.7). Previous studies reported that oxoiron(IV) porphyrin π-cation radical complexes oxidize *N*,*N*-dimethyl-*p*-nitroaniline to *N*-methyl-*p*-nitroaniline via an electron transfer mechanism and 1,4-cyclohexadiene to benzene via a hydrogen abstraction mechanism.[34,35] The second-order rate constants of $[(TMTMP^{+\bullet})Fe^{IV}O(Im)](NO_3)$ and $(TMTMP^{+\bullet})Fe^{IV}O(3\text{-F-4-}NO_2\text{-PhO})$ for *N*,*N*-dimethyl-*p*-nitroaniline were 70 times higher than that of $(TMTMP^{+\bullet})Fe^{IV}O(NO_3)$, and those for 1,4-dihydrocyclohexadiene were 10 times higher. Coordination of imidazole and phenolate axial ligands enhanced the reactivity of oxoiron(IV) porphyrin π-cation radical complex not only for the epoxidation reaction, but also for the aniline *N*-demethylation and hydrogen abstraction reactions.

Regarding the catalase reactions, we examined the reactions of $(TMTMP^{+\bullet})Fe^{IV}O(NO_3)$, $[(TMTMP^{+\bullet})Fe^{IV}O(Im)](NO_3)$, and $(TMTMP^{+\bullet})Fe^{IV}O$-$(3\text{-F-4-}NO_2\text{-PhO})$ with hydrogen peroxide in dichloromethane at –80 °C. Whereas $(TMTMP^{+\bullet})Fe^{IV}O(NO_3)$ reacted in a few minutes with the addition of 10 equiv of hydrogen peroxide in methanol (k_{app} = 2.0 × 10^{-2} s^{-1} for 1 mM hydrogen peroxide), $[(TMTMP^{+\bullet})Fe^{IV}O(Im)](NO_3)$, and $(TMTMP^{+\bullet})Fe^{IV}O(3\text{-F-4-}NO_2\text{-PhO})$ reacted immediately to form iron(III) porphyrin complexes. Because these reactions occurred so rapidly, the reaction rate constants could not be determined. While a drastic axial ligand effect was found for the hydrogen peroxide oxidation, predominance of the phenolate axial ligand over the imidazole axial ligand was not observed.

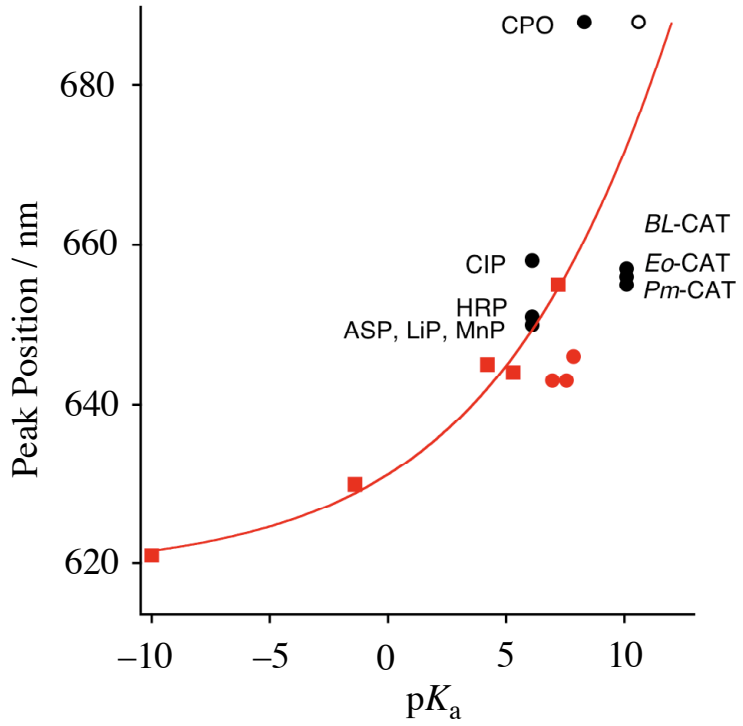

Figure 2.1.12. Correlation of pK_a value of the axial ligand (L) of (TMTMP$^{+\bullet}$)-Fe^{IV}O(L) with its absorption peak position. Red square; anion liagnd, L from left; ClO_4^-, NO_3^-, benzoate, 3-F-4-NO_2-PhO^-, 4-NO_2-PhO^-, red circle; neutral ligand, L from left; Im, 5-MeIm, 2-MeIm. The solid red line was a correlation curve based on the anion ligands (red square). Black circle; compound-I of heme enzymes listed in Table 1. The pK_a values for peroxidases other than CPO, catalases, and CPO are used those for histidine (6.1), tyrosine (10.1), and cysteine (8.3) residues, respectively.[36] Circle; CPO compound-I for the pK_a (10.6) of ethanethiol.[36]

Discussion

Effect of Axial Ligand on Electronic Structure. All oxoiron(IV) porphyrin π-cation radical complexes characterized in this study showed the Soret band with decreased intensity around 400 nm and a characteristic absorption around 650 nm. The peak positions for TMP complexes were hardly changed by the axial ligand effect; however, those for TMTMP complexes were sensitive to the axial ligand effect (Table 2.1.1). In particular, the absorption peak at around 650 nm for TMTMP complexes

showed ~ 35 nm shift due to the axial ligand. It is worth noting that the peak position of $(TMTMP^{+\bullet})Fe^{IV}O(L)$ shifted to lower energy as the pK_a value of the axial ligand (L) increased (Figure 2.1.12).[36] The axial anion ligands showed a good correlation line, while the axial neutral ligands, L = Im, 2-MeIm, 5-MeIm, exhibited slight shifts from the correlation line for the axial anion ligands. The absorption peak at around 650 nm may be a good marker for estimation of the electron donor ability of the axial ligand. Because of the structural similarity of protoporphyrin IX with TMTMP, a similar correlation was also observed for peak positions of compound I of peroxidases and catalases (Table 2.1.1 and 2.1.2). The peak positions of the compound I of peroxidases and catalases also shifted from 650 to 688 nm, and were correlated with the pK_a values of the proximal ligands (Figure 2.1.12). Although other factors, such as the steric and electrostatic environment around heme must be considered, the peak position observed for compound I can be explained by the donor effect of the proximal ligand in these heme enzymes. For peroxidases other than CPO, the observed peak positions (650 ~ 658 nm) were close to the correlation line and were reasonable for the character of the imidazolate anion, resulting from hydrogen bonding interactions of the proximal histidines with the aspartate residues (see Figure 2.1.1). The peak positions (655 ~ 657 nm) for catalases can be explained by hydrogen bonding between the proximal tyrosine ligand (phenolate) and a nearby arginine residue, which shifted the phenolate character of the proximal ligand to a phenol and weakens the electron donor effect of the proximal tyrosine ligand. The absorption peak (688 nm) for CPO compound I indicates extremely strong electron donor effect of the proximal cysteine ligand. The donor effect was much stronger than that expected from the pK_a value (8.3) of cysteine, but comparable to that expected from alkylthiol (pK_a 10 ~ 11).[36]

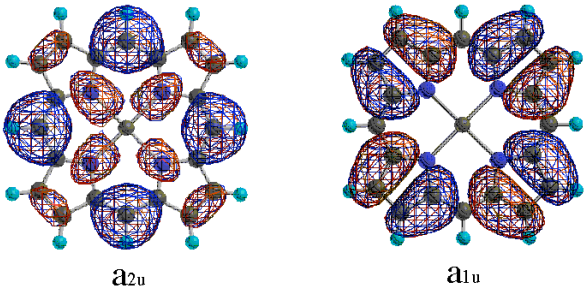

Figure 2.1.13. Electron spin density distribution of the a_{2u} and a_{1u} porphyrin π-cation radical orbitals. Red and blue colors represent signs of wave functions.

Previously, we showed that the porphyrin π-cation radical (a_{1u} or a_{2u}) state depends on the porphyrin substitution pattern (Figure 2.1.13).[29a] Meso-substituted porphyrins, such as TMP, form the a_{2u} radical state, which shifts to the a_{1u} state with an increase in the electron-withdrawing effect of the meso-substituent. Pyrrole β-substituted porphyrins, like TMTMP, form the a_{1u} radical state, which is not changed even with an increase in the electron-withdrawing effect of the pyrrole β-substituent. On the other hand, the present ^{1}H NMR results clearly show that the axial ligand effect does not change the porphyrin π-cation radical state. Even if the electron donating axial ligand, such as imidazole and phenolate, were coordinated to the ferryl iron, TMTMP and TMP complexes remained in the a_{1u} and a_{2u} radical states, respectively. These results indicate that compound I in all peroxidases and catalases with pyrrole β-substituted porphyrin, like protoporphyrin IX, would be in the a_{1u} radical state, because one-electron oxidation of protoporphyrin IX usually yields the a_{1u} radical state.

The paramagnetic shifts of the iron-bound axial ligands allow the estimation of spin transfer from ferryl iron and porphyrin π-cation radical spins to the iron-bound oxo and axial ligand. The radical character of the oxo ligand has been discussed in relation

to the oxygenation reactivity of oxoiron(IV) porphyrin π-cation radical complex,[37] but the spin transfer from the porphyrin π-cation radical to the axial ligand has not been studied in detail. As summarized in Figure 2.1.6 and Table 2.1.5, the iron-bound imidazole signals showed paramagnetic shifts, induced by ferryl iron and porphyrin π-cation radical spins. We assume here that the dipolar contribution of oxoiron(IV) porphyrin π-cation radical complex is close to that of oxoiron(IV) porphyrin complex.[38] As previously analyzed for oxoiron(IV) porphyrin complexes, two unpaired electrons in the ferryl iron d_π (d_{xz} and d_{yz}) orbitals delocalize into the imidazole π-orbital (the highest occupied π-molecular orbital), leading to up-field shifts of all protons belonging to the iron-bound imidazoles.[38] On the other hand, porphyrin π-cation radical spin would be transferred to the axial imidazole s-orbital via the unoccupied ferryl iron d_{z^2} orbital, resulting in downfield shifts of the imidazole signals, especially the imidazole 1-H and 5-H signals, as observed for high spin iron(III) porphyrin complexes (see Table 2.1.5).[39] Therefore, the up-field shifts of the imidazole 2-H and 4-H signals for oxoiron(IV) porphyrin π-cation radical complexes were mainly induced by the spin delocalization of the ferryl iron d_π spins. This result was further confirmed by the large downfield shifts with the 2-methyl substitutions. Compared with the NMR shifts of the iron-bound imidazole signals of oxoiron(IV) porphyrin complexes, the upfield shifts of the imidazole 2-H and 4-H signals for TMTMP complexes become smaller with the formation of porphyrin π-cation radicals, while those for TMP complexes hardly change. Since the NMR shifts of the iron-bound imidazole signals of oxoiron(IV) TMP complexes were similar to those of TMTMP complexes (Table 2.1.5), the observed change suggests that spin transfer of the ferryl iron spins to the axial ligands is weakened with the formation of the a_{1u} radical complex (TMTMP), but unchanged with the formation of the a_{2u} radical complex (TMP). On the other hand, with the formation

of the porphyrin π-cation radical, the imidazole 5-H(D) signals showed large downfield shifts for the TMP complexes, but small shifts for the TMTMP complexes. Large downfield shifts of the 5-H(D) signals for TMP complexes indicate effective spin transfer from the a_{2u} porphyrin radical, but the small shifts for TMTMP complexes indicate ineffective transfer from the a_{1u} porphyrin radical. Overall, the ferryl iron and porphyrin π-cation radical spins were effectively transferred to the axial imidazole for the a_{2u} radical complex, but not for the a_{1u} radical complex. This is consistent with a previous EPR study of zinc(II) porphyrin π-cation radical complexes.[40] With molecular vibration of the propyhrin plane, e.g. doming, the a_{2u} orbital is allowed to overlap with the ferryl iron d_{z^2} orbital, but the a_{1u} orbital is not. Moreover, the π-spin density of the pyrrole nitrogen is large in the a_{2u} orbital, but not in the a_{1u} orbital (see Figure 2.1.13). These differences should result in differing spin transfer between the a_{1u} and a_{2u} complexes. This argument is applicable to the axial oxo ligand of oxoiron(IV) porphyrin π-cation radical complex, suggesting different spin density on the oxo ligand in the a_{1u} and a_{2u} radical complexes.

The effect of the axial ligand on spin interaction between the ferryl iron and porphyrin π-cation radical spins of oxoiron(IV) porphyrin π-cation radical complex is manifested in its EPR spectrum. The difference in spin interaction between the TMP and TMTMP complexes might result from differences in both the π-spin density on the pyrrole nitrogen atom between the a_{2u} and a_{1u} radical states (see Figure 2.1.13), and the flexibility of the porphyrin plane of TMTMP due to less steric hindrance than in TMP. The EPR spectra of compound I in heme enzymes more closely resemble those of TMTMP complexes, confirming the a_{1u} radical state. The similarity of the EPR spectra of the compound I of heme enzymes with those of model complexes with similar axial ligands suggests that the axial ligand effect is an important determinant of the

intramolecular spin interaction of the compound I, as well as the steric effect of amino acid residues around the heme.

Effect of the Axial Ligand on Reactivity. Previously, the axial ligand effect on styrene oxidation was studied using $(TMP^{+\bullet})Fe^{IV}O(X)$, where X is either chloride, fluoride, acetate, methanol, or trifluoromethylsulfonate.[18] The second-order rate constant for the styrene oxidation was increased about 15 times when the axial ligand was changed from the least reactive trifluoromethylsulfonate to the most reactive fluoride. In this study, we also found similar increments when the axial ligand was changed from nitrate to chloride (~15-fold). More importantly, this study showed a significant effect of axial ligands of imidazole and phenolate derivatives on the reactivity of oxoiron(IV) porphyrin π-cation radical complex. As clearly shown in Figure 2.1.14, the effect of the axial imidazole and phenolate was much more prominent than that of the axial chloride. For the 3-fluoro-4-nitrophenolate axial ligand, the second-order rate constants for the TMP and TMTMP complexes were comparable. However, for the imidazole and 5-methylimidazole axial ligands, the second-order rate constants for the TMP complexes were about twice those of the TMTMP complexes. For the 2-methylimidazole axial ligand, the TMTMP complex was much more reactive than the TMP complex. The low reactivity of $(TMP^{+\bullet})Fe^{IV}O$(2-MeIm) may be due to steric interaction between the methyl groups of TMP and 2-methylimidazole, which was detected in its ^{1}H NMR spectra. As reported for 1,2-dimethylimidazole complexes of ferric TMP,[41] the steric interaction might induce ruffling of the porphyrin plane of $(TMP^{+\bullet})Fe^{IV}O$(2-MeIm), leading to a drastic decrease in epoxidation reactivity.

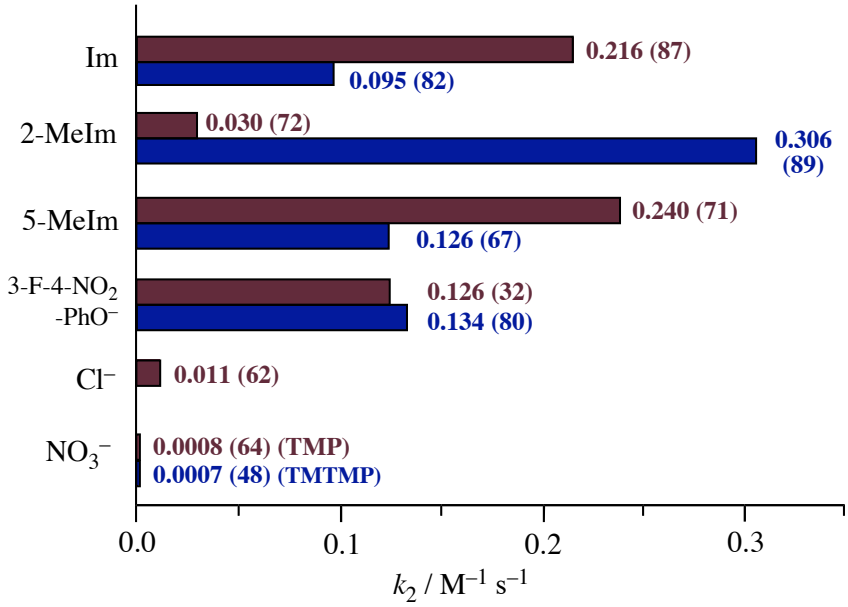

Figure 2.1.14. Comparison of second-order rate constants for the cyclooctene epoxidation of oxoiron(IV) TMP (brown bar) and TMTMP (blue bar) π-cation radical complexes with various axial ligands. The numbers in parentheses are yields of cyclooctene oxide.

A drastic axial ligand effect of imidazole and phenolate derivatives was also found in the reactions with 1,4-cyclohexadiene, *N*,*N*-dimethyl-*p*-nitroaniline, and hydrogen peroxide. However, the axial ligand effect (~10-fold) for 1,4-cyclohexadiene is not so significant than those (~100-fold) for *N*,*N*-dimethyl-*p*-nitroaniline and cyclooctene (Table 2.1.7). Although we attempted to correlate these reactivities with the present spectroscopic results of oxiron(IV) porphyrin π-cation radical complexes, we could not find any clear correlation. Therefore, the explanation for the dramatic axial ligand effect on the reactivity must be effects other than the electronic state of the oxiron(IV) porphyrin π-cation radical complex. For example, differences in the reaction mechanism, such as hydrogen abstraction and electron transfer, would form different

transition states, which might result in different axial ligand effects. The axial ligand effect on oxoiron(IV) porphyrin π-cation radical complex would be different from that on iron(III) porphyrin complex as a reaction product. Moreover, the thermodynamic parameters for substrate oxidation must also be considered. For example, the change in an enthalpy (ΔH) for conversion of 1,4-cyclohexadine to benzene and water is ~ –260 kJ/mol, while that of cyclohexene to cyclohexene oxide is ~ –120 kJ/mol.[42] The large enthalpy contribution from the substrate oxidation would weaken the enthalpy contribution from the axial ligand effect.

Conclusion

Previously, the axial ligand effect of imidazole and phenolate has been reported in catalytic oxygenation reactions with iron and manganese porphyrin complexes.[12-17] Previously, Watanabe et al. studied the axial ligand effect on the former process, in which the coordination of the axial imidazole ligand increased the rate of the O-O bond cleavage of iron bound *m*-chloroperbenzoate and the rate correlated with the donor effect of the axial imidazole ligand.[5] On the other hand, this study clearly showed that the axial imidazole and phenolate ligands drastically increased the reaction rates of oxoiron(IV) porphyrin π-cation radical complexes with substrates. In the catalytic system, the axial ligand works to accelerate not only the formation of the high-valent oxo complex, but also the oxo-transfer to substrate.

References

(1) Dunford, H. B. *Heme Peroxidases*, Wiley-VCH: New York, 1999.

(2) Schonbaum, G. R.; Chance, B. In *The Enzymes*; Boyer, P. D., Ed.; Academic Press: New York, 1976; Vol. 13, pp 363-408.

(3) (a) Watanabe, Y.; Groves, J. T. In *The Enzymes*; Sigman, D. S., Ed.; Academic Press: New York, 1992; Vol. 20, pp 405-452. (b) Oritz de Montellano, P. R. *Cytochrome P450. Structure, Mechanism, and Biochemistry*, 2nd ed.; Plenum Publishing Corporation: New York, 1995.

(4) (a) Smulevich, G.; Mauro, J. M.; Fishel, L. A.; English, A. M.; Kraut, J.; Spiro, T. G. *Biochemistry* **1988**, *27*, 5477-5485. (b) Goodin, D. B.; McRee, D. E. *Biochemistry* **1993**, *32*, 3313-3324.

(5) Yamaguchi, K.; Watanabe, Y.; Morishima, I. *J. Am. Chem. Soc.* **1993**, *115*, 4058-4065.

(6) Schluz, C. E.; Rutter, R.; Sage, J. T.; Debrunner, P. G.; Hager, L. P. *Biochemistry* **1984**, *23*, 4743-4754.

(7) (a) Rutter, R.; Hager, L. P. *J. Biol. Chem.* **1982**, *257*, 7958-7961. (b) Rutter, R.; Hager, L. P.; Dhonau, H.; Hendrich, M.; Valentine, M.; Debrunner, P. *Biochemistry* **1984**, *23*, 6809-6816.

(8) Benecky, M. J.; Frew, J. E. Scowen, N.; Jones, P.; Hoffman, B. M. *Biochemsitry* **1993**, *32*, 11929-11933.

(9) Patterson, W.; Polous, T. L.; Goodin, D. B. *Biochemistry* **1995**, *34*, 4342-4345.

(10) Ivancich, A.; Jouve, H. M.; Sartor, B.; Gaillard, J. *Biochemistry* **1997**, 36, 9356-9364.

(11) Khindaria, A.; Aust, S. *Biochemistry* **1996**, 35, 13107-13111.

(12) Traylor, T. G.; Lee, W. A.; Stynes, D. V. *J. Am. Chem. Soc.* **1984**, *106*, 755-764.

(13) (a) Dicken, C. M.; Woon, T. C.; Bruice, T. C. *J. Am. Chem. Soc.* **1986**, *108*, 1636-1643. (b) Beck, M. J.; Gopinath, E.; Bruice, T. C. *J. Am. Chem. Soc.* **1993**, *115*, 21-29.

(14) Battioni, P.; Renaud, J. P.; Bartoli, J. F.; Reina-Artiles, M.; Fort, M.; Mansuy, D. *J. Am. Chem. Soc.* **1988**, *110*, 8462-8470.

(15) Robert, A.; Loock, B.; Momenteau, M.; Meunier, B. *Inorg. Chem.* **1991**, *30*, 706-711.

(16) (a) Higuchi, T.; Uzu, S.; Hirobe, M. *J. Am. Chem. Soc.* **1990**, *112*, 7051-7052. (b) Suzuki, N.; Higuchi, T.; Urano, Y.; Kikuchi, K.; Uekusa, H. Ohashi, Y.; Uchida, T.; Kitagawa, T.; Nagano, T. *J. Am. Chem. Soc.* **1999**, *121*, 11571-11572. (c) Urano, Y.; Higuchi, T.; Hirobe, M.; Nagano, T. *J. Am. Chem. Soc.* **1997**, *119*, 12008-12009.

(17) Ohno, T.; Suzuki, N.; Dokoh, T.; Urano, Y.; Kikuchi, K.; Hirobe, M.; Higuchi, T.; Nagano, T. *J. Inorg. Biochem.* **2000**, *82*, 123-125.

(18) a) Gross, Z.; Nimri, S. *Inorg. Chem.* **1994**, *33*, 1731-1732. (b) Gross, Z.; Nimri, S.; Barzilay, C. M.; Simkhovich, L. *J. Biol. Inorg. Chem.* **1997**, *2*, 492-506.

(19) Song, W. J.; Ryu, Y. O.; Song, R.; Nam, W. *J. Biol. Inorg. Chem.* **2005**, *10*, 294-304.

(20) (a) Kuramochi, H.; Noodleman, L.; Case, D. A. *J. Am. Chem. Soc.* **1997**, *119*, 11442-11451. (b) de Visser, S. P.; Ogliaro, F.; Sharma, P. K.; Shaik, S. *Angew. Chem. Int. Ed.* **2002**, *41*, 1947-1951. (c) Kamachi, T.; Kouno, T.; Nam, W.; Yoshizawa, K. *J. Inorg. Biochem.* **2006**, *101*, 1464-1472. (d) Wang, R.; de Visser, S. P. *J. Inorg. Biochem.* **2007**, *101*, 1464-1472.

(21) Fujii, H.; Yoshimura, T.; Kamada, H. *Inorg. Chem.* **1997**, *36*, 6142-6143.

(22) Czarnecki, K.; Kincaid, J. R.; Fujii, H. *J. Am. Chem. Soc.* **1999**, *121*, 7953-7954.

(23) Dunford, H. B. *Adv. Inorg. Biochem.* **1982**, *4*, 41-68.

(24) Lad, L.; Mewies, M.; Raven, E. L. *Biochemistry* **2002**, *41*, 13774-13781.

(25) Renganathan, V.; Gold, M. H. *Biochemistry* **1986**, *25*, 1626-1631.

(26) Wariishi, H.; Akileswaran, L.; Gold, M. H. *Biochemistry* **1988**, *27*, 5365-5370.

(27) Anderson, M. B.; Hsuanyu, K.; Welinder, K. G.; Scheider, P.; Dunford, H. P. *Acta. Chem. Scand.* **1991**, *45*, 1080-1086.

(28) Palcic, M. M.; Rutter, R.; Araiso, T.; Hager, L. P.; Dunford, H. B. *Biochem. Biophys. Res. Commun.* **1980**, *94*, 1123-1127.

(29) (a) Fujii, H. *J. Am. Chem. Soc.* **1993**, *115*, 4641-4648. (b) Fujii, H.; Ichikawa, K. *Inorg. Chem.* **1992**, *31*, 1110-1112.

(30) Fujii, H.; Yoshimura, T.; Kamada, H. *Inorg. Chem.* **1996**, *35*, 2373-2377.

(31) Browett, W. R.; Stillman, M. J. *Biochica. Biophys. Acta* **1980**, *623*, 21-31.

(32) Hara, I.; Ichise, N.; Kojima, K.; Kondo, H.; Ohgiya, S.; Matsuyama, H.; Yumoto, I. *Biochemistry* **2007**, *46*, 11-22.

(33) Time course of the absorptions for $[(TMP^{+\bullet})Fe^{IV}O(5\text{-MeIm})](NO_3)$ could not fit well with a single exponential function, but with a bi-exponential function, suggesting some sequential reaction. The rate constant for the first reaction was assigned as that for $[(TMP^{+\bullet})Fe^{IV}O(5\text{-MeIm})](NO_3)$ with cyclooctene.

(34) (a) Goto, Y.; Watamabe, Y.; Fukuzumi, S.; Jones, J. P.; Dinnocenzo, J. P. *J. Am. Chem. Soc.* **1998**, *120*, 10762-10763. (b) Chiavarino, B.; Cipollini, R.; Crestonei, M. E.; Fornarini, S.; Lanucara, F.; Lapi, A. *J. Am. Chem. Soc.* **2008**, *130*, 3208-3217.

(35) Jeong, Y. J.; Kang, Y.; Han, A.-R.; Lee, Y.-M.; Kotani, H.; Fukuzumi, S.; Nam, W. *Angew. Chem. Int. Ed.* **2008**, *47*, 7321-7324.

(36) (a) Albert, A. In *Physical Methods in Hetrocyclic Chemistry*; Katritzky, A. R.,

Ed.; Academic Press: New York, 1971; Vol. III, pp 1-108. (b) Pine, S. H.; Hendrickson, J. B.; Vram, D. J.; Hammond, G. S. In *Organic Chemistry* 4th Edition; MaGRAW-HILL: Auckland, 1981, Chapter 6, 196-239. (c) Albert, A.; Serjeant, E. P. In *The Determination of Ionization Constants* 3th Edition; Chapman and Hall: Lonadon, 1962, Chapter 9, pp 136-175. (d) Chapman, E.; Bryan, M. C.; Wong, C.-H. *Proc. Natl. Acad. Sci. U.S.A.* **2003**, *100*, 910-915.

(37) (a) Groves, J. T.; Nemo, T. E. *J. Am. Chem. Soc.* **1983**, *105*, 6243-6248. (b) Champion, P. M. *J. Am. Chem. Soc.* **1989**, *111*, 3434-3436. (c) Bernadou, J.; Fabiano, A.-S.; Robert, A.; Meunier, B. *J. Am. Chem. Soc.* **1994**, *116*, 9375-9376.

(38) Balch, A. L.; La Mar, G. N.; Latos-Grazynski, L.; Renner, M. W.; Thanabal, V. *J. Am. Chem. Soc.* **1985**, *107*, 3003-3007.

(39) Cheng, R.-J.; Chen, P.-Y.; Lovell, T.; Liu, T.; Noodleman, L.; Case, D. A. *J. Am. Chem. Soc.* **2003**, *125*, 6774-6783.

(40) Fujita, I.; Hanson, L. K.; Walker, F. A.; Fajer, J. *J. Am. Chem. Soc.* **1983**, *105*, 3296-3300.

(41) Munro, O. Q.; Marques, H. M.; Debrunner, P. G.; Mohanrao, K.; Scheidt, W. R. *J. Am. Chem. Soc.* **1995**, *117*, 935-954.

(42) (a) Pedley, J. B.; Naylor, R. D.; Kirby, S. P. "*Therochemical Data of Organic Compounds*", Chapman and Hall: London, 1986. (b) Stull, D. R.; Westrum, E. F.; Sinke, G. C. "*The Chemical Thermodynamics of Organic Compounds*", Jone Wiley: New York, 1969. (c) Nagano, H. In *Kagaku-Binran* 5th Edition; Atake, T.; Sorai, M.; Matsuo, T. Eds.; Maruzen: Tokyo, Vol. II, pp 301-313.

(43) Hardacre, C.; Holbrey, J. D.; McMath, S. E. J. *Chem. Commum.* **2001**, 367-368.

(44) (a) Lindsey, J.; Wagner, R. *J. Org. Chem.* **1989**, *54*, 828-836. (b) Ono, N.; Kawamura, H.; Bougauchi, M.; Maruyama, K. *Tetrahedron* **1990**, *46*, 7483-7496.

(45) Groves, J. T.; Gross, Z.; Stern, M. K. *Inorg. Chem.* **1994**, *33*, 5065-5072.

(46) Reed, C. A.; Mashiko, T.; Bentley, S. P.; Kastner, M. E.; Scheidt, W. R.; Spartalian, K.; Lang, G. *J. Am. Chem. Soc.* **1979**, *101*, 2948-2958.

(47) Phillippi, M. A.; Baenziger, N.; Goff, H. M. *Inorg. Chem.* **1981**, *20*, 3904-3911.

(48) (a) Tang, S. C.; Koch, S.; Papaefthymiou, G. C.; Foner, S.; Frankel, R. B.; Ibers, J. A.; Holm, R. H. *J. Am. Chem. Soc.* **1976**, *98*, 2414-2434. (b) Ainscough, E. W.; Addison, A. W.; Dolphin, D.; James, B. R. *J. Am. Chem. Soc.* **1978**, *100*, 7585-7591.

(49) (a) Quinn, R.; Nappa, M.; Valentine, J. S. *J. Am. Chem. Soc.* **1982**, *104*, 2588-2595. (b) Scheidt, W. R.; Geiger, D. K.; Lee, Y. J.; Reed, C. A.; Lang, G. *J. Am. Chem. Soc.* **1985**, *107*, 5693-5699.

Table 2.1.1. UV-visible Spectral Data of $[(P^{+\bullet})Fe^{IV}O(L)]X$, in CH_2Cl_2 at –80°C.

Porphyrin	L	X	λ / nm	ref
TMP	ClO_4^-		403, 660	
	NO_3^-		401, 666	
	Im	ClO_4^-, NO_3^-	403, 667	
	2-MeIm	ClO_4^-, NO_3^-	403, 667	
	5-MeIm	ClO_4^-, NO_3^-	404, 667	
	3-F-4-NO_2-PhO		406, 666	
TMTMP	ClO_4^-		387, 621	
	NO_3^-		391, 630	
	$C_6H_5CO_2^-$		396, 645	
	Im	ClO_4^-, NO_3^-	394, 643	
	2-MeIm	ClO_4^-, NO_3^-	389, 646	
	5-MeIm	ClO_4^-, NO_3^-	394, 643	
	3-F-4-NO_2-PhO		388, 644	
	4-NO_2-PhO		392, 655	21

Table 2.1.2. UV-vis and EPR data for compound I of peroxidases and catalases.

Enzyme	Axial ligand	λ / nm	EPR	ref
HRP	His	400, 651	~ 2	6, 23
ASP	His	404, 650	3.27, 1.99	9, 24
LiP	His	408, 650	3.42, 2.00	11, 25
MnP	His	406, 650		26
CIP	His	402, 658		27
CPO	Cys	367, 688	2.00, 1.73, 1.64	7, 28
BL-CAT	Tyr	400, 656	1.96 (1.98)	10, 31
Eo-CAT	Tyr	402, 657		32
Pm-CAT	Tyr	655	~ 2	10
Ml-CAT	Tyr		3.32, ~ 2	8

Table 2.1.5. NMR Chemical Shifts (ppm) of iron-bound imidazole signals of iron porphyrin complexes in dichloromethane.

Complex	2-H(D)	4-H(D)	5-H(D)	*T* / °C	ref
$(TMP^{+\bullet})Fe^{IV}O(Im\text{-}d_4)$ [a]	–30.2	–17.4	19.1	–80	
$(TMP^{+\bullet})Fe^{IV}O(2\text{-}MeIm\text{-}d_6)$ [a]	29.4 [c]	–15.0	12.4	–80	
$(TMP^{+\bullet})Fe^{IV}O(5\text{-}MeIm\text{-}d_6)$ [a]	–34.3	–17.4	6.1 [c]	–80	
$(TMTMP^{+\bullet})Fe^{IV}O(Im\text{-}d_4)$ [a]	–14.5	–3.7	5.9	–80	
$(TMTMP^{+\bullet})Fe^{IV}O(2\text{-}MeIm\text{-}d_6)$ [a]	23.9 [c]	–2.7	n.d. [d]	–80	
$(TMTMP^{+\bullet})Fe^{IV}O(5\text{-}MeIm\text{-}d_6)$ [a]	–17.3	–2.5	6.1 [c]	–80	
$(TMP)Fe^{IV}O(1\text{-}MeIm)$	–28.5	–21.6	–3.6	–80	
$(TMP)Fe^{IV}O(1,2\text{-}DiMeIm)$	n.d. [d]	–20.7	–4.1	–80	
$(TMTMP)Fe^{IV}O(1\text{-}MeIm)$	–29.1	–22.7	–4.2	–80	
$(TMTMP)Fe^{IV}O(1,2\text{-}DiMeIm)$	n.d. [d]	n.d. [d]	–3.8	–80	
$(TmTP)Fe^{IV}O(1\text{-}MeIm\text{-}d_6)$ [b]	–22.5	–17.5	–2.8	–50	38
$(TmTP)Fe^{IV}O(1,2\text{-}DiMeIm\text{-}d_8)$ [b]	n.d. [d]	–13.7	–1.7	–50	38
$(TmTP)Fe^{IV}O(1,5\text{-}DiMeIm\text{-}d_8)$ [b]	–23.5	–15.8	–1.3 [c]	–50	38
$(TMP)Fe^{III}(Im\text{-}d_4)$ [a,e]	–28.6	33.6	111.7	–60	
$(TMP)Fe^{III}(2\text{-}MeIm\text{-}d_6)$ [a,e]	18.4 [c]	42.3	89	–60	
$(TMP)Fe^{III}(5\text{-}MeIm\text{-}d_6)$ [a,e]	–36.3	33.8	24.6 [c]	–60	
$(TMTMP)Fe^{III}(Im\text{-}d_4)$ [a,e]	–45.2	30.1	115.3	–80	
$(TMTMP)Fe^{III}(2\text{-}MeIm\text{-}d_6)$ [a,e]	20.3 [c]	45.9	91.3	–80	
$(TMTMP)Fe^{III}(5\text{-}MeIm\text{-}d_6)$ [a,e]	–49.4	31.2	22.9 [c]	–80	

[a] Counter anion is perchlorate ion (ClO_4^-). [b] TmTP; Tetra-*m*-tolylporphyrin, in toluene-d_8. [c] Methyl signal. [d] Not determined. [e] Assignments of the signals are based on the methyl substitutions.

Table 2.1.6. The parent peak values of $[(P^{+\bullet})Fe^{IV}O(L)](ClO_4)$ determined by ESI-MS.

Por =	TMP		TMTMP	
Ligand	Observed	Calculated	Observed	Calculated
None	852.35	852.36	908.11	908.12
Im	920.44	920.38	976.06	976.45
2-MeIm	934.36	934.40	990.96	990.46
5-MeIm	934.49	934.40	990.19	990.46

Table 2.1.3. ^{1}H NMR Chemical Shifts (ppm) and EPR data for (TMP$^{+\bullet}$)Fe^{IV}O(L).

L =	*T*, °C	pyrrole-H	*ortho*-CH_3	*meta*-H	*para*-CH_3	*g*-values	*E*/*D*
Im[a]	–60	–10.4	22.8, 23.8	63.9, 65.4	10.3	4.41, 3.55, 1.98	0.070
	–80	–11.3	26.4, 27.5	73.1, 74.8	11.7		
2-MeIm[a]	–60	–8.8	25.6	70.6, 72.2	10.8	4.47, 3.45, 1.97	0.085
	-80	-9.8	broad	broad	11.3		
5-MeIm[a]	–60	–9.8	22.8, 24.0	64.4, 65.8	10.4	4.42, 3.57, 1.98	0.070
	–80	–11.1	24.2, 25.8	73.2, 74.9	11.2		
3-F-4-NO_2-PhO	–80	–13.7	25.4, 26.9	71.7	11.3	4.59, 3.40, 1.95	0.100
ClO_4^-	–80	–27.4	26.4, 23.9	66.4	11.3	4.42, 3.55, 1.98	0.075
NO_3^-	–80	–19.4	25.3, 27.8	72.5	10.2	4.45, 3.45, 1.96	0.090

[a] Counter ion is perchlorate ion (ClO_4^-). NMR; in dichloromethane-d_2. EPR; in dichloromethane-toluene (5:1) at 4 K.

Table 2.1.4. ^{1}H NMR Chemical Shifts (ppm) and EPR data for (TMTMP$^{+\bullet}$)Fe^{IV}O(L).

L =	pyrrole-CH_3	meso-H	*ortho*-CH_3	*meta*-H	*para*-CH_3	*g*-values	*J*/*D*
Im [a]	113.2	0.0	7.5, 8.7	12.6, 13.4	3.2	2.97, 2.00	0.3
2-MeIm [a]	123.7	–14.8	8.0, 9.3	14.2, 15.0	2.9	3.67, 2.00	0.7
5-MeIm [a]	111.8	–4.0	7.4, 8.6	12.6, 13.4	3.1	3.84, 2.00	0.9
3-F-4-NO_2-PhO	101.9	–1.0	6.6, 7.7	13.3, 13.7	3.2	2.0	0
ClO_4^-	135.5	55.6	7.6, 9.6	14.2, 15.0	3.6	3.23, 2.00	0.4
NO_3^-	127.7	34.7	7.4, 8.3	13.8, 14.6	3.3	3.69, 2.00	0.7
	132.1	45.8	8.3, 9.6	13.7, 14.6	3.4		

[a] Counter ion is perchlorate ion (ClO_4^-). NMR; in dichloromethane-d_2. EPR; in dichloromethane-toluene (5:1) at 4 K.

Table 2.1.7. The second-order rate constants for the reaction of $(P^{+\cdot})Fe^{IV}O(L)$ with the various substrates in CH_2Cl_2 at –80 °C

Porphyrin	Ligand	k_2, $M^{-1}s^{-1}$		
		Cyclooctene[a]	1,4-Cyclohexadiene	*N*,*N*-Dimethyl-*p*-nitroaniline
TMP	Im	0.216 ± 0.003 (87 ± 3)		
	2-MeIm	0.030 ± 0.002 (72 ± 4)		
	5-MeIm[b]	0.240 ± 0.003 (71 ± 3)		
	3-F-4-NO_2-PhO	0.126 ± 0.001 (32 ± 8)		
	Cl^-	0.011 ± 0.001 (62 ± 2)		
	NO_3^-	$8.21 \pm 0.31 \times 10^{-4}$ (64 ± 2)		
TMTMP	Im	0.095 ± 0.001 (82 ± 2)	0.868 ±0.005	3.470 ±0.225
	2-MeIm	0.306 ± 0.002 (89 ± 3)		
	5-MeIm	0.126 ± 0.001 (67 ± 5)		
	3-F-4-NO_2-PhO	0.134 ± 0.001 (80 ± 3)	1.043 ±0.016	3.383 ±0.050
	NO_3^-	$7.13 \pm 0.25 \times 10^{-4}$ (48 ± 1)	0.082 ±0.005	0.048 ±0.002

[a] Numbers in parentheses are yield (%) of cyclooctene oxide. [b] Rate for the second slow reaction was 0.020 ± 0.001 $M^{-1}s^{-1}$.[33]

Chapter 2.

Thermodynamic Factor Determining the Reactivity of Oxoiron(IV) Porphyrin π-Cation Radical Complexes Bearing Various Anionic Axial Ligands: Linear Relationship between Reaction Rate and Free Energy of Reaction

Abstract

Effect of axial anion ligand on reactivity of oxoiron(IV) porphyrin π-cation radical complex was investigated by the reactions of $Fe^{IV}O(TMP^{+\bullet})(L)$, where TMP = tetramesitylporphyrin and L = F^-, Cl^-, BnO^-, AcO^-, HcO^-, TFA^-, and NO_3^-,with cyclooctene, 1,4-cyclohexadiene, and *N*,*N*-dimethyl-*p*-nirtoaniline. The second-order rate constants for cyclooctene epoxidation reactions increased in the order of $F^- > BnO^- > HcO^- > Cl^- > AcO^- > TFA^- > NO_3^-$. The same order was also observed for the oxidations of 1,4-cyclohexadiene and *N*,*N*-dimethyl-*p*-nirtoaniline. To explain this reactivity order, electronic states of $Fe^{IV}O(TMP^{+\bullet})(L)$ complexes were investigated by various physical methods. Although resonance Raman shift of $\nu_{Fe=O}$ band, ^1H NMR chemical shifts of the TMP proton signals, and EPR g-values for $Fe^{IV}O(TMP^{+\bullet})(L)$ complexes did not correlate to the second-order rate constants for the reactions of $Fe^{IV}O(TMP^{+\bullet})(L)$, the redox potentials ($E_{1/2}$ values) for $Fe^{III/II}$ couple linearly correlated. To further confirm these results, the effects of the axial anion ligands on thermodynamic stability of $O=Fe^{IV}por^{+\bullet}$ and $Fe^{III}por$ was investigated by ligand-exchange reactions with tetra(*n*-butyl)ammonium salts $nBu_4N^+(L^-)$. The axial anion ligand changed thermodynamic stability of $Fe^{III}por$ complex more drastically than that of $O=Fe^{IV}por^{+\bullet}$ complex. Moreover, as observed for the correlation with redox potential, the second-order rate constants correlate to the difference of thermodynamic stability between $O=Fe^{IV}por^{+\bullet}$ and $Fe^{III}por$ complexes, which is mainly determined by that of $Fe^{III}por$ complex. All of these results clearly indicate the idea that the reactivity of $O=Fe^{IV}por^{+\bullet}$ complex is controlled by the thermodynamic stability of $Fe^{III}por$ complex, not but by that of $O=Fe^{IV}por^{+\bullet}$ complex.

Abbreviations

$Fe^{IV}O(TMP^{+\bullet})$: oxoiron(IV) meso-tetramesitylporphyrin π-cation radical complex

BnO : benzoate ion

HcO : hydrocinnamate ion

AcO : acetate ion

ImH : imidazole

cpd I ($O=Fe^{IV}por^{+\bullet}$) : compound I (oxoiron(IV) porphyrin π-cation radical)

cpd II : compound II (oxoiron(IV) porphyrin)

TBAP : tetra(*n*-butyl)ammonium perchlorate

Introduction

High-valent metal oxo species (e.g., $Fe^{IV}=O$, $Mn^{V}=O$, $Mo^{VI}=O$ etc) participate in the biological processes of metal enzymes.[1] In particular, the roles of iron-oxo, Fe=O, species are important in chemical and biological oxidation systems.[2-4] In biological systems, the Fe=O species have been implicated as a key reaction intermediate, which is involved in hydrogen abstraction of C-H bond from alkane and insertion an oxygen atom into C=C bond of alkene. For instance, the Fe=O species in cytochromes P450 has been proposed to react with the most difficult C-H bond in a wide variety of organic compounds in biological systems.[5-7] The Fe=O species in cytochromes P450 is an oxoiron(IV) porphyrin π-cation radical, so-called compound I, with a thiolate axial ligand from protein cysteine.[8,9] Compounds I are also characterized as reactive intermediates in catalytic cycles of peroxidases and catalases, in which imidazole axial ligand from histidine and phenolate axial ligand form tyrosine are coordinated to the heme iron, respectively.[5,10] In heme enzymes, proximal ligand, such as cystein

(cytochromes P450), histidine (peroxidases), and tyrosine (catalases) are believed to play crucial roles in generating and tuning reactivities of compound I state.[8a,11]

In order to study the axial ligand effects in heme enzymes, many systematic studies have been reported with synthetic biomimetic model complexes.[12-20] Gross et al. showed that reaction rate of epoxidation of styrene by $O=Fe^{IV}por^{+\bullet}$ complexes was changed by the axial anion ligands.[17] However, mechanisms how to control the reactivity with the axial ligand effect have been still poorly understood. Despite many efforts to reveal the axial ligand effect on $O=Fe^{IV}por^{+\bullet}$, conclusive evidence for correlations between the reactivity and electronic properties of $O=Fe^{IV}por^{+\bullet}$, e.g., the Fe=O bond strength or the spin density at oxo-group (=O), has not yet been obtained.[17,18,21] To reveal the axial anion ligand effect reported by Gross et al, the effects of the axial anion ligands on thermodynamic stability of $O=Fe^{IV}por^{+\bullet}$ and $Fe^{III}por$ was investigated by ligand-exchange reactions with tetra(*n*-butyl)ammonium salts $n Bu_4N^+(L^-)$. The results in this study clearly indicate the idea that the reactivity of $O=Fe^{IV}por^{+\bullet}$ complex is controlled by the thermodynamic stability of $Fe^{III}por$ complex, not but by that of $O=Fe^{IV}por^{+\bullet}$ complex.

Experimental Section

Instrumentation. UV-visible absorption spectra were recorded on an Agilent 8453 (Agilent Technologies) equipped with a USP-203 low-temperature chamber (UNISOKU). ^1H NMR spectra were measured on a Lambda-500 spectrometer (JEOL). Chemical shifts were referenced to the residual peak of dichloromethane-d_2, (5.32 ppm). The concentration of samples for NMR spectra were 1-3 mM. Gas chromatography-mass spectroscopy (GC/MS) analysis was performed on a QP-5000

GC-MS system (Shimadzu) equipped with a capillary gas chromatograph (GC-17A, CBP5-M25-025 capillary column). Cyclic voltammograms were measured with an ALS612A electrochemical analyzer in degassed dichloromethane containing 0.1M nBu$_4$N$^+$ClO$_4^-$ (TBAP) as a supporting electrolyte. The working electrode was a glassy carbon. The counter electrode was a platinium-wire. The potentials were recorded with respect to a saturated calomel electrode (S.C.E) as a referenced electrode. Resonance Raman scattering was excited at 406.7nm from a Kr^+ laser (Spectra Physics, Beam Lok 2060), dispersed by a single polychromator (Chromex, 500IS) and detected with a liquid-nitrogen cooled CCD detector (Roper Scientific, Spex10 400B/LN). Sample concentration was 1 mM. Laser power at the sample was 20 mW. Mechanical slit width was 50 mm. The resonance Raman measurements were carried out using a rotating NMR tube (outer diameter = 5 mm) thermostated at –80 °C by flashing cold nitrogen gas. A 135° back-scattering geometry was used.

UV-vis Measurements upon Controlled-Potential Electrochemical Oxidation. Controlled-potential electrochemical oxidation was conducted in a thin layer quartz cell (0.5 mm) using a gold-mesh working electrode, a platinium-wire counter electrode, and Ag reference electrode, which are connected to a HA-151 potentiostat-galvanostant (Hokuto Denko). $Fe^{IV}O$(TMP) complex was prepared according to the procedure shown in the chapter 1. The dichloromethane solution containing $Fe^{III}(TMP^{+\bullet})(ClO_4)_2$ was passed through a short basic alumina column (0.5 × 2 cm) at ambient temperature, and the elute was poured into a thin layer quartz cell cooling at –60°C, and then the constant potential was applied at the voltage which was higher by 100 mV than the one-electron oxidation potential. UV-vis spectral changes were monitored during electrochemical oxidation

Materials. Dichloromethane was purchased from commercial company as anhydrous solvent and was stored in the presence of 4A molecular sieves. Cyclooctene and 1,4-cyclohexadiene were purchased from commercial company. To remove trace of impurity, cyclooctene and 1,4-cyclohexadiene were passed through activated alumina just before use. Other chemicals were purchased from commercial company, and used without further purification. *meso*-Tetramesitylporphyrin ($TMPH_2$) was prepared according to the literature.[22] Insertion of iron was carried out in acetic acid using $FeCl_2$ and sodium acetate. Chloride iron(III) porphyrin $Fe^{III}(TMP)(Cl)$ was purified by silica gel column using by dichloromethane/methanol as an eluting agent, which was recrystallized from dichloromethane/*n*-hexane.[23] Iron(III) tetramesityl-porphyrins with different axial ligands $Fe^{III}(TMP)(L)$ were obtained from $Fe^{III}(TMP)(OH)$ by the ligand conversion from hydroxide ion to the other anion (fluoride ion ; F^-, acetate ion ; AcO^-, benzoate ion ; BnO^-, trifluoroacetate ion ; TFA^-, hydrocinnamate ion ; HcO^-, and nitrate ion ; NO_3^-) in toluene solution, and these complexes were re-crystallized from ether/*n*-hexane.

Kinetics. The dichloromethane solution of oxoiron(IV) meso-tetramesityl-porphyrin π-cation radical $Fe^{IV}O(TMP^{+\bullet})(L)$, where L = F^-, Cl^-, BnO^-, $AcO,^-$ HcO^-, and NO_3^-, (100 μM) were prepared in a 1-cm quartz cuvette by bubbling O_3 through the solution of iron(III) porphyrin at –60°C. After generation of $Fe^{IV}O(TMP^{+\bullet})(L)$, excess O_3 was removed by bubbling with Ar gas in dichloromethane solution before addition of substrate (cyclooctene, 1,4-cyclohexadiene, and *N,N*-dimethyl-*p*-nitroaniline). Then, excess of substrate (20-1000x) was added to the solution with vigorous stirring, and the reaction rates were determined by monitoring the decay of near 500nm and 667nm optical absorption bands of $Fe^{IV}O(TMP^{+\bullet})(L)$. $Fe^{IV}O(TMP^{+\bullet})(L)$ disappeared within

1~2 h, and changed to that of $Fe^{III}(TMP)(L)$ with clear isosbestic point. The observed rate constants (k_{obs}) were linearly dependent on the concentration of cyclooctene with near-zero intercepts. Thereafter the reaction mixture was quenched by addition of 10 equiv of tetrabutylammonium iodide (n-$Bu_4N^+I^-$) at –60°C. The reaction rate constants were determined by computer simulation of absorption versus time for the reactions.

Thermochemical analysis. The relative energies for $Fe^{IV}O(TMP^{+\bullet})(L)$ and $Fe^{III}(TMP)(L)$ were estimated through the ligand-exchange reactions. Ligand-exchange reactions of $Fe^{IV}O(TMP^{+\bullet})(L^1)$ or $Fe^{III}(TMP)(L^1)$ with n-$Bu_4N^+(L^2)$ were monitored by using ^1H NMR spectra. Samples of $Fe^{IV}O(TMP^{+\bullet})(L^1)$ for ligand-exchange reactions were prepared by ozone oxidations in NMR tubes. To remove a trace of HCl, CD_2Cl_2 was passed through activated alumina just before use. n-$Bu_4N^+(L^2)$ were slowly added to the iron porphyrin solution in NMR tubes. The addition of n-$Bu_4N^+(L^2)$ showed a spectral change, indicating the progression of ligand-exchange reaction without reduction of porphyrin π-cation radical.

Equilibrium constants, K_{Fe4+}, for the ligand-exchange reactions, $Fe^{IV}O(TMP^{+\bullet})(L^1)$ + n-$Bu_4N^+(L^2)$ $\rightleftarrows$ $Fe^{IV}O(TMP^{+\bullet})(L^2)$ + n-$Bu_4N^+(L^1)$, is given as:

$$K_{Fe4+} = ([Fe^{IV}O(TMP^{+\bullet})(L^2)]\,[n\text{-}Bu_4N^+(L^1)]) / ([Fe^{IV}O(TMP^{+\bullet})(L^1)]\,[n\text{-}Bu_4N^+(L^2)])$$
$$= \alpha^2 / \{(1-\alpha)\,(n-\alpha)\}$$

where the term α denotes the molar fraction of $Fe^{IV}O(TMP^{+\bullet})(L^2)$, which can be obtained by the ratio of the peak areas for *m*-H, *o*-Me, *p*-Me and pyrrole-H resonance signals, and n is the molar ratio $[n\text{-}Bu_4N^+(L^2)]_0$ / the total heme. K_{Fe4+} were determined by least squares fit for the plot of α against n. Free energies ΔG_{Fe4+} for ligand-exchange reactions were obtained from the equilibrium constants K_{Fe4+} with the

relation $\Delta G_{Fe4+} = -RT \ln K_{Fe4+}$. The zero of the relative scale is arbitrarily chosen by setting the value for $Fe^{IV}O(TMP^{+\bullet})(NO_3)$ and $Fe^{III}(TMP)(NO_3)$, 0.0 kJ mol^{-1}. Equilibrium constants K_{Fe3+} and free energies ΔG_{Fe3+} for the ligand-exchange reactions, $Fe^{III}(TMP)(L^1) + n Bu_4N^+(L^2) \rightleftarrows Fe^{III}(TMP)(L^2) + n Bu_4N^+(L^1)$, were also estimated by the same method.

Result and Discussion

Preparation and Characterization of Various Oxoiron(IV) Porphyrin π-Cation Radical complexes. Oxoiron(IV) meso-tetramesitylporphyrin π-cation radical complexes bearing different axial ligands, $Fe^{IV}O(TMP^{+\bullet})(L)$, where L is F^-, Cl^-, BnO^-, AcO^-, HcO^-, TFA^-, and NO_3^-, were prepared in dichloromethane solution by oxidations of $Fe^{III}(TMP)(L)$ with O_3 gas at low temperature.[17a,24] O_3 gas appeared to be an ideal oxidant for this study, since neither O_3 nor O_2 gas was potential ligand for $Fe^{IV}O(TMP^{+\bullet})(L)$ complex. $Fe^{IV}O(TMP^{+\bullet})(L)$ complexes were characterized by various spectroscopic techniques including UV-visible, hyperfine-shifted ^1H NMR, electron paramagnetic resonance (EPR), and resonance Raman (RR) spectroscopy. The solution color changed to brilliant green upon oxidation of $Fe^{III}(TMP)(L)$ (reduced soret-band intensity; ~410nm, and characteristic visible band; 665nm), suggesting the formation of porphyrin π-cation radical.[23-26] The EPR spectra of the oxidized green complexes showed two signals around g = 4 and one signal at about g = 2 at 4 K, indicating strong ferromagnetic coupling (S_{total} = 3/2) between the two unpaired electrons of ferryl iron spins Fe^{IV} (S = 1) and single electron of the porphyrin radical (S = 1/2).[27,28] The UV-visible and EPR spectra of $Fe^{IV}O(TMP^{+\bullet})(L)$ were hardly changed by axial ligand, L, suggesting similar electronic structure of all complexes.[17a,27c-d]

Table 2.2.1. Selected resonance Raman, NMR, and EPR spectra for the various oxoiron(IV) porphyrin π-cation radical complexes, $Fe^{IV}O(TMP^{+\bullet})(L)$.

L =	F^-	Cl^-	BnO^-	HcO^-	AcO^-	TFA^-	NO_3^-
$\nu_{Fe=O}$ (cm^{-1}) [a]	801	801	804	802	800	816	821
py-H (ppm) [b]	–11.5	–5.8	–8.6	–7.6	–7.1	–13.5	–17.3
meta-H (ppm) [b]	63.4, 63.9	54.8	59.4, 60.8	61.9, 62.7	65.6	58.7, 59.7	64.0, 64.4
Δg ($g_y - g_x$) [c]	0.92	0.50	0.90	0.96	0.94	0.93	1.06

[a] In CH_2Cl_2 at –60℃. [b] In CD_2Cl_2 at –60℃. [c] In CH_2Cl_2 / toluene (5/1) at 4K.

^1H NMR spectra of $Fe^{IV}O(TMP^{+\bullet})(L)$ were similar, but ^1H chemical shifts were slightly changed by the axial ligand.[17a] These ^1H NMR change indicated binding of the axial ligand in $Fe^{IV}O(TMP^{+\bullet})(L)$ (see Table 2.2.1). RR spectra of $Fe^{IV}O(TMP^{+\bullet})(L)$ were recorded with an exitation wavelength of 407nm, and the bands are summarized in Table 2.2.1. The frequency of Fe=O stretching bands ($\nu_{Fe=O}$) of $Fe^{IV}O(TMP^{+\bullet})(L)$ were

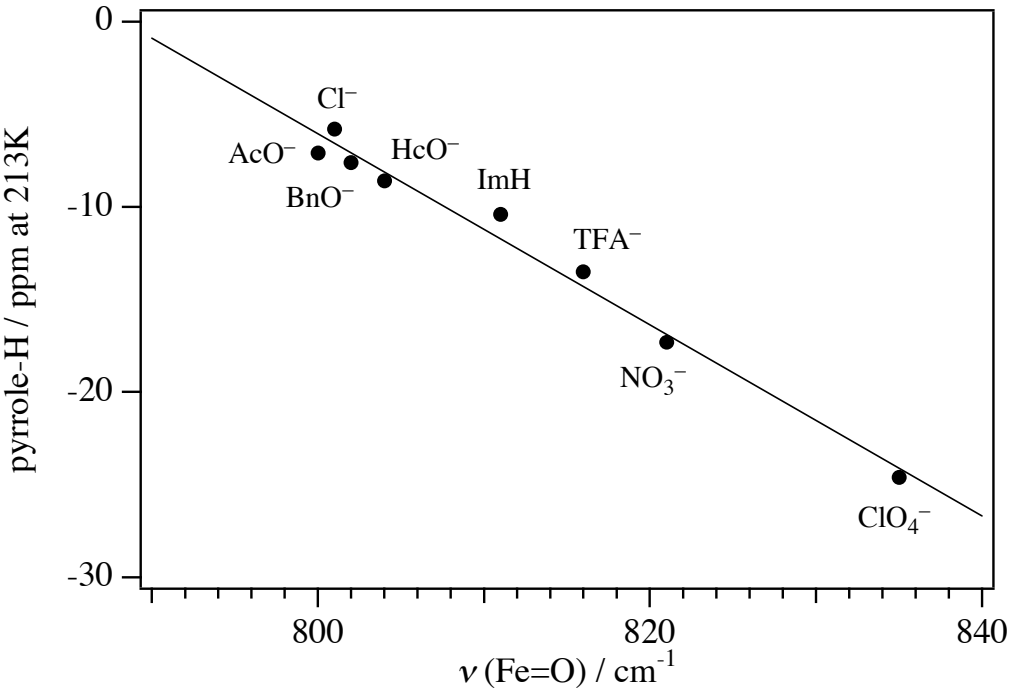

Figure 2.2.1. Plot of pyrrole ^1H chemical shift and $\nu_{Fe=O}$ for $Fe^{IV}O(TMP^{+\bullet})(L)$.

sensitive to the axial ligand.[18] The $\nu_{Fe=O}$ of $Fe^{IV}O(TMP^{+\bullet})(L)$ was observed near 800 cm^{-1} for F^-, Cl^-, AcO^-, BnO^-, HcO^- complexes, and 816 and 821 cm^{-1} for TFA^- and NO_3^- complexes, respectively. It is well known that the $\nu_{Fe=O}$ is sensitive to electron donating ability of axial ligand. Interestingly, the $\nu_{Fe=O}$ band and the ^1H NMR shift of pyrrole-H signal showed a linear relationship, as shown in Figure 2.2.1. This correlation means that the pyrrole-H NMR signal shifts more upfield with an increase in the RR shift of the $\nu_{Fe=O}$ band. With an increase in the donor effect of the axial ligand, deviation of the ferryl iron position from the porphyrin plane decreases, leading to effective spin transfer to the porphyrin ligand.

Reactivity of Various Oxoiron(IV) Porphyrin π-Cation Radical Complexes. Reactivity of $Fe^{IV}O(TMP^{+\bullet})(L)$ complexes, where L = F^-, Cl^-, BnO^-, AcO^-, HcO^-, TFA^-, and NO_3^-, was investigated with oxo transfer reaction to cyclooctene, hydrogen abstraction reaction from 1,4-cyclohexadiene, and electron transfer reaction from *N*,*N*-dimethyl-*p*-nirtoaniline. The detailed reaction mechanisms of these reactions were reported over the past two decades.[29-31] The reaction rate constants for the reaction of $Fe^{IV}O(TMP^{+\bullet})(L)$ complexes with these substrates in dichloromethane at –60°C were determined by UV-vis spectral changes. The second-order rate constants k_2 for these reactions were obtained from the linear dependence of the pseudo-order rate constants on the concentrations of these substrates. The results, which are collected in Table 2.2.2, revealed a pronounced axial ligand effect on the reactivity of $(TMP^{+\bullet})Fe^{IV}O(L)$. The reactivity is increased in the order of $F^- > BnO^- > HcO^- > Cl^- > AcO^- > TFA^- > NO_3^-$ for all of these substrates.

It is well known that the push (electron donation) effect of the axial ligand

Table 2.2.2. Rate constant (k_2, $M^{-1}s^{-1}$ in CH_2Cl_2 at –60°C) for the reaction of the various oxoirn(IV) porphyrin π-cation radical complexes with substrates.

Substrates	F^-	Cl^-	BnO^-	HcO^-	AcO^-	TFA^-	NO_3^-
Cyclooctene	0.29	0.09	0.20	0.15	0.05	0.05	0.02
1,4-cyclohexadiene	24.0	12.6	19.8	16.4	11.9	6.0	3.6
N,N-Dimethyl-*p*-nitroaniline	30.0	6.4	14.9	12.6	6.5	3.2	1.6

accelerates the heterolytic cleavage of O-O bond of the iron bound dioxygen or peroxy acid.[8a,11,16,32,33] In fact, the thiolate ligation in cytochrome P450 promotes the O-O heterolysis more than the imidazole and chloride ligands.[34,35] However, there was no correlation between electron donating ability of axial ligand and the RR band of the $\nu_{Fe=O}$ band, ^1H NMR shifts, and reaction rates of $(TMP^{+\bullet})Fe^{IV}O(L)$. This means that the electron donating ability of axial ligand is not a critical factor on the reactivity of $O=Fe^{IV}por^{+\bullet}$.

Electrochemical Measuremenst. The cyclic voltammogram (CV) of $Fe^{IV}O(TMP)$ has been recorded in dichloromethane solution containing 0.1 M $(n\text{Bu})_4N^+ClO_4^-$ as a supporting electrolyte as shown in Figure 2.2.2. At a scan rate 100 mV s^{-1}, $Fe^{IV}O(TMP)$ complex exhibited a quasi-reversible one-electron potential at $E_{1/2}$ = + 0.89 V (E_{ox} = + 0.98 V, E_{red} = + 0.80 V, E_{ox} and E_{red} denote the peak potentials for oxidation and reduction, respectively). Consistent with the one reversible oxidation wave, a controlled-potential electrochemical oxidation of $Fe^{IV}O(TMP)$ at –60°C lead to UV-vis spectral change with clear isosbestic points, suggesting that the one-electron oxidized species was generated (Figure 2.2.2). The thin layer of the cell enables a fast oxidation of the contained solution. This one-electron oxidized species is generated

through controlled-potential oxidation at 1.05 V versus S.C.E for 30 min. Upon the one-electron oxidation, an intense absorption at 545 nm for $Fe^{IV}O$(TMP) complex completely disappeared, while a characteristic absorption around 660 nm grow. The observed absorption band around 660 nm is a characteristic for oxoiron(IV) porhyrin π-cation radical complex. Therefore, the redox potential $E_{1/2}$ at + 0.89 V of $Fe^{IV}O$(TMP) complex can be assigned to the one-electron oxidation at porphyrin macrocycle to yield $Fe^{IV}O(TMP^{+\bullet})(ClO_4)$, not the oxidation potential for Fe^{IV}-center.

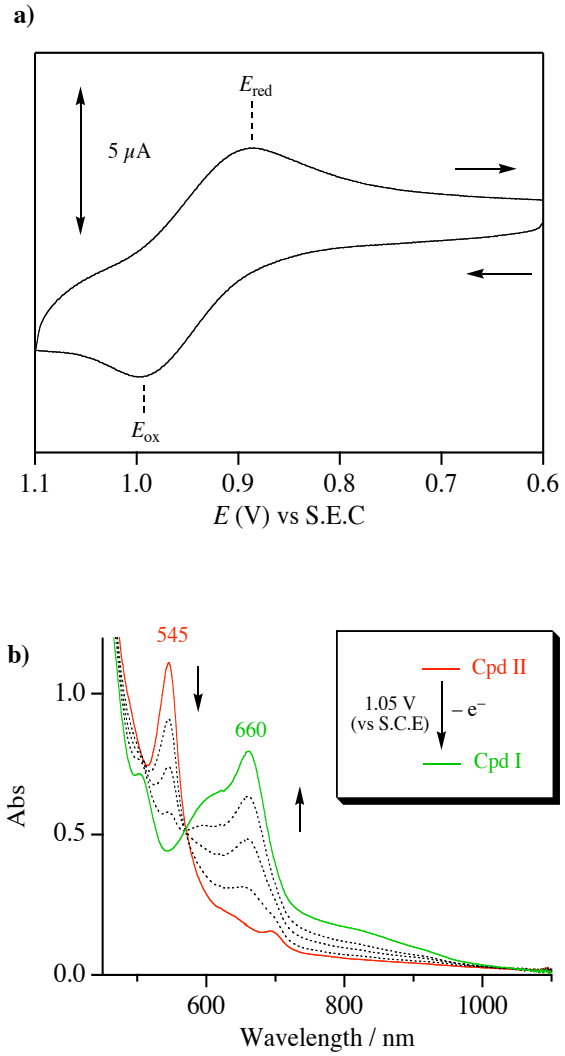

Figure 2.2.2. a) Cyclic voltammogram of $Fe^{IV}O$(TMP) complex in 0.1 M TBAP / dichloromethane solution at –60°C. b) Thin-layer spectra recorded during the controlled-potential oxidation of $Fe^{IV}O$(TMP) complex at 1.05 V vs S.C.E.

Table 2.2.3. Electrochemical parameters for various iron porphyrin complexes.

$E_{1/2}$ / V	F^-	Cl^-	BnO^-	HcO^-	AcO^-	TFA^-	NO_3^-
Cpd-I / Cpd-II	0.95	0.94	1.04	—	0.95	0.96	0.94
$Fe^{III/II}$	–0.63	–0.45	–0.51	–0.48	–0.46	–0.32	–0.18

To investigate into the effect of axial ligand on the $E_{1/2}$ value for Cpd-I/Cpd-II couple, CVs of the $Fe^{IV}O(TMP)$ solutions containing adequate amount of $(n\text{Bu})_4N^+(L)$, where L = F, Cl, BnO, AcO, TFA, and NO_3, were measured under the same condition. Upon addition of $(n\text{Bu})_4N^+(F^-)$ to the solution, it is interestingly to note that the $E_{1/2}$ value is shifted cathodically by 70 mV in comparison to the corresponding potential of $Fe^{IV}O(TMP)$ complex. Upon addition of other $(n\text{Bu})_4N^+(L)$, however, alternation of the $E_{1/2}$ values for Cpd-I/Cpd-II couple were scarcely observed as shown in Table 2.2.3. It is worth noting that the reaction rate of $Fe^{IV}O(TMP^{+\bullet})(F)$ with cyclooctene is almost 20 times faster than that of $Fe^{IV}O(TMP^{+\bullet})(NO_3)$, but $Fe^{IV}O(TMP^{+\bullet})(F)$ and $Fe^{IV}O(TMP^{+\bullet})(NO_3)$ have an identical $E_{1/2}$ value for Cpd-I/Cpd-II couple. Therefore, the reactivity order of the $Fe^{IV}O(TMP^{+\bullet})(L)$ can not be explained by the $E_{1/2}$ value for Cpd-I/Cpd-II couple.

The $E_{1/2}$ values for $Fe^{III/II}$ couple of the $Fe^{III}(TMP)(L)$ were also measured at the same conditions. The $E_{1/2}$ values for $Fe^{III/II}$ couple shifted negative in the order of NO_3 (–0.18) < TFA (–0.32) < Cl (–0.45) < AcO (–0.46) < HcO (–0.48) < BnO (–0.51) < F (–0.63). Surprisingly, this order is very similar to the reactivity order of the $Fe^{IV}O(TMP^{+\bullet})(L)$ ($F^- > BnO^- > HcO^- > Cl^- > AcO^- > TFA^- > NO_3^-$). As shown in Figure 2.2.3, there is a linear correlation between the $E_{1/2}$ values for $Fe^{III/II}$ couple of the $Fe^{III}(TMP)(L)$ and the reactivity order of the $Fe^{IV}O(TMP^{+\bullet})(L)$. It has been known that

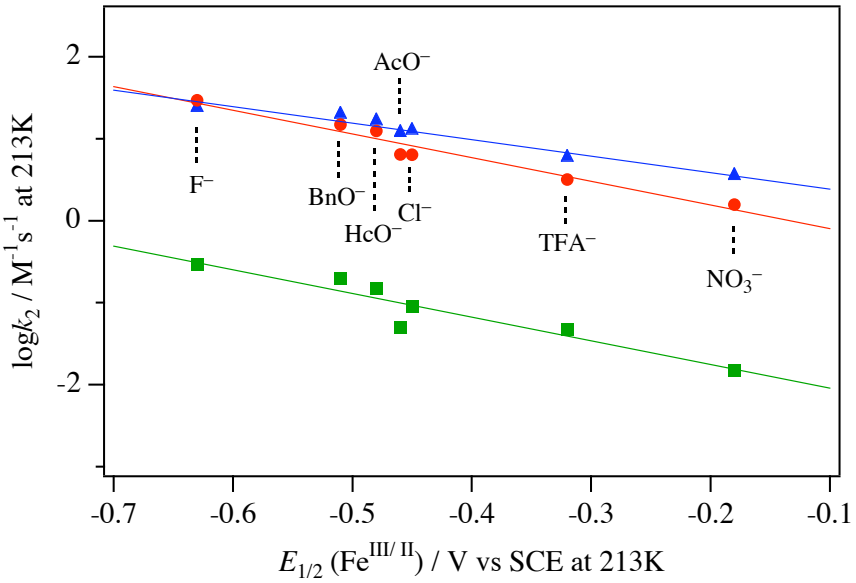

Figure 2.2.3. Plot of logk_2 and the $E_{1/2}$ values for Fe$^{III/II}$ couple. (■; cyclooctene, ▲; 1,4-cyclohexadiene, ●; *N*,*N*-dimethyl-*p*-nitroaniline)

the $E_{1/2}$ value for Fe$^{III/II}$ couple is influenced by the relative stability of the Fe^{III}-ligand interaction.[36] An increases in the Fe^{III}-ligand bond strength results in a negative shift of $E_{1/2}$ value while a decreases in the Fe^{III}-ligand bond strength shift the $E_{1/2}$ value to a positive direction. Therefore, the $E_{1/2}$ value for Fe$^{III/II}$ couple reflects the relative stability of Fe^{III}por complex. This result suggests that the reactivity order may be controlled by the thermodynamic stability of reactant (O=Fe^{IV}por$^{+\bullet}$) and/or product (Fe^{III}por).[37,38]

Thermodynamic stability of iron porphyrins. The thermodynamic stabilites of Fe^{IV}O(TMP$^{+\bullet}$)(L) and Fe^{III}(TMP)(L) were estimated by ligand-exchange reactions as follows:

$$Fe^{IV}O(TMP^{+\bullet})(L^1) + n Bu_4N^+(L^2) \rightleftarrows Fe^{IV}O(TMP^{+\bullet})(L^2) + n Bu_4N^+(L^1) \qquad \Delta G_{Fe4+}$$

$$Fe^{III}(TMP)(L^1) + n Bu_4N^+(L^2) \rightleftarrows Fe^{III}(TMP)(L^2) + n Bu_4N^+(L^1) \qquad \Delta G_{Fe3+}$$

Free energies (ΔG_{Fe4+}, ΔG_{Fe3+}) were measured for seven iron porphyrins and six nBu$_4$N$^+$(L^2) salts, and the estimated values are summarized in Figure 2.2.4. The relative stability of Fe^{IV}O(TMP$^{+\bullet}$)(L) and Fe^{III}(TMP)(L) was estimated from free energies obtained from the ligand-exchanges experiments.[39,40] While the stability of Fe^{III}(TMP)(L) was consistent to the redox potential for Fe$^{III/II}$ couple, the stability of Fe^{IV}O(TMP$^{+\bullet}$)(L) was totally different from the redox potential of Fe^{III}(TMP)(L) series. While Fe^{III}(TMP)(F) complex, which was the most reactive in the series of complexes,

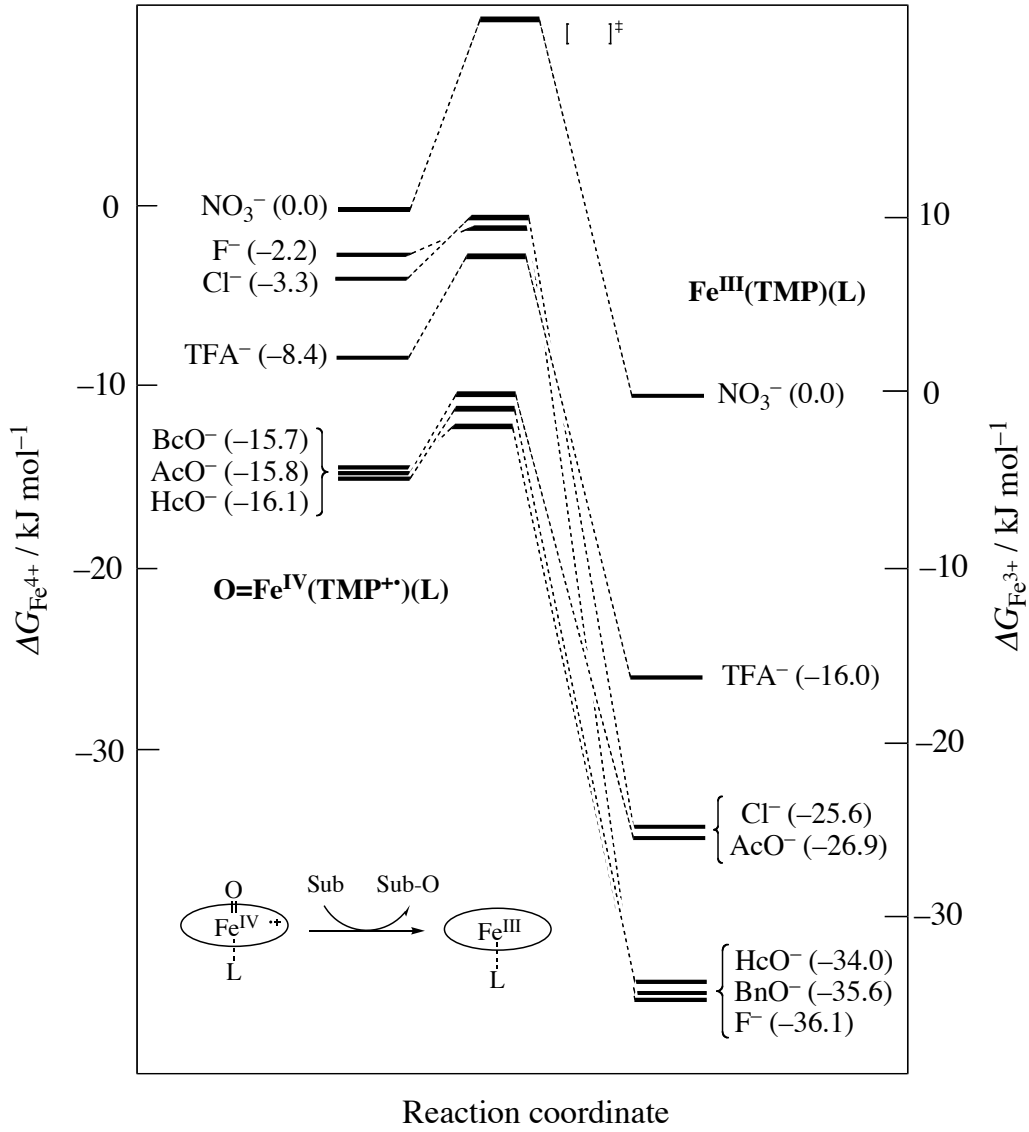

Figure 2.2.4. Energy level diagrams for Fe^{IV}O(TMP$^{+\bullet}$)(L) and Fe^{III}(TMP)(L).

was the most stable in these complexes, $Fe^{IV}O(TMP^{+\bullet})(F)$ complex was not the most unstable. The highest oxidation power of $Fe^{IV}O(TMP^{+\bullet})(F)$ may be derived from free energy gap ($\Delta\Delta G$) between $Fe^{IV}O(TMP^{+\bullet})(F)$ and $Fe^{III}(TMP)(F)$, so the free energy gap $\Delta\Delta G$ was estimated as follows:

$$Fe^{III}(TMP)(L^1) + n\text{Bu}_4N^+(L^2) \rightleftharpoons Fe^{III}(TMP)(L^2) + n\text{Bu}_4N^+(L^1) \qquad \Delta G_{Fe3+}$$

$$-) \; Fe^{IV}O(TMP^{+\cdot})(L^1) + n\text{Bu}_4N^+(L^2) \rightleftharpoons Fe^{IV}O(TMP^{+\cdot})(L^2) + n\text{Bu}_4N^+(L^1) \qquad \Delta G_{Fe4+}$$

$$Fe^{III}(TMP)(L^1) + Fe^{IV}O(TMP^{+\cdot})(L^2) \rightleftharpoons Fe^{III}(TMP)(L^2) + Fe^{IV}O(TMP^{+\cdot})(L^1) \qquad \Delta\Delta G$$

The free energy $\Delta\Delta G$ for the ligand-exchange reaction is defined as

$$\Delta\Delta G = RT \ln K_{ex} = RT \ln (K_{Fe3+} / K_{Fe4+}) = \Delta G_{Fe3+} - \Delta G_{Fe4+}$$

The free energy gap $\Delta\Delta G$ for seven iron porphyrins were calculated, and summarized in Table 2.2.4. These $\Delta\Delta G$ values showed a very good correlation with $\log k_2$, as shown in Figure 2.2.5. This correlation suggests that the reactivity of $O=Fe^{IV}por^{+\bullet}$ is controlled by the thermodynamic stability of $O=Fe^{IV}por^{+\bullet}$ and $Fe^{III}por$. More interestingly, the range of the free energy for the $Fe^{III}(TMP)(L)$ was two times larger than that of the $Fe^{IV}O(TMP^{+\bullet})(L)$. In other words, the stability of $Fe^{III}por$ is more important factor to the reactivity than that of $O=Fe^{IV}por^{+\bullet}$.

Finally, correlations between the free energy gap $\Delta\Delta G$ and second-order rate constants for the oxidations of $Fe^{IV}O(TMP^{+\bullet})(L)$ complexes with various substrates (cyclooctene, 1,4-cyclohexadiene, and *N,N*-dimethyl-*p*-nitroaniline) were also examined. When the reaction rates $\log k_2$ and $\Delta\Delta G$ were plotted, the slopes of –3.72 (cyclooctene), –2.43 (1,4-cyclohexadiene), and –3.57 (*N,N*-dimethyl-*p*-nitroaniline) were obtained. It is noteworthy that the slope for 1,4-cyclohexadiene was smaller than those for other two substrates. The large enthalpic contribution from the substrate

Table 2.2.4. Free energy gaps $\Delta\Delta G$ (kJ mol^{-1} at –60°C) values for the various iron porphyrins.

L =	F^-	Cl^-	BnO^-	HcO^-	AcO^-	TFA^-	NO_3^-
$\Delta\Delta G$	–33.9	–22.3	–19.9	–17.9	–11.1	–7.6	0.0

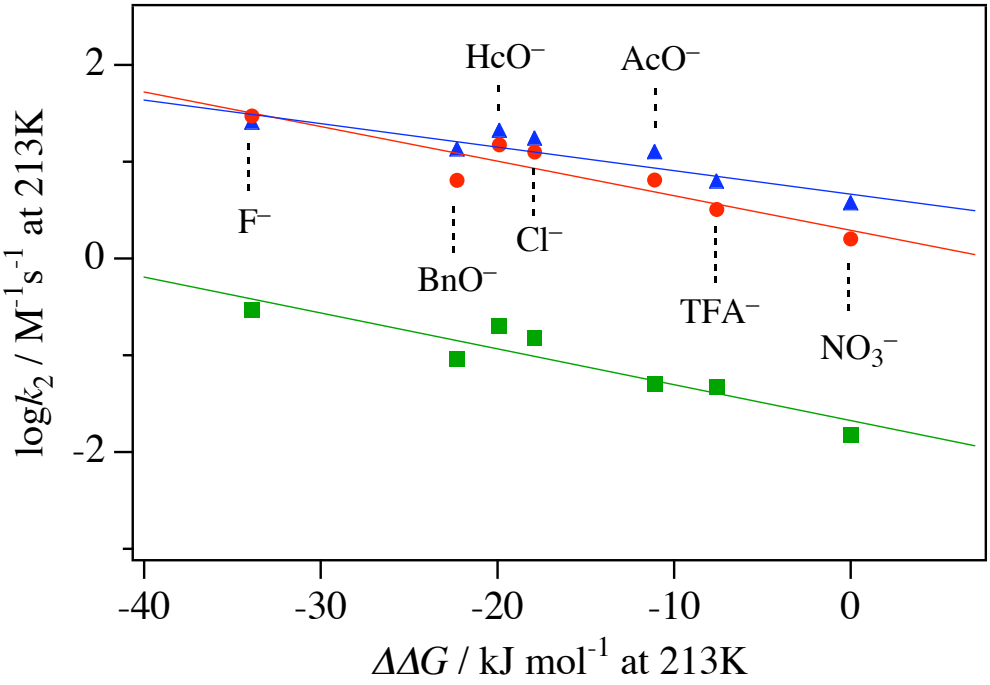

Figure 2.2.5. Plot of logk_2 and free energy gap $\Delta\Delta G$ for the various iron porphyrins. (■; cyclooctene, ▲; 1,4-cyclohexadiene, ●; *N,N*-dimethyl-*p*-nitro- aniline)

oxidation would weaken enthalpy contribution from the effect of axial ligand, leading to the small slope. Actually, change in an enthalpy (ΔH) from 1,4-cyclohexadine to benzene and water would be ~ –260 kJ/mol while that from cyclohexene to cyclohexene oxide would be ~ –120 kJ/mol.[41-43]

Conclusion

Effect of axial anion ligand on reactivity of oxoiron(IV) porphyrin π-cation radical complex was investigated by the reactions of $Fe^{IV}O(TMP^{+\bullet})(L)$ with cyclooctene, 1,4-cyclohexadiene, and *N*,*N*-dimethyl-*p*-nirtoaniline. The axial anion ligand changed thermodynamic stability of Fe^{III}por complex more drastically than that of $O=Fe^{IV}por^{+\bullet}$ complex. The second-order rate constants correlate to the difference of thermodynamic stability between $O=Fe^{IV}por^{+\bullet}$ and Fe^{III}por complexes, which is mainly determined by that of Fe^{III}por complex. All of these results clearly indicate the idea that the reactivity of $O=Fe^{IV}por^{+\bullet}$ complex is controlled by the thermodynamic stability of Fe^{III}por complex, not but by that of $O=Fe^{IV}por^{+\bullet}$ complex.

References

(1) Lippard, S. J.; Berg. J. M. In *Principles of Bioinorganic Chemistry*; University Science Books: California, chapter 12, 1994.

(2) Sono, M.; Roach, M. P.; Coulter, E. D.; Dawson, J. H. *Chem. Rev.* **1996,** *96*, 2841-2887.

(3) Costas, M.; Mehn, M, P.; Jensen, M, P.; Que, L., Jr. *Chem. Rev.* **2004,** *104*, 939-986.

(4) Meunier, B. *Chem. Rev.* **1992,** *92*, 1411-1456.

(5) Schonbaum, G. R.; Chance, B. In *The Enzymes*; Boyer, P. D., Ed.; Academic Press: New York, 1976; Vol. 13, pp 363-408.

(6) Watanabe, Y.; Groves, J. T. In *The Enzymes*; Sigman, D. S., Ed.; Academic Press: New York, 1992; Vol. 20, pp 405-452.

(7) Oritz de Montellano, P. R. In *Cytochrome P450: Structure, Mechanism, and*

Biochemistry, 2nd ed.; Plenum Publishing Corporation: New York, 1995.

(8) (a) Dawson, J. H. *Science* **1988,** *240*, 433-438. (b) Dawson, J. H.; Sono, M. *Chem. Rev*. **1987,** *87*, 1255-1276.

(9) (a) Kellner, D. G.; Hung, S.-C.; Weiss. K. E.; Sligar, S. G. J. Bio. Chem. **2002,** *277*, 9641-9644. (b) Sheng, X.; Horner, J. H.; Newcomb, M.

(10) (a) Dunford, H. B. *Heme Peroxidases*, Wiley-VCH: New York, 1999. (b) Dunford, H. B.; Stillman, J. S. *Coord. Chem.* **1976,** *19,* 187-251.

(11) Poulos, T. L. *J. Biol. Inorg. Chem.* **1996,** *1*, 356-359.

(12) Traylor, T. G.; Lee, W. A.; Stynes, D. V. *J. Am. Chem. Soc*. **1984**, *106*, 755-764.

(13) Battioni, P.; Renaud, J. P.; Bartoli, J. F.; Reina-Artiles, M.; Fort, M.; Mansuy, D. *J. Am. Chem. Soc*. **1988**, *110*, 8462-8470.

(14) Robert, A.; Loock, B.; Momenteau, M.; Meunier, B. *Inorg. Chem.* **1991**, *30*, 706-711.

(15) Beck, M. J.; Gopinath, E.; Bruice, T. C. *J. Am. Chem. Soc*. **1993**, *115*, 21-29.

(16) Yamaguchi, K.; Watanabe, Y.; Morishima, I. *J. Am. Chem. Soc*. **1993**, *115*, 4058-4065.

(17) (a) Gross, Z.; Nimri, S. *Inorg. Chem.* **1994**, *33*, 1731-1732. (b) Gross, Z.; Nimri, S. *J. Am. Chem. Soc*. **1995**, *117*, 8021-8022. (c) Gross, Z. *J. Biol. Inorg. Chem.* **1996**,1, 368-371. (d) Gross, Z.; Nimri, S.; Barzilay, C. M.; Simkhovich, L. *J. Biol. Inorg. Chem.* **1997**, *2*, 492-506.

(18) Czarnecki, K.; Nimri, S.; Gross, Z.; Proniewicz, L. M.; Kincaid, J. R. *J. Am. Chem. Soc*. **1996**, *182*, 2929-2935.

(19) (a) Higuchi, T.; Uzu, S.; Hirobe, M. *J. Am. Chem. Soc*. **1990**, *112*, 7051-7052. (b) Suzuki, N.; Higuchi, T.; Urano, Y.; Kikuchi, K.; Uekusa, H. Ohashi, Y.; Uchida, T.; Kitagawa, T.; Nagano, T. *J. Am. Chem. Soc*. **1999**, *121*, 11571-11572.

(c) Urano, Y.; Higuchi, T.; Hirobe, M.; Nagano, T. *J. Am. Chem. Soc.* **1997**, *119*, 12008-12009. (d) Ohno, T.; Suzuki, N.; Dokoh, T.; Urano, Y.; Kikuchi, K.; Hirobe, M.; Higuchi, T.; Nagano, T. *J. Inorg. Biochem.* **2000**, *82*, 123-125.

(20) (a) Song, W. J.; Ryu, Y. O.; Song, R.; Nam, W. *J. Biol. Inorg. Chem.* **2005,** *10,* 294-394. (b) Nam, W.; Lim, M. H.; Oh, S.-Y.; Lee, J. H.; Lee, H.J.; Woo, S.K.; Kim, C.; Shin, W. *Angew. Chem., Int. Ed.* **2000,** *39,* 3646-3649. (c) Nam, W.; Lim, M. H.; Oh, S.-Y. *Inorg. Chem.* **2000**, *39*, 5572-5575. (d) Nam, W.; Jin, S. K.; Lim, M. H.; Ryu, J. Y.; Kim, C. *Inorg. Chem.* **2002**, *41*, 3647-3652.

(21) Kamachi, T.; Kouno, T.; Nam, W.; Yoshizawa, K. *J. Inorg. Biochem.* **2006**, *100*, 751-754.

(22) Lindsey, J.; Wagner, R. *J. Org. Chem.* **1989,** *54,* 828-836.

(23) Fujii, H. *J. Am. Chem. Soc.* **1993**, *115*, 4641-4648.

(24) Sugimoto, H.; Tung, H,; Sawyer, D. H. *J. Am. Chem. Soc.* **1988**, *110*, 2465-2470.

(25) (a) Groves, J. T.; Haushalter , R. C.; Nakamura, M.; Nemo, T. E.; Evans, B. J. *J. Am. Chem. Soc.* **1981**, *103*, 2884-2886. (b) Groves, J. T.; Watanabe, Y. *J. Am. Chem. Soc.* **1986**, *108*, 3507-508.

(26) Balch, A. L.; Latos-Grazynski, L.; Renner, M W. *J. Am. Chem. Soc.* **1985**, *107*, 2983-2985.

(27) (a) Bill, E.; Ding, X.-Q.; Bominaar, E. L.; Trautwein, A. X.; Winkler, H.; Mandon, D.; Wiess, R.; Gold. A.; Jayaraj, K.; Hatfield, W. E.; Kirk, M. *Eur. J. Biochem.* **1900,** *188,* 665-672. (b) Mandon, D.; Wiess, R.; Jayaraj. K.; Gold, A.; Terner, J.; Bill, E.; Trautwein, A. X. *Inorg. Chem.* **1992,** *31,* 4404-4409. (c) Jayaraj. K.; Terner, J.; Roberts, D. A.; Austin, R. N.; Mandon, D.; Wiess, R.; Bill, E.; Müther, M.; Trautwein, A. X. *Inorg. Chem.* **1996,** *35,* 1632-1640. (d) Wiess, R.; Mandon, D.; Wolter, T.; Trautwein, A. X.; Müther, M.; Bill, E.; Gold. A.; Jayaraj.

K.; Terner, J. *J. Biol. Inorg. Chem.* **1996**,1, 377-383. (e) Wolter, T.; Meyer-Klaucke, W.; Müther, M.; Mandon, D.; Winkler, H.; Trautwein, A. X.; Wiess, R. *J. Inorg. Biochem.* **2000**, 78, 117-122.

(28) (a) Fujii, H.; Yoshimura, T.; Kamada, H. *Inorg. Chem.* **1996**, *35*, 2373-2377. (b) Fujii, H. *Coord. Chem.* **2002,** *226,* 51-60.

(29) Goto, Y.; Watamabe, Y.; Fukuzumi, S.; Jones, J. P.; Dinnocenzo, J. P. *J. Am. Chem. Soc.* **1998**, *120*, 10762-10763.

(30) Chiavarino, B.; Cipollini, R.; Crestonei, M. E.; Fornarini, S.; Lanucara, F.; Lapi, A. *J. Am. Chem. Soc.* **2008**, *130*, 3208-3217.

(31) Jeong, Y. J.; Kang, Y.; Han, A.-R.; Lee, Y.-M.; Kotani, H.; Fukuzumi, S.; Nam, W. *Angew. Chem. Int. Ed.* **2008**, *47*, 7321-7324.

(32) Dawson, J. H.; Holm, R. H.; Trudell, J. R.; Barth, G.; Linder, R. E.; Bunnenberg, E.; Dejerassi, C.; Tang, S. C. *J. Am. Chem. Soc.* **1976**, *98*, 3707-3709.

(33) Traylor, T. G.; Lee, W. A.; Stynes, D. V. *J. Am. Chem. Soc.* **1984**, *106*, 755-764.

(34) Higuchi, T.; Shimada, K.; Maruyama, N.; Hirobe, M. *J. Am. Chem. Soc.* **1993**, *115*, 7551-7552.

(35) Adachi, S.; Nagano, T.; Ishimori, K.; Watanabe, Y.; Morishima, I. *Biochmistry.* **1993,** *32,* 241-252.

(36) Bottomley, L. A.; Kadish, K. M. *Inorg. Chem.* **1981,** *20,* 1348-1357.

(37) Decker, A.; Rohde, J.-U.; Klinker, E. J.; Wong, S. D.; Oue, L, Jr.; Solomon, E, I. *J. Am. Chem. Soc.* **2007**, *129*, 15983-15996.

(38) Ray, K.; England, J.; Fiedler, A. T.; Martinho, M.; Munck, E.; Oue, L, Jr. *Angew. Chem., Int. Ed.* **2008,** *47,* 8068-8071.

(39) (a) Uppal, J. S.; Staley, R. H.; *J. Am. Chem. Soc.* **1982**, *104*, 1235-1238. (b) Uppal, J. S.; Staley, R. H.; *J. Am. Chem. Soc.* **1982**, *104*, 1235-1243. (c) Jones,

R. W.; Staley, R. H.; *J. Am. Chem. Soc*. **1982**, *104*, 2296-2300.

(40) Operti, L.; Tews, E. C.; Freiser, B. S. Staley, R. H.; *J. Am. Chem. Soc*. **1988**, *110*, 3847-3853.

(41) Pedley, J. B.; Naylor, R. D.; Kirby, S. P. "*Therochemical Data of Organic Compounds*", Chapman and Hall: London, 1986.

(42) Stull, D. R.; Westrum, E. F.; Sinke, G. C. "*The Chemical Thermodynamics of Organic Compounds*", Jone Wiley: New York, 1969.

(43) Nagano, H. In *Kagaku-Binran* 5th Edition; Atake, T.; Sorai, M.; Matsuo, T. Eds.; Maruzen: Tokyo, Vol. II, pp 301-313.

Chapter 3.

Functional Role of Neutral Axial Ligand on the Reactivity of Oxoiron(IV) Porphyrin π-Cation Radical Complexes: Comparison between Anionic and Neutral Axial Ligand Effects

Abstract

To understand how the biomimetic axial ligands, phenolate and imidazole, control the reactivity of compound I, the stability for $Fe^{IV}O(TMP^{+\bullet})(L)$ and $Fe^{III}(TMP)(L)$, where L = 3-F-4-NO_2-PhO^-, ImH, 2-MeIm, and 5-MeIm, was estimated from equilibrium constants for ligand exchange reactions. The free energy gap ($\Delta\Delta G$), which was estimated from difference in stability between $Fe^{IV}O(TMP^{+\bullet})(L)$ and $Fe^{III}(TMP)(L)$, for the phenolate complex was larger than those for the other anionic ligands studied in the chapter 2. Therefore, higher reactivity of $O=Fe^{IV}por^{+\bullet}$ complex with the phenilate axial ligand, shown in the chapter 1, was due to large free energy gap induced by stabilization of its Fe^{III}-state. In contrast, the free energy gaps for the neutral imidazole ligands were not similar to that for the phenolate complex. The highest reactivity for the imidazole complexes observed in the chapter 1 could not be explained by free energy gap, as the case for the anionic ligands. However, drastic difference between the neutral and anionic ligands was observed for affinity to the ferryl-oxo speices, $O=Fe^{IV}por$ complex, which would be formed in the oxidation reaction after one-electron transfer from substrate to $Fe^{IV}O(TMP^{+\bullet})(L)$. The higher affinity of the neutral imidazole ligands than the anionic ligands may stabilize the *transition states*, resulting in the highest reactivity of the imidazole complexes.

Abbreviations

$Fe^{IV}O(TMP^{+\bullet})$: oxoiron(IV) meso-tetramesitylporphyrin π-cation radical complex

3-F-4-NO_2-PhO^- : 3-fluoro-4-nitrophenolate

ImH : imidazole

2-MeIm : 2-methylimidazole

5-MeIm : 5-methylimidazole

MeCN : acetonitrile

BnO^- : benzoate

HcO^- : hydrocinnamate

AcO^- : acetate

$O=Fe^{IV}por^{+\bullet}$: oxoiron(IV) porphyrin π-cation radical

compound I : oxoiron(IV) porhyrin π-cation radical

compound II : oxoiron(IV) porphyrin

Introduction

Heme is one of the most important coenzymes in biology.[1-7] Heme consists of an iron ion bound to the four central nitrogen atoms of a porphyrin ring. One or two axial ligands complete the octahedral coordination around the heme iron ion.[1,2] These are various types of the axial ligands in heme proteins, and it is believed that the axial ligand controls the properties of heme active centers.[8-11] Cytochromes P450, chloroperoxidases, and nitric oxide synthases, have a thiolate (Cys) axial ligand, whereas peroxidases have an imidazole (His) axial ligand and catalases have a phenolate (Tyr) axial ligand. These enzymes have different functions *in vivo*:

cytochromes P450 catalyze monooxygenation reactions, whereas catalases detoxify hydrogen peroxide to water and oxygen gas.[1-7] Despite the different reactivity, it is well-known that the catalytic cycles of these enzymes proceed via an oxoiron(IV) porphyrin π-cation radical species, so-called compound I, as a common reactive intermediate.[1-7] It has been proposed that a key element, which distinguishes enzyme functions, is the axial ligand.[12] Previously, Gross et al. reported that there is a pronounced axial ligand effect on the epoxidation of styrene by oxoiron(IV) tetramesitylporhyrin π-cation radical complexes bearing different axial ligands, $Fe^{IV}O(TMP^{+\bullet})(L)$, where TMP = tetramesitylporphyrin and L = F^-, Cl^-, AcO^-, $CF_3SO_3^-$, ClO_4^-, and MeOH.[13] Although the result clearly showed the axial ligand effect on the reactivity of compound I, it has not been studied the axial ligand effect in heme enzyme. This is due to the difficulty of direct comparison of the reactivity of compound I in heme enzymes because of different protein structures, and due to the absence of stable compound I model complexes with imidazole, phenolate, and thiolate axial ligands because of rapid reduction of compound I model complexes by these axial ligands.[14] In the chapter 1, the author has clearly showed that the phenolate and imidazole ligands activate $O=Fe^{IV}por^{+\bullet}$ complexes more than anionic axial ligands, like Cl^- and NO_3^-. This means that the axial ligands in heme nezymes play an important role in activation of the reaction intermediate. To further reveal the axial ligand effect in heme enzyme, in this chapter, the author has evaluated the thermodynamic stability of $Fe^{IV}O(TMP^{+\bullet})(L)$ and $Fe^{III}(TMP)(L)$, where L = 3-fluoro-4-nitrophenolate (3-F-4-NO_2-PhO^-), imidazole (ImH), 2-methylimidazole (2-MeIm), and 5-methylimidazole (5-MeIm). This study clearly showed unique activation mechanisms of the axial ligands in heme enzymes.

Experimental Section

Instrumentation. UV-vis absorption spectra were recorded on an Agilent 8453 (Agilent Technologies) equipped with a USP-203 low-temperature chamber (UNISOKU). ^{1}H NMR were measured on a Lambda-500 spectrometer (JEOL). Chemical shifts were referenced to the residual peak of dichloromethane-d_2, (5.32 ppm). The concentrations of NMR samples were 1-3 mM. Cyclic voltammogram was measured with an ALS612A electrochemical analyzer in degassed dichloromethane containing 0.1M nBu$_4$N$^+$(ClO_4^-) as a supporting electrolyte. The working electrode was a glassy carbon. The counter electrode was a platinium-wire. The potentials were recorded with respect to a saturated calomel electrode (SCE) as a referenced electrode.

Materials. Dichloromethane-d_2 was purchased from commercial company. To remove a trace of HCl, dichloromethane-d_2 was passed through activated alumina just before use. Other chemicals were purchased from commercial company, and used without further purification. Oxoiron(IV) meso-tetramesitylporhyrin π-cation radical complexes with various axial ligands, $Fe^{IV}O(TMP^{+\bullet})(L)$, where L = Cl^-, NO_3^-, BnO^-, HcO^-, TFA^-, and 3-F-4-NO_2-PhO^-, were prepared and purified by publish methods[15-17], and all spectroscopic data of these complexes were consistent with assigned structures.[13,14b,16-20] Oxoiron(IV) meso-tetramesitylporhyrin complex $Fe^{IV}O(TMP^{+\bullet})$ was prepared according to the published procedure.[21]

Thermodynamic Analysis. Stability of the $Fe^{IV}O(TMP^{+\bullet})(L)$ and $Fe^{III}(TMP)(L)$ with 3-F-4-NO_2-PhO^- was estimated according to the procedure shown in the chapter 2.[22,23] Binding constants (K_{Fe4+}, K_{Fe3+}) of neutral ligands, like ImH, 2-MeIm, 5-MeIm,

and MeCN, to $Fe^{IV}O(TMP^{+\bullet})(NO_3^-)$ and $Fe^{III}(TMP)(NO_3^-)$ were examined in dichloromethane at –80°C according to the published procedure.[24-26] Free energies (ΔG) for association reactions were obtained from the binding constants K_{Fe4+} with the relation $\Delta G = -RT \ln K$. The free energy gap $\Delta\Delta G$ (= $\Delta G_{Fe3+} - \Delta G_{Fe4+}$) is defined as following:

$$
\begin{array}{rcl}
Fe^{III}(TMP)(NO_3) + L & \rightleftharpoons & [Fe^{III}(TMP)(L)](NO_3) \quad \Delta G_{Fe3+} \\
-) \; Fe^{IV}O(TMP^{+\cdot})(NO_3) + L & \rightleftharpoons & [Fe^{IV}O(TMP^{+\cdot})(L)](NO_3) \quad \Delta G_{Fe4+} \\
\hline
Fe^{III}(TMP)(NO_3) + [Fe^{IV}O(TMP^{+\cdot})(L)](NO_3) & \rightleftharpoons & [Fe^{III}(TMP)(L)](NO_3) + Fe^{IV}O(TMP^{+\cdot})(NO_3) \quad \Delta\Delta G
\end{array}
$$

where L = ImH, 2-MeIm, 5-MeIm and MeCN. To compare the present result with the results in the chapter 2, free energies of $Fe^{IV}O(TMP^{+\bullet})(NO_3^-)$ and $Fe^{III}(TMP)(NO_3^-)$ were set as zero points.

Result and Discussion

The stability (ΔG_{Fe4+}, ΔG_{Fe3+}) of $Fe^{IV}O(TMP^{+\bullet})(L)$ and $Fe^{III}(TMP)(L)$ s, where L = 3-F-NO_2-PhO^-, ImH, 2-MeIm, 5-MeIm, NCMe, were evaluated by the methods similar to those used in the chapter 2, and summarized in Figure 2.3.1 and 2.3.4. Correlation between the free energy gaps $\Delta\Delta G$ and the second-order rate constants k_2 in log unit for cyclooctene epoxidation by $Fe^{IV}O(TMP^{+\bullet})(L)$ is given in Figure 2.3.2. Data for anionic ligands like Cl^-, NO_3^-, benzoate (BnO^-), hydrocinnamate (HcO^-), and trifluoroacetate (TFA^-) were used in the chapter 2. A good linear correlation could be found for the anionic axial ligands including 3-F-4-NO_2-PhO^-. Thus, higher reactivity of the phenolate axial ligand, which is a model for compound I of catalases, can be explained by large free energy gap $\Delta\Delta G$ between $Fe^{IV}O(TMP^{+\bullet})$(3-F-4-NO_2-PhO) and

Fe^{III}(TMP)(3-F-4-NO_2-PhO) complexes. As shown in Figure 2.3.1, $Fe^{IV}O(TMP^{+\bullet})$-(3-F-4-NO_2-PhO) was relatively unstable in $Fe^{IV}O(TMP^{+\bullet})$(L) complexes, Fe^{III}(TMP)-(3-F-NO_2-PhO) was the most stable in Fe^{III}(TMP)(L) complexes. The stability of Fe^{III}(TMP)(L) complexes was consistent to the redox potential $E_{1/2}$ for $Fe^{III/II}$ couple (NO_3^-: –0.18 < TFA^-: –0.32 < 3-F-4-NO_2-PhO^-: –0.43 < Cl^-: –0.45 < HcO^-: –0.48 < BnO^-: –0.51 (V) vs SCE at –60°C). These results indicate that large free energy gap $\Delta\Delta G$, induced by stabilization of Fe^{III}(TMP)(3-F-4-NO_2-PhO), renders high oxidation activity in $Fe^{IV}O(TMP^{+\bullet})$(3-F-4-NO_2-PhO).

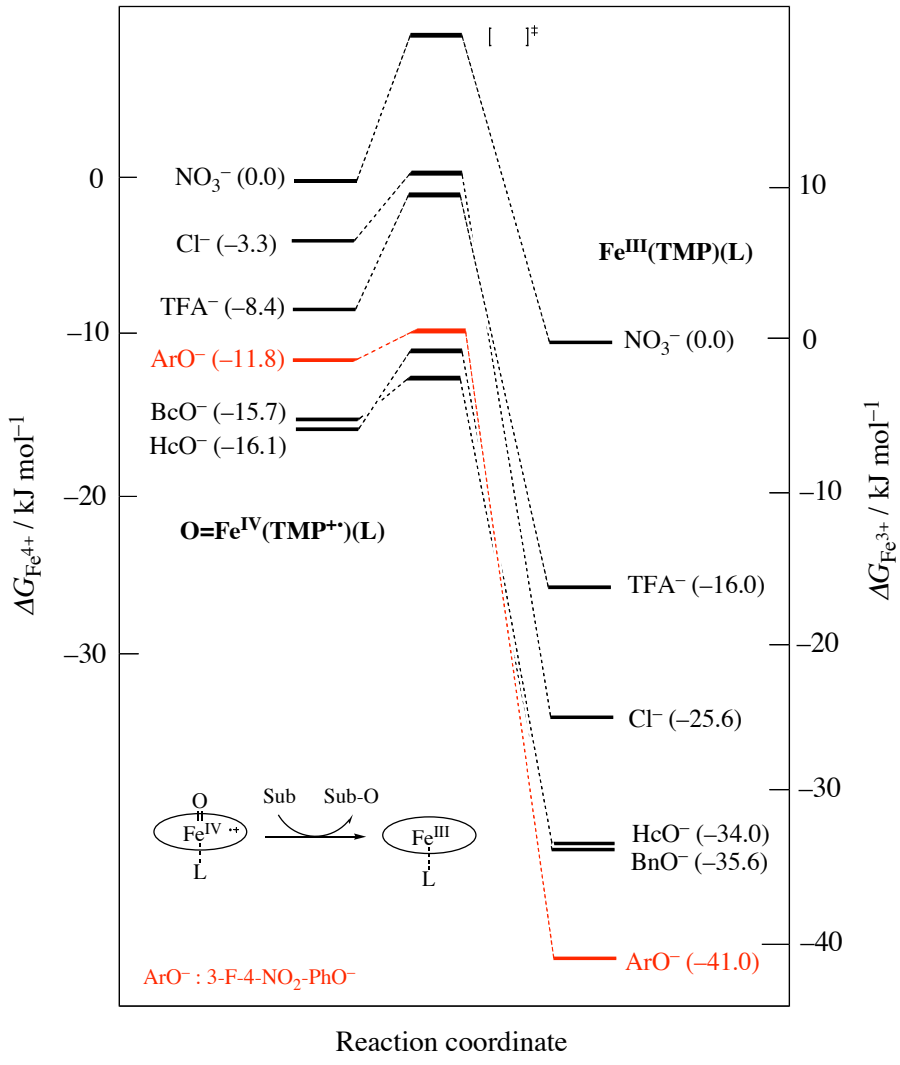

Figure 2.3.1. Energy level diagrams for $Fe^{IV}O(TMP^{+\bullet})$(L) and Fe^{III}(TMP)(L).

Table 2.3.1. The second-order rate constants for the reaction of $Fe^{IV}O(TMP^{+\bullet})(L)$ with cyclooctene in dichloromethane at –80°C.

L =	Cl^-	BnO^-	HcO^-	TFA^-	NO_3^-	MeCN
k_2 / $M^{-1}s^{-1}$ (10^3)	11	30	18	4	1	4

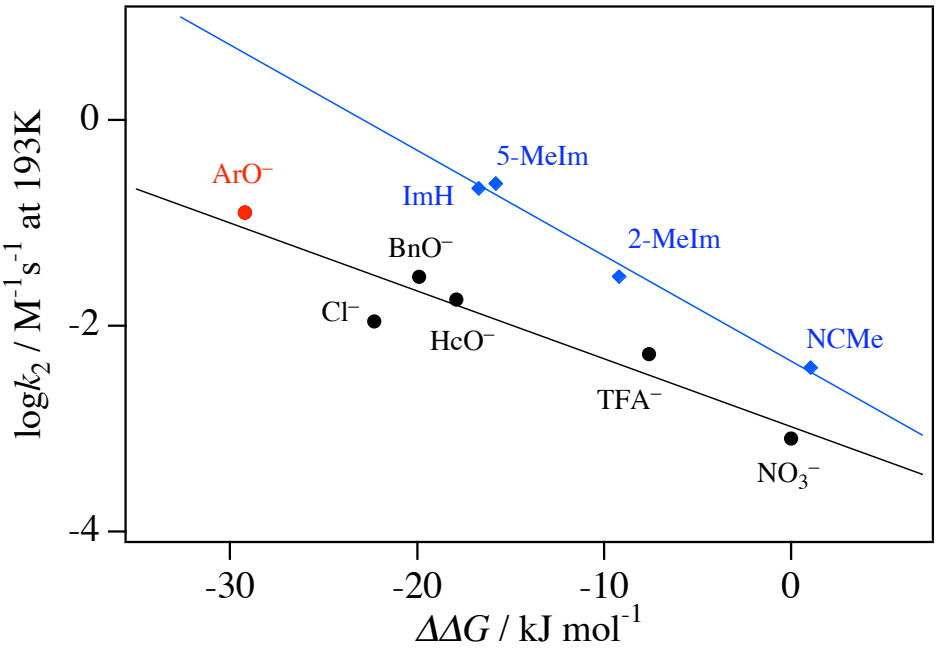

Figure 2.3.2. Plot of logk_2 for the reaction of $Fe^{IV}O(TMP^{+\bullet})(L)$ with cyclooctene and free energy gap $\Delta\Delta G$ for iron porphyrins. k_2 for the reaction of $Fe^{IV}O(TMP^{+\bullet})(L)$, where L = ArO^-, ImH, 2-MeIm, and 5-MeIm, with cyclooctene were used in the chapter 1.

On the other hand, the neutral axial ligands show a different correlation line. Although the difference in $\Delta\Delta G$ between ImH and HcO^- is not significantly large, the ImH ligand renders higher oxidation ability to $O{=}Fe^{IV}por^{+\bullet}$ than the HcO^- ligand. To investigate the role of the neutral ligand, the author examined the binding of the axial ligand to ferryl-oxo species, $Fe^{IV}O(TMP)$ complex, because it may be formed in the oxidation reaction of $Fe^{IV}O(TMP^{+\bullet})(L)$ with substrate after one-electron transfer.[27-32] Imidazole ligands bound to $Fe^{IV}O(TMP)$ complex with high affinities. Upon addition

of ~1.2 equiv ImH, the Soret peak of $Fe^{IV}O$(TMP) shifted from 417 to 422 nm, and the Q-band peak shifted from 543 nm to 569 and 603 nm with clear isosbestic points.[33,34] The similar absorption spectral changes were observed for 2-MeIm and 5-MeIm ligands (see Figure 2.3.3). The binding constants for these imidazole ligands could not be determined numerically because of extremely high affinity. On the other hand, in the case of anionic ligands, absorption spectral change could not be observed even when large excess of anionic ligands was added. These spectral changes suggest that oxoiron(IV) porphyrin complexes bearing imidazole ligands are more stable than that without axial ligand or with anionic axial ligands. This can be explained by net charge of the complex; a neutral character of $Fe^{IV}O$(TMP) complex increases affinity to the neutral axial ligand. The higher affinity of the neutral imidazole ligands than the anionic ligands may stabilize the *transition states*, resulting in the highest reactivity of the imidazole complexes.

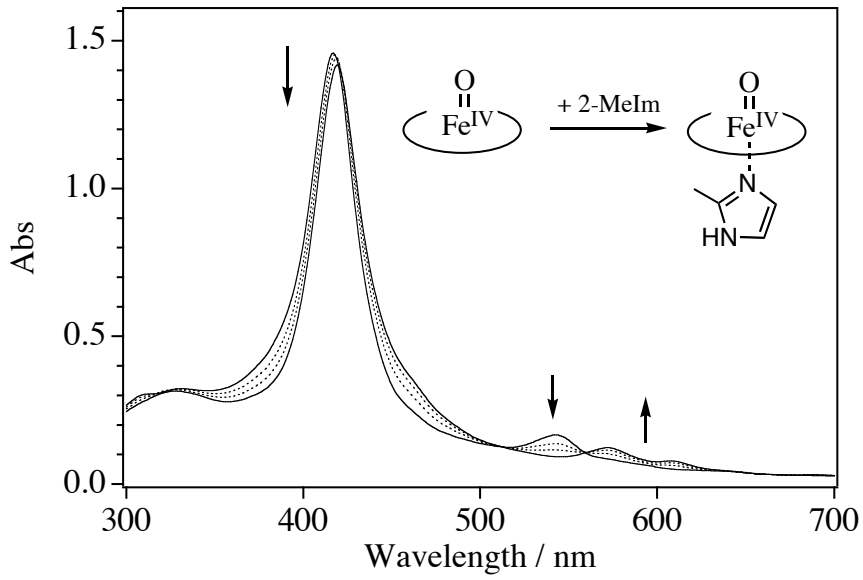

Figure 2.3.3. Absorption spectral changes observed upon addition of 2-methylimidazole (0 – 1.2 equiv) to a solution of $Fe^{IV}O$(TMP) in chlorobenzene at –40°C.

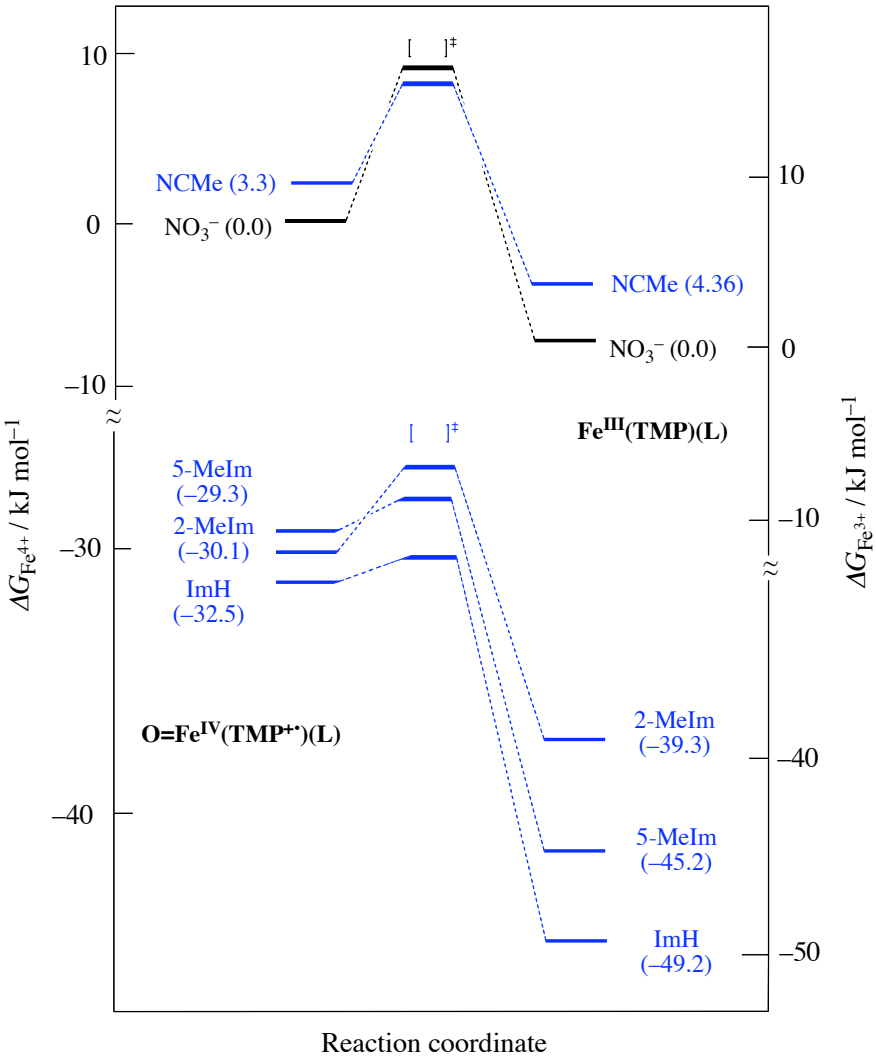

Figure 2.3.4. Energy level diagrams for $Fe^{IV}O(TMP^{+\bullet})(L)$ and $Fe^{III}(TMP)(L)$.

Conclusion

The author studied how the biomimetic axial ligands, like phenolate and imidazole, control the reactivity of compound I. The higher reactivity of $O=Fe^{IV}por^{+\bullet}$ complex with the phenilate axial ligand was due to large free energy gap induced by stabilization of its Fe^{III}-state. In contrast, the higher affinity of the neutral imidazole ligands than the anionic ligands may stabilize the *transition states*, resulting in the highest reactivity of the imidazole complexes.

References

(1) See, for example: Lippard, S. J.; Berg. J. M. In *Principles of Bioinorganic Chemistry*; University Science Books: California, 1994.

(2) Hewson, W. D.; Harger, L. P.; In The Porphyrins; Dolphin, D., Ed.; Academic Press: New York, 1979; Vol. 7.

(3) Schonbaum, G. R.; Chance, B. In *The Enzymes*; Boyer, P. D., Ed.; Academic Press: New York, 1976; Vol. 13, pp 363-408.

(4) Watanabe, Y.; Groves, J. T. In *The Enzymes*; Sigman, D. S., Ed.; Academic Press: New York, 1992; Vol. 20, pp 405-452.

(5) Oritz de Montellano, P. R. In *Cytochrome P450: Structure, Mechanism, and Biochemistry*, 2nd ed.; Plenum Publishing Corporation: New York, 1995.

(6) Dunford, H. B. *Heme Peroxidases*, Wiley-VCH: New York, 1999.

(7) Sono, M.; Roach, M. P.; Coulter, E. D.; Dawson, J. H. *Chem. Rev.* **1996,** *96*, 2841-2887.

(8) (a) Dawson, J. H. *Science* **1988,** *240*, 433-438. (b) Dawson, J. H.; Holm, R. H.; Trudell, J. R.; Barth, G.; Linder, R. E.; Bunnenberg, E.; Dejerassi, C.; Tang, S. C. *J. Am. Chem. Soc.* **1976**, *98*, 3707-3709.

(9) Poulos, T. L. *J. Biol. Inorg. Chem.* **1996,** *1*, 356-359.

(10) Goodin, D. B.; McRee, D. E. *Biochemistry.* **1993,** *32*, 3313-3324.

(11) (a) Adachi, S.; Nagano, T.; Ishimori, K.; Watanabe, Y.; Morishima, I. *Biochmistry.* **1993,** *32,* 241-252. (b) Yoshioka, S.; Takahashi, S.; Ishimori, K.; Morishima, I. *J. Inorg. Biochem.* **2000**, 81, 141-151.

(12) (a) Wang, R.; de Visser, S. P. *J. Biol. Inorg. Chem.* **2007**, *101*, 1464-1472. (b) de Visser, S. P. *J. Biol. Inorg. Chem.* **2006**, *101*, 168-178. (c) de Visser, S. P. *J. Phys. Chem. B* **2006**, *110*, 20759-20761. (d) de Visser, S. P. *J. Phys. Chem. B*

2007, *110*, 12299-12302.

(13) (a) Gross, Z.; Nimri, S. *Inorg. Chem.* **1994**, *33*, 1731-1732. (b) Gross, Z.; Nimri, S.; Barzilay, C. M.; Simkhovich, L. *J. Biol. Inorg. Chem.* **1997**, *2*, 492-506.

(14) (a) Fujii, H.; Yoshimura, T.; Kamada, H. *Inorg. Chem.* **1997**, *36*, 6142-6143. (b) Czarnecki, K.; Kincaid, J. R.; Fujii, H. *J. Am. Chem. Soc.* **1999**, *121*, 7953-7954.

(15) Lindsey, J.; Wagner, R. *J. Org. Chem.* **1989,** *54,* 828-836.

(16) (a) Fujii, H. *J. Am. Chem. Soc.* **1993**, *115*, 4641-4648. (b) Fujii, H.; Yoshimura, T.; Kamada, H. *Inorg. Chem.* **1996**, *35*, 2373-2377.

(17) Sugimoto, H.; Tung, H,; Sawyer, D. H. *J. Am. Chem. Soc.* **1988**, *110*, 2465-2470.

(18) (a) Groves, J. T.; Haushalter , R. C.; Nakamura, M.; Nemo, T. E.; Evans, B. J. *J. Am. Chem. Soc.* **1981**, *103*, 2884-2886. (b) Groves, J. T.; Watanabe, Y. *J. Am. Chem. Soc.* **1986**, *108*, 3507-508.

(19) Balch, A. L.; Latos-Grazynski, L.; Renner, M W. *J. Am. Chem. Soc.* **1985**, *107*, 2983-2985.

(20) (a) Bill, E.; Ding, X.-Q.; Bominaar, E. L.; Trautwein, A. X.; Winkler, H.; Mandon, D.; Wiess, R.; Gold. A.; Jayaraj, K.; Hatfield, W. E.; Kirk, M. *Eur. J. Biochem.* **1900,** *188,* 665-672. (b) Mandon, D.; Wiess, R.; Jayaraj. K.; Gold, A.; Terner, J.; Bill, E.; Trautwein, A. X. *Inorg. Chem.* **1992,** *31,* 4404-4409.

(21) (a) Groves, J. T.; Gross, Z.; Stern, M. K. *Inorg. Chem.* **1994**, *33*, 5065-5072.

(22) (a) Uppal, J. S.; Staley, R. H.; *J. Am. Chem. Soc.* **1982**, *104*, 1235-1238. (b) Gross, Z.; Nimri, S.; Barzilay, C. M.; Simkhovich, L. *J. Biol. Inorg. Chem.* **1997**, *2*, 492-506. Uppal, J. S.; Staley, R. H.; *J. Am. Chem. Soc.* **1982**, *104*, 1235-1243. (c) Jones, R. W.; Staley, R. H.; *J. Am. Chem. Soc.* **1982**, *104*, 2296-2300.

(23) Operti, L.; Tews, E. C.; Freiser, B. S. Staley, R. H.; *J. Am. Chem. Soc.* **1988**, *110*, 3847-3853.

(24) Walker, F. A.; Lo, M.-W.; Ree, T. *J. Am. Chem. Soc.* **1976**, *98*, 5552-5560.

(25) Yoshimura, T.; Ozaki, T. *Bull. Chem. Soc. Jpn.* **1979,** *52*, 2268-2275.

(26) Stephenson, N. A.; Bell, A. T. *Inorg. Chem.* **2006**, *45*, 5591-5599.

(27) (a) Ortiz de Montellano, P. R.; Kunze, K. L. *Biochemistry.* **1981**, *20*, 7266-7271. (b) Ortiz de Montellano, P. R.; Kunze, K. L. *Biochemistry.* **1982**, *21*, 1331-13.

(28) (a) Guengerich, F. P.; Macdonald, T L. *Acc. Chem. Res.* **1984,** *17,* 9-16. (b) Guengerich, F. P.; Willard, R. J.; Shea, J. P.; Richard, L. E.; Macdonald, T L. *J. Am. Chem. Soc.* **1984**, *106*, 6446-6447.

(29) Groves , J. T.; Watanabe, Y. *J. Am. Chem. Soc.* **1986**, *108*, 507-508.

(30) (a) Traylor, T. G.; Nakano, T.; Dunlap, B. E.; Traylor, P. S.; Dolphin, D. *J. Am. Chem. Soc.* **1986**, *108*, 2782-2784. (b) Traylor, T. G.; Miksztal, A. R. *J. Am. Chem. Soc.* **1987**, *109*, 2770-2774. (c) Traylor, T. G.; Nakano, T.; Miksztal, A. R.; Dunlap, B. E. *J. Am. Chem. Soc.* **1987**, *109*, 3625-3632.

(31) (a) Ostovic, D.; Bruice, T. C. *Acc. Chem. Res.* **1992,** *25,* 314-320 and references therein. (b) He, G,-X.; Arasasingham, R. D.; Zhang, G-H.; Bruice, T, C. *J. Am. Chem. Soc.* **1991**, *113*, 9828-9833. (c) Garrison, M. J.; Bruice, T. C. *J. Am. Chem. Soc.* **1989**, *111*, 191-198. (d) Garrison, M. J.; Ostovic , D.; Bruice, T. C. *J. Am. Chem. Soc.* **1989**, *111*, 4960-4966.

(32) (a) Gross, Z.; Nimri, S. *J. Am. Chem. Soc.* **1995**, *117*, 8021-8022. (b) Gross, Z. *J. Biol. Inorg. Chem.* **1996**,1, 368-371.

(33) Chin, D.-H.; Balch, A.; La Mar, G. N. *J. Am. Chem. Soc.* **1980**, *102*, 1446-1448.

(34) Oertling, W. A.; Kean, R. T.; Waver, R.; Babcock, G. T. *Inorg. Chem.* **1990**, *29*, 2633-2645.

PART III.

CHEMOSELECTIVITY AND ELECTRONIC STRUCTURE OF COMPOUND I

Chapter 1. Activation Parameters for Cyclohexene Oxygenation by an Oxoiron(IV) Porphyrin π-Cation Radical Complex: Entropy Control of an Allylic Hydroxylation Reaction

Chapter 2. ENDOR Study of Oxoiron(IV) Porphyrin π-Cation Radical Complexes as Models for Compound I of Heme Enzymes

---

Chapter 1.

Activation Parameters for Cyclohexene Oxygenation by an Oxoiron(IV) Porphyrin π-Cation Radical Complex: Entropy Control of an Allylic Hydroxylation Reaction

Published in *Inorganic Chemistry* **2007**, *46*, 6227-6229.

Akihiro Takahashi, Takuya Kurahashi, and Hiroshi Fujii

Abstract

Activation parameters for epoxidation and allylic hydroxylation reactions of cyclohexene with $Fe^{IV}O(TMP^{+\bullet})(Cl)$ **1** were determined. Within the experimental temperature range, the epoxidation reaction was enthalpy-controlled (i.e., $\Delta H^{\neq} > -T\Delta S^{\neq}$) while the allylic hydroxylation reaction was entropy-controlled (i.e., $-T\Delta S^{\neq} > \Delta H^{\neq}$). Unexpectedly large contribution of entropy term for the allylic hydroxylation reaction indicated that the free energy of activation, $\Delta G^{\neq}$, rather than the activation energy, E_a, should be used to discuss the reaction mechanism and chemoselectivity. The results of this study bring caution to previous DFT studies, in which reaction mechanism and chemoselectivity are evaluated from calculated E_a.

Abbreviations

$Fe^{III}(TMP)(Cl)$; chloro iron(III) *meso*-tetramesitylporphyrin

$Fe^{IV}O(TMP^{+\bullet})(Cl)$; chloro oxoiron(IV) *meso*-tetramesitylporphyrin π-cation radical

Introduction

Cytochromes P450 (P450) are very versatile catalysts, which activate molecular oxygen and catalyze hydrocarbon hydroxylation or alkene epoxidation with high stereoselectivity.[1,2] Reaction of P450 with cyclohexene yields a mixture of two major products: cyclohexene oxide (an epoxidation product) and 2-cyclohexen-1-ol (an allylic hydroxylation product).[3] Interestingly, the ratio of epoxidation to allylic hydroxylation products, i.e., the chemoselectivity, is changed by P450 isozymes and by mutation of a single amino acid near the proximal or distal side.[3] In addition, P450 model studies using synthetic iron porphyrin complexes showed that the chemoselectivity depends on various other factors, such as the nature of the porphyrin and axial ligands, solvents, and reaction temperature.[4-7] While these enzymatic and model studies suggest that chemoselectivity is dependent on the electronic structure of the reactive intermediate, oxoiron(IV) porphyrin π-cation radical species (compound I), it is not clear how compound I controls chemoselectivity. Recently, the reaction mechanism and chemoselectivity of P450 have been studied by theoretical calculations based on density functional theory (DFT).[8] In DFT studies, reaction mechanism and chemoselectivity are predicted from calculated activation energy, E_a, for epoxidation and allylic hydroxylation reactions of oxoiron(IV) porphyrin π-cation radical species. These studies are based on the assumption that the contribution of entropy of activation, $\Delta S^{\neq}$, is much smaller than that of enthalpy of activation, $\Delta H^{\neq}$. However, the validity of this assumption remains unproven because the activation parameters for epoxidation and allylic hydroxylation reactions of compound I species are yet to be determined. To better understand epoxidation and allylic hydroxylation reactions, the present study ascertained the activation parameters for epoxidation and allylic hydroxylation reactions of cyclohexene with compound I species, $Fe^{IV}O(TMP^{+\bullet})(Cl)$ **1**, (see Figure 3.1.1). This

study demonstrated that epoxidation is an enthalpy-controlled reaction, while allylic hydroxylation is an entropy-controlled reaction. The large contribution of the entropy term, $-T\Delta S^{\neq}$, to the free energy of activation, $\Delta G^{\neq}$, indicated that $\Delta G^{\neq}$, rather than E_a, should be used to predict reaction mechanisms and chemoselectivity.

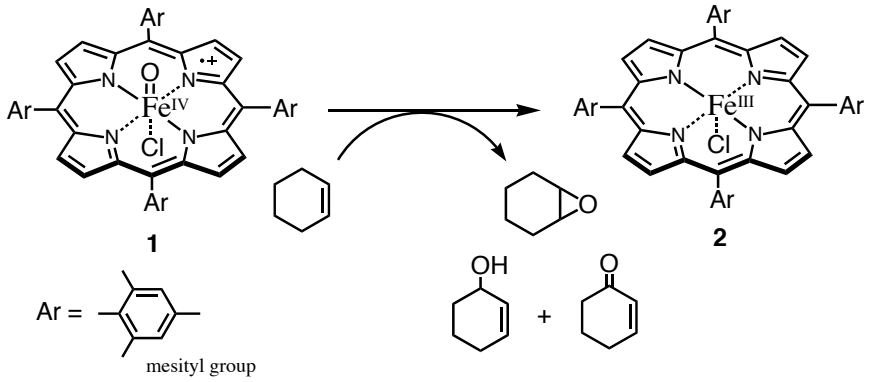

Figure 3.1.3. Epoxidation vs allylic C-H hydroxylation reactions of cyclohexene by $Fe^{IV}O(TMP^{+\bullet})Cl$ **1**.

Experimental Section

Instruments. UV-vis spectra were recorded on an Agilent 8453 (Agilent Technologies) equipped with USP-203 low temperature chamber (UNISOKU). Gas chromatography-mass spectroscopy (GC-MS) analysis was performed on a QP-5000 GC-MS system (Shimadzu) equipped with a capillary gas chromatograph (GC-17A, CBP5-M25-025 capillary column).

Materials. Methylene chloride was purchased from Kanto as anhydrous solvent and was stored in the presence of 4A molecular sieves. Cyclohexene was purchased from Kanto. Cyclohexene-d_{10} was purchased from ISOTEC. To remove a trace of impurity, cyclohexene and cyclohexene-d_{10} were passed through activated alumina just before use. Undecane was purchased from Kanto. $Fe^{III}(TMP)(Cl)$ **1** was synthesized according to the published procedure.[15]

Product Analysis. $Fe^{IV}O(TMP^{+\bullet})Cl$ **1** was generated by **2** (0.5 μmol) and O_3 gas at 193 K in 500 μL of anhydrous CH_2Cl_2 solution. To remove excess O_3 gas, the resulting solution was then frozen in liquid nitrogen, and thawed at 193 K under vacuum. This freeze-thaw cycle was repeated five times. The solution of **1** was stirred at 193, 203, 213, 223, and 233 K for 5 min, and then cyclohexene (50 μmol) was added to the solution under the Ar atmosphere. **1** disappeared within 1–2 h, and thereafter the reaction mixture was quenched by addition of tetrabutylammonium iodide (5.0 μmol) at the same temperature. Analysis of the reaction mixture with GC-MS revealed that cyclohexene oxide, 2-cyclohexen-1-ol and 2-cyclohexen-1-one were generated. Other possible oxidation products such as 2-cyclohexen-1-one oxide and bicyclohexene were not detected. Quantitative analysis was performed with GC-MS using undecane as an internal standard. Experiments were repeated three times, and averaged yields relative to **1** were summarized in Table 3.1.1. The yield of each product is not changed upon prolonged reaction time, indicating that isomerization between cyclohexene oxide and 2-cyclohexen-1-ol does not occur under the experimental conditions.

Kinetics. The CH_2Cl_2 solution of **1** (1.1×10^{-5} M) was prepared in a 1-cm quartz cuvette by bubbling O_3 through the solution of **2** at 193, 203, 213, 223, and 233 K. Then, cyclohexene (1.1×10^{-3} –1.1×10^{-1} M) was added to the solution with vigorous stirring, and the time-dependent absorption spectral changes were recorded every 10–60 s over 3600 s immediately after the addition of cyclohexene. The absorption spectrum of **1** was changed to that of **2** with clear isosbestic points. In the absence of cyclohexene, the decay of **1** was negligibly small in this temperature range.

Plots of the absorbance at 418 and 667 nm vs time obeyed the pseudo-first-order rate kinetics in the presence of excess cyclohexene. The pseudo-first-order rate constants were linearly dependent on the concentration of cyclohexene with near-zero intercepts. Thus, the second-order rate constants (k_{ox}) for the decay of **1** were determined at each temperature from eq (1),

$$k_{obs} = k_0 + k_{ox}[\text{cyclohexene}] \quad (1)$$

where k_{obs} is the pseudo-first-order rate constant for the decay of **1** in the presence of excess cyclohexene, k_0 is the first-order rate constant for the decay in the absence of cyclohexene.

The second-order rate constants for the formation of epoxidation product (k_{oxide}) and allylic hydroxylation product (k_{ol}) were determined from k_{ox} and product distributions using eq (2), which is typical for the parallel reaction.

$$k_{oxide} = \frac{Y_{oxide}}{Y_{oxide} + Y_{ol}} k_{ox} \qquad k_{ol} = \frac{Y_{ol}}{Y_{oxide} + Y_{ol}} k_{ox} \quad (2)$$

where Y_{oxide} is the yield of cyclohexene oxide, and Y_{ol} is the yield of 2-cyclohexen-1-ol and 2-cyclohexen-1-one. Results are summarized in Table 3.1.1. Kinetics for the reaction of **1** with cyclohexene-d_{10} at 213 K are summarized in Table 3.1.2.

Activation energies (ΔE_a) were obtained from the Arrhenius plots for epoxidation and allylic hydroxylation ($\ln k_{oxide}$, $\ln k_{ol}$ vs 1/T) by a linear least-squares fit to the data. The enthalpy of activation ($\Delta H^{\neq}$) and the entropy of activation ($\Delta S^{\neq}$) were obtained from the Eyring plots for epoxidation and allylic hydroxylation ($\ln(k_{oxide}/T)$, $\ln(k_{ol}/T)$ vs $1/T$) by a linear least-squares fit to the data.

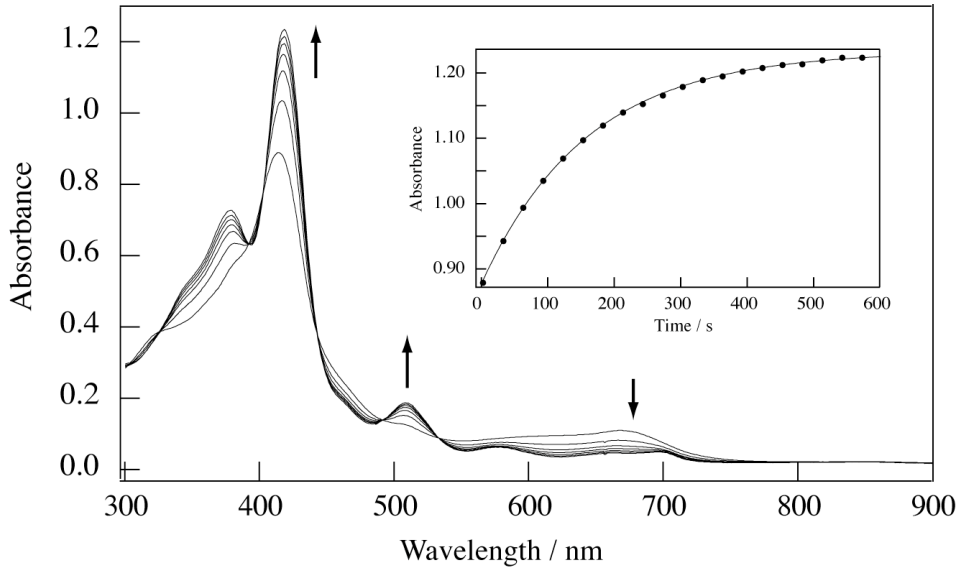

Figure 3.1.2. Absorption spectral change upon addition of cyclohexene (1.0×10^{-2} M) to the dichloromethane solution **1** (1.0×10^{-5} M) at 223K. Inset: time course for the absorbance change at 417nm.

Result and Discussion

The absorption spectrum of **1**, which was prepared by ozone oxidation of Fe^{III}(TMP)(Cl) (**2**) in CH_2Cl_2,[9] was changed to that of **2** with clear isosbestic points upon addition of cyclohexene as shown in Figure 3.1.2. The clear isosbestic points indicated the absence of accumulation of any reaction intermediate; moreover, formation of the first transition state was the rate-limiting step for both the epoxidation and allylic hydroxylation reactions of cyclohexene oxygenation by **1**. Therefore, the activation parameters estimated in this study correspond to those of the rate-limiting steps.

The E_a values for the epoxidation and allylic hydroxylation reactions of cyclohexene, estimated from an Arrhenius plot over temperatures ranging from 193 to 233 K, were found to be 35.4 ± 1.7 and 20.9 ± 2.4 kJ mol^{-1}, respectively. Interestingly,

the E_a value for the epoxidation reaction was about two-fold greater than that for the allylic hydroxylation reaction. This result is inconsistent with DFT calculations for propene oxygenation, which predicted that E_a for the epoxidation reaction was less than that for the allylic hydroxylation reaction.[8] According to previous DFT studies using E_a values, the result of the present study, shown in Figure 3.1.3, leads to the conclusion that allylic C-H hydroxylation is more favorable than epoxidation. However, this conclusion is erroneous, as epoxidation is favored over allylic hydroxylation at room temperature.[4c]

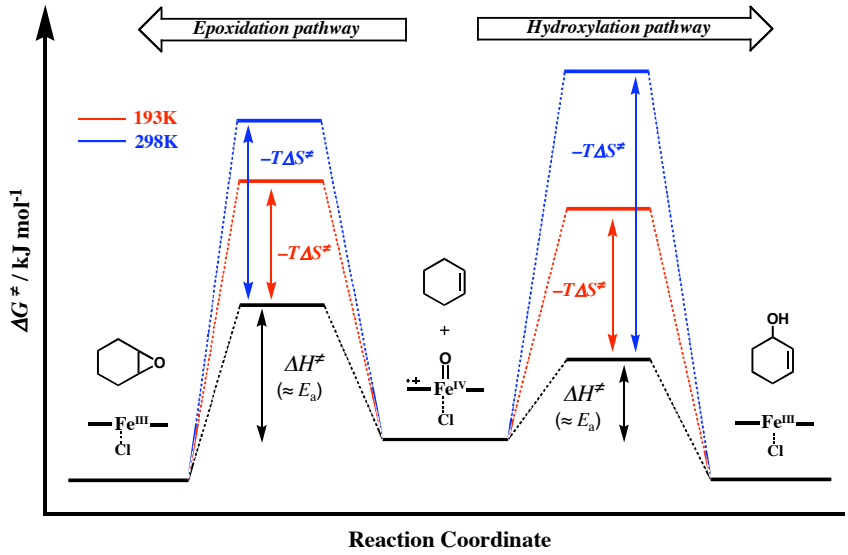

Figure 3.1.3. Diagram for cyclohexene oxygenation by **1**. The black lines show energy profiles with E_a ($\Delta H^{\neq}$). The red and blue lines show energy profiles with $\Delta G^{\neq}$ ($\Delta H^{\neq} - T\Delta S^{\neq}$) at 193 and 298 K, respectively.

To further analyze the cyclohexene oxygenation reaction, $\Delta H^{\neq}$ and $\Delta S^{\neq}$ values were estimated from an Eyring plot over temperatures ranging from 193 to 233 K. The $\Delta H^{\neq}$ values for epoxidation and allylic hydroxylation reactions were estimated to be 33.6 ± 1.7 and 19.2 ± 2.4 kJ mol^{-1}, and the $\Delta S^{\neq}$ values were estimated to be –101.2 ± 6.7 and

-169.1 ± 9.0 J K^{-1} mol^{-1}, respectively. As expected from the equation, $\Delta H^{\neq} = E_a - RT$,[10] the $\Delta H^{\neq}$ values were similar to the E_a values. In contrast, the $\Delta S^{\neq}$ values for both the epoxidation and allylic hydroxylation reactions were large negative values, and the $\Delta S^{\neq}$ value for the allylic hydroxylation reaction was about two-fold greater than that of the epoxidation reaction. The $\Delta S^{\neq}$ value for the epoxidation reaction was reasonable for a typical bimolecular reaction. However, the $\Delta S^{\neq}$ value for the allylic hydroxylation reaction was larger than that of a typical bimolecular reaction, approaching $\Delta S^{\neq}$ values observed for bimolecular reactions with a high degree of order in the transition state, such as the Diels-Alder reaction.[11]

The contribution of the entropy term, $-T\Delta S^{\neq}$, to the epoxidation and allylic hydroxylation reactions was unexpectedly large. $-T\Delta S^{\neq}$ became greater than $\Delta H^{\neq}$ at temperatures exceeding 114 K for allylic hydroxylation and 334 K for epoxidation.

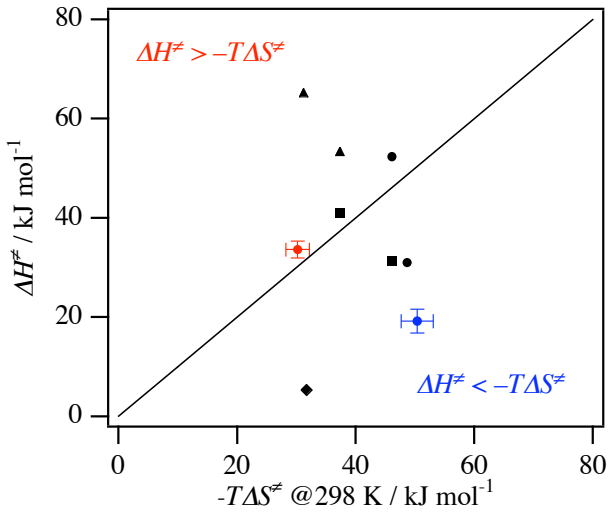

Figure 3.1.4. Plot of $\Delta H^{\neq}$ vs $-T\Delta S^{\neq}$ at 298 K for epoxidation (red circle and allylic C-H hydroxylation (blue circle) of cyclohexe oxygenation by **1** and for othor related reactions. Black circle: Diels-Alder reactions.[12] Black diamond: tert-butoxy radical and triphenylmethane.[13] Black squares: rhodium porphyrin and methane.[14] Black triangle: $KMnO_4$ or CrO_2Cl_2 and toluene.[15]

Within the experimental temperature range, for the allylic hydroxylation reaction, $-T\Delta S^{\neq}$ was approximately two-fold greater than $\Delta H^{\neq}$ (entropy control). In contrast, the epoxidation reaction was enthalpy-controlled, but $-T\Delta S^{\neq}$ was comparable to $\Delta H^{\neq}$ at room temperature (see Figure 3.1.4). Entropy-controlled reactions are uncommon, but have been reported for hydrogen abstraction by *t*-butoxyl radical and rhodium(II) porphyrin.[11-13a]

In previous experimental and DFT studies, the reaction mechanism and chemoselectivity were discussed based on E_a values.[7,8] These studies assume that, for the epoxidation and allylic hydroxylation reactions, $-T\Delta S^{\neq}$ values are much smaller than $\Delta H^{\neq}$ values, indicating enthalpy control. However, the results of the current study bring the result of these previous studies into question. The large contribution of the entropy term to both the epoxidation and allylic hydroxylation reactions indicates that free energy of activation, $\Delta G^{\neq}$, rather than E_a, should be used to discuss reaction mechanism and chemoselectivity. In fact, temperature affected chemoselectivity of cyclohexene oxygenation: at 173 K, the major product of cyclohexene oxygenation by **1** was cyclohexene oxide, while at 233 K it was 2-cyclohexen-1-ol (see Table 3.1.1). This temperature dependence of chemoselectivity cannot be explained by E_a, but only by $\Delta G^{\neq}$, because E_a is independent of temperature. The observed temperature effect on chemoselectivity of cyclohexene can be seen with $\Delta G^{\neq}$, as shown in Figure 3.1.3. Furthermore, reaction mechanisms also can be predicted by $\Delta G^{\neq}$, but not by E_a. In previous DFT studies, reaction mechanisms were predicted from E_a values of possible reaction pathways. However, due to the large contribution of $-T\Delta S^{\neq}$, the reaction pathway having a higher E_a value may be favored over a pathway with a lower E_a.

The difference in $\Delta S^{\neq}$ values between epoxidation and allylic hydroxylation was reasonable because the reactions proceed via independent pathways with different

transition states.[4c] The large negative $\Delta S^{\neq}$ value for the allylic hydroxylation reaction suggested a highly ordered transition state, indicating that allylic hydroxylation occurs only when **1** and cyclohexene interact at a specific orientation. Allylic hydroxylation demonstrated a drastic kinetic isotope effect (see Table 3.1.2), suggesting involvement of C-H bond breakage in the transition state. Bond formation (orbital overlapping) between the oxo ligand of **1** and the allylic hydrogen may result in a highly ordered transition state for the allylic hydroxylation reaction, as indicated by the large negative $\Delta S^{\neq}$ value. In contrast, the $\Delta S^{\neq}$ value for the epoxidation reaction was typical for a bimolecular reaction. Furthermore, the epoxidation reaction did not show kinetic isotope effect (see Table 3.1.2). The epoxidation transition state does not involve interaction of **1** with the C-H moiety of cyclohexene and a complex with weak interactions, such as charge transfer complex, may form.

Conclusion

In summary, this study determined the activation parameters for cyclohexene oxygenation by **1**. Chemoselectivity of cyclohexene oxygenation by **1** was not controlled by the E_a value, but by the $\Delta S^{\neq}$ value, suggesting that previous DFT studies should be interpreted with caution. Additional studies investigating the porphyrin and axial ligand effects on activation parameters are being conducted using synthetic iron porphyrin complexes and heme enzymes by this research group.

References

(1) *Cytochrome P-450: Structure, Mechanism, and* Biochemistry, 2nd ed. (Ed.: P. R. Ortiz de Montellano), Plenum Press, New York, 1995.

(2) Y. Watanabe, J. T. Groves in *The Enzymes*, (Eds.: D. S. Sigman, P. D. Boyer), Academic Press, San Diego, 1992, Vol. 20, p. 405–452.

(3) a) White R. E.; Groves, J. T.; McClusky, G. A. *Acta. Biol. Med. Germ.* **1979**, *38*, 475-482. b) Vaz. A. D. N.; McGinnity. D. F.; Coon, M. J. *Proc. Natl. Acad. Sci. USA*. **1998**, *95*, 3555–3560. c) Yoshioka, S.; Takahashi, S.; Ishimori, K.; Morishima, I. *J. Inorg. Biochem.* **2000**, *81*, 141–151.

(4) a) Groves, J. T.; Nemo, T. E. *J. Am. Chem. Soc.* **1983**, *105*, 5786–5791. b) Groves, J. T.; Subramanian, D. V. *J. Am. Chem. Soc.* **1984**, *106*, 2177–2181. c) Groves, J. T.; Gross, Z. in *Bioinorganic Chemistry: An Inorganic Perspective of Life*, (Ed. D. P. Kessissoglou), NATO Advanced Study Institute Series 459, Kluwer Academic Publishers, The Netherlands, 1995, p. 39–47.

(5) Bartoli, J. F.; Brigaud, O.; Battioni, P.; Mansuy, D. *J. Chem. Soc., Chemm. Commun.* **1991**, 440-442.

(6) a) Ohno, T.; Suzuki, N.; Dokoh, T.; Urano, Y.; Kikuchi, K.; Hirobe, M.; Higuchi, T.; Nagano, T. *J. Inorg. Biochem.* **2000**, *82*, 123-125. b) Suzuki, N.; Higuchi, T.; Urano, Y.; Kikuchi, K.; Uekusa, H.; Ohashi, Y.; Uchida, T.; Kitagawa, T.; Nagano, T. *J. Am. Chem. Soc.* **1999**, *121*, 11571-11572.

(7) Song, W. J.; Ryu, Y. O.; Song, R.; Nam, W. *J. Biol. Inorg. Chem.* **2005**, *10*, 294–304.

(8) a) Shaik, S.; Kumar, D.; de Visser, S. P.; Altun, A.; Thiel, W. *Chem. Rev.* **2005**, *105*, 2279–2328. b) de Visser, S. P.; Ogliaro, F.; Sharma, P. K.; Shaik, S. *J. Am. Chem. Soc.* **2002**, *124*, 11809–11826. c) de Visser, S. P.; Ogliaro, F.; Sharma, P. K.;

Shaik, S. *Angew. Chem. Int. Ed.* **2002**, *41*, 1947–1951. d) de Visser, S. P. *J. Biol. Inorg. Chem.* **2006**, *11*, 168–178. e) de Visser, S. P. *J. Am. Chem. Soc.* **2006**, *128*, 9813-9824. f) de Visser, S. P. *J. Am. Chem. Soc.* **2006**, *128*, 15809-15818.

(9) a) Sugimoto, H.; Tung, H.-C.; Sawyer, D. T. *J. Am. Chem. Soc.* **1988**, *110*, 2465-2470. b) Gross, Z.; Nimri, S. *Inorg. Chem.* **1994**, *33*, 1731-1732. c) Fujii, H.; Yoshimura, T.; Kamada, H. *Inorg. Chem.* **1997**, *36*, 6142-6143.

(10) Espenson, J. H. Chemical Kinetics and Reaction Mechanisms; McGraw-Hill: New York, 1981.

(11) Andrews, L. J.; Keefer, R. M. *J. Am. Chem. Soc.* **1955**, *77*,6284-6289.

(12) Finn, M.; Friedline, R.; Suleman, N. K.; Wohl, C. J.; Tanko, J. M. *J. Am. Chem. Soc.* **2004**, *126*, 7578-7584.

(13) a) Sherry, L. I.; Wayland, B. B. *J. Am. Chem. Soc.* **1990**, *112*, 1259-1261. b) Cui, W.; Zhang, X. P.; Wayland, B. B. *J. Am. Chem. Soc.* **2003**, *125*, 4994-4995.

(14) a) Gardner, K. A.; Mayer, J. M. *Science*, **1995**, *269*, 1849-1851. b) Cook, G. K.; Mayer, J. M. *J. Am. Chem. Soc.* **1995**, *117*, 7139-7156.

(15) Fujii, H. *J. Am. Chem. Soc.* **1993**, *115*, 4641–4648.

Table 3.1.2. Product yields and rate constants for cyclohexene oxygenation by **1** at 193 – 233K.

	Cyclohexene oxide		Cyclohexanol Cyclohexenone			Total		
Temp (K)	Yield (%)	k_{oxide} ($M^{-1}s^{-1}$)	Yield (%)	Yield (%)	k_{ol} ($M^{-1}s^{-1}$)	Yield (%)	k_{ox} ($M^{-1}s^{-1}$)	$k_0 \times 10^3$ (s^{-1})
233	61±2	0.848±0.028	25±2	4±0	0.403±0.013	90±4	1.252±0.041	0.726±0.290
223	49±2	0.288±0.020	33±1	8±1	0.241±0.017	90±4	0.529±0.037	0.387±0.256
213	46±3	0.113±0.013	37±3	6±0	0.106±0.013	89±6	0.219±0.026	0.262±0.193
203	37±1	0.048±0.003	46±1	3±0	0.063±0.004	86±2	0.111±0.007	0.020±0.229
193	28±1	0.018±0.001	66±1	6±0	0.047±0.001	100±2	0.065±0.001	0.172±0.032

Table 3.1.2. Product yields and rate constants for cyclohexene oxygenation by **1** at 193 – 233K.

	Cyclohexene oxide		Cyclohexanol Cyclohexenone			Total		
	Yield (%)	k_{oxide} ($M^{-1}s^{-1}$)	Yield (%)	Yield (%)	k_{ol} ($M^{-1}s^{-1}$)	Yield (%)	k_{ox} ($M^{-1}s^{-1}$)	$k_0 \times 10^3$ (s^{-1})
Cyclohexene	46±3	0.113±0.013	37±1	6±0	0.106±0.013	89±6	0.219±0.026	0.262±0.193
Cyclohexene-d_{10}	74±10	0.092±0.001	N.D. [a]	N.D. [a]	0	74±10	0.092±0.001	0.615±0.001

[a] Not determined.

Chapter 2.

ENDOR Study of Oxoiron(IV) Porphyrin π-Cation Radical Complexes as Models for Compound I of Heme Enzymes

Published in *Chemistry Letters* **2009,** *38*, 68-69.

Akihiro Takahashi, Yasunori Ohba, Seigi Yamauchi, and Hiroshi Fujii

Abstract

Electron nuclear double resonance (ENDOR) spectroscopy of oxoiron(IV) porphyrin π-cation radical complexes (**1** – **4**) with pyrrole β-substituted porphyrins is reported. Hyperfine coupling constants (A^H) of the pyrrole β-methyl groups were determined. Comparison of the A^H values with those of compound I of peroxidases and catalase indicated the a_{1u} porphyrin π-cation radical states of these compound I.

Abbreviations

compound I : oxoiron(IV) porphyrin π-cation radical

HRP : horseradish peroxidase

Ml-CAT : *Micrococcus lysodeikticus* Catalase

CPO : chloroperoxidase

ENDOR : electron nuclear double resonance

mCPBA : *m*eta-chloroperbenzoic acid

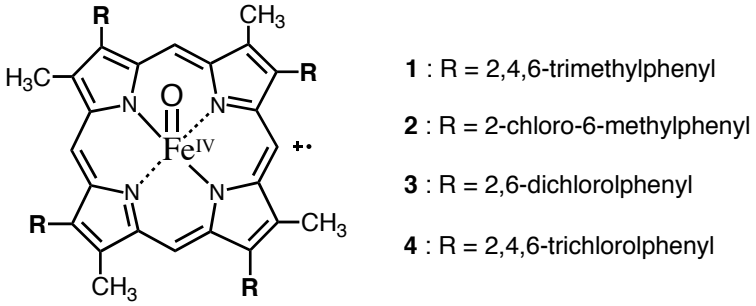

Figure 3.2.1. Structures of oxoiron(IV) porphyrin π-cation radical complexes (**1** – **4**) in this study.

Introduction

Oxoiron(IV) porphyrin π-cation radical species is a reaction intermediate in the catalytic cycles of heme-containing peroxidases and catalases.[1] This intermediate, formally two oxidation equivalents above the ferric porphyrin resting state, is commonly known as compound I.[1] A similar compound I intermediate has been proposed as an active oxygen atom donor in catalytic cycles of cytochromes P450.[2] For over a decade, because of the importance in biological functions, the electronic states of compound I have been studied by several physicochemical methods, such as electronic absorption, NMR, resonance Raman, EPR, MCD, Mössbauer, and EXAFS spectroscopy. However, our understanding of the relationship between electronic structure and reactivity of compound I remains incomplete.

Electron nuclear double resonance (ENDOR) spectroscopy is a powerful tool to determine the electronic state of compound I. Roberts et al. first reported ^{1}H and ^{14}N ENDOR spectra of compound I of horseradish peroxidase (HRP), which suggested the a_{2u} porphyrin π-cation radical state of HRP compound I.[3] Moreover, the ^{17}O ENDOR signals of HRP compound I allow estimation of spin density on the iron-bound oxo ligand.[4] Benecky et al. showed EPR and ^{1}H ENDOR spectra of compound I of *Micrococcus lysodeikticus* Catalase (*Ml*-CAT),[5] which differ from those of HRP, suggesting a different porphyrin π-cation radical state. Recently, ENDOR spectra of compound I of chloroperoxidase (CPO) were reported.[6] Analysis of hyperfine coupling constants indicated that spin delocalization to the axial thiolate ligand is not so large; $r_S < 0.23$. While these ENDOR studies clearly demonstrate that ENDOR spectroscopy provides considerable insight into the relationship between the electronic structure and reactivity, application of ENDOR spectroscopy to compound I has been limited. This is due to absence of ENDOR spectral data of compound I model

complexes, which are expected to provide a direct probe for the ENDOR assignment of compound I. Here we report the first ENDOR spectroscopy of compound I model complexes, oxoiron(IV) porphyrin π-cation radical complexes.

Experimental Section

Instruments. EPR spectra were recorded at 4 K on Bruker E500 X-band spectrometer with an Oxford Instruments EPR910 helium-flow cryostat (Bruker). ENDOR spectra were recorded at 4 K on Varian E1700 spectrometer with Oxford Instruments EPR-9 helium cryostat.

Materials. Oxygen-17 gas (40% enriched) was purchased from Cambridge Isotope Laboratories. Other chemicals were purchased commercial companies, and without further purification. ^{17}O labeled mCPBA was prepared from *m*-chlorobenzoyl chloride and ^{17}O labeled potassium peroxide obtained from the reaction of ^{17}O labeled oxygen gas with benzydrol.[11] 2-chloro-6-methylbenzaldehyde and 2,4,6-trichloro-benzaldehyde were prepared by methods described in the literature.[7a,12] 2,7,12,17-Tetramethyl-3,8,13,18-tetraarylporphyrin, **1** – **4**, were synthesized from the previous method. Iron(III) Chloride porphyrin complexes of **1 - 4** were prepared by refluxing in a chloroform-acetic acid mixture with ferrous chloride and sodium acetate.[7a] Iron(III) Perchlorate porphyrin complexes **1** – **4** were prepared by anion exchange by silver perchlorate.[13] The iron(III) Perchlorate porphyrin complexes, **1** – **4**, (10 mM) in a dichloromethane / toluene / methanol (1:3:1) mixture were placed in to a sample tube, and these solutions were cooled to –80°C in a methanol-liquid nitrogen bath. mCPBA (1.0 ~ 1.2 equiv) in methanol was slowly added to these solutions. After the solution color changed to green, these solutions were immediately frozen to 77 K and were subject to ENDOR and EPR measurements.

Result and Discussion

Because of similarity in the porphyrin structure to those of naturally occurring compounds, we utilized oxoiron(IV) porphyrin π-cation radical complexes with the pyrrole β-substituted porphyrins, **1** – **4**, shown in Figure 3.2.1. The electronic structures of **1** – **4** were characterized by absorption, ^{1}H NMR and EPR spectroscopy, which showed the a_{1u} porphyrin π-cation radical state with weak ferromagnetic coupling with the ferryl iron spins.[7] The EPR spectrum of **1** in dichloromethane / toluene / methanol shows perpendicular and parallel components of the ESR signal at g = 3.6 and 2.0, which was identical to our previous result in dichloromethane-methanol (5:1).[7] Moreover, the EPR spectrum of **1** was close to those of compound I of ascorbate peroxidase, lignin peroxidase, and *Ml*-CAT.[5,8] Figure 3.2.2 a) shows the ENDOR spectrum of **1** with magnetic field set at 324.4 mT, where the peak of the parallel component ESR signal is. The signals, located in the frequency range of 12 - 16 MHz, result from ^{1}H ENDOR signals, which exhibit a pair of ENDOR lines separated by a hyperfine coupling constant, A^H, and mirrored about the proton Larmor frequency, n_H (13.9 MHz). We can identify at least two sets of magnetically distinguishable ^{1}H ENDOR resonances in Figure 3.2.2 b). To assign these ENDOR signals, we measured the ENDOR spectrum of meso-d_4 labeled **1** (Figure 3.2.2 c). The ENDOR signals for the meso proton were assigned at 13.7 and 14.1 MHz from a difference spectrum between Figures 3.2.2 b) and c). A pair of signals around 12.5 and 15.3 MHz was assigned to the pyrrole β-methyl proton and the other pyrrole β-mesityl signals were in the peaks from 13.5 to 14.3 MHz. Therefore, hyperfine-coupling constants (A^H) of the meso proton and the pyrrole β-methyl protons were estimated to be 0.4 MHz and 2.7 MHz, respectively, which are consistent with the a_{1u} radical state as previously assigned.[7]

We examined ^{1}H ENDOR measurements of **1** at different magnetic field sets, but the ENDOR signal was not detected. Moreover, we could not observe ^{14}N ENDOR for **1**. To examine ^{17}O ENDOR spectroscopy, the oxo ligand of **1** was labeled with 40% ^{17}O enriched mCPBA. However, we have not been able to observe ^{17}O ENDOR. These may be due to insufficient saturation of the EPR signal of **1** at 4 K.

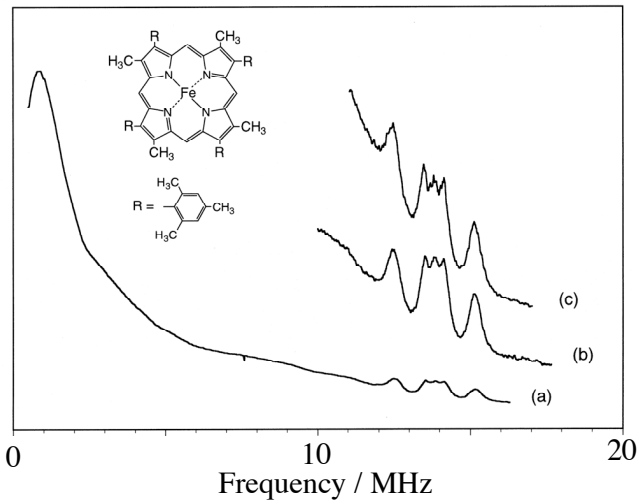

Figure 3.2.2. ^{1}H ENDOR spectra of **1** at 4 K; (a). (b); Expansion of ^{1}H ENDOR region of (a). (c); ^{1}H ENDOR region of meso-d_4 labeled **1**.

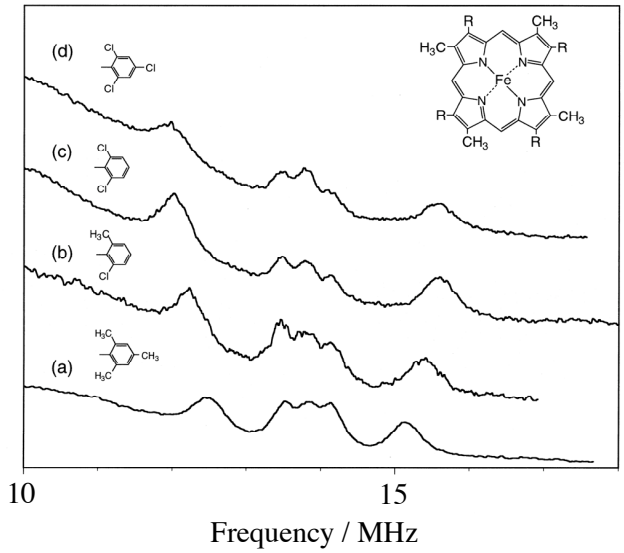

Figure 3.2.3. ^{1}H ENDOR spectra of (a) **1**, (b), **2**, (c) **3**, and (d) **4** at 4 K.

To investigate the electron-withdrawing effect on the spin density, we measured ENDOR spectra of **2** – **4** at 4K with magnetic field set at 324.4 mT (Figure 3.2.3) and the hyperfine coupling constants for **1** – **4** are summarized in Table 3.2.1. Interestingly, the A^H value for the pyrrole β-methyl proton increases with increasing electron withdrawing effect of the pyrrole β-substituent, **1** < **2** < **3** < **4**. This is consistent with a previous ^{1}H NMR study, in which paramagnetic down field shift of the pyrrole β-methyl proton signal became larger as the electron withdrawing effect of the pyrrole β-substituent was stronger.[7]

Table 1. Hyperfine coupling constants for the pyrrole β-methyl groups of **1** – **4** and compound I of heme proteins.

Compound	A^H (MHz)	a_{iso} [c] (MHz)	r [c]
1	2.67	3.45	0.049
2	3.16	3.78	0.054
3	3.58	4.11	0.059
4	3.37	4.16	0.059
HRP [a]	~ 4.4		
***Ml*-CAT** [b]	~ 6		

a) ref 3. b) ref 5. c) calculated from ^{1}H NMR shifts (ref 7).

The hyperfine coupling constant (A^H) of the pyrrole β-methyl proton can be estimated by an equation, $A^H = A_{aniso} + r(B_1 + B_2\cos^2 q)$, where A_{aniso} is an anisotropic hyperfine coupling constant, r is a π-spin density on the pyrrole β-position, q is the angle between the $C_{py\text{-}b}$–C_{methyl}–H plane and the pyrrole β-carbon $2P_z$ axis, and $B_1 = 0$ – 10 MHz and B_2 = 140 MHz for the methyl proton. Since rotation of the pyrrole

β-methyl group is frozen at 4 K, the observed A^H value would result from the methyl proton(s) with one orientation. As expected from the above equation, the observed A^H values for **1** – **4** linearly correlated to the a_{iso} values calculated from their ^{1}H NMR shifts (Table 1),[7] indicating $A^{//}_{aniso} \sim -2$ MHz and $q \sim 30°$.[9] This is reasonable orientation to avoid steric interaction with either the meso-proton or the pyrrole β-phenyl group.

From the present ^{1}H ENDOR results, we expect that the A^H value of the pyrrole β-methyl proton in ^{1}H ENDOR of frozen solution is less than 10 MHz for compound I with the a_{1u} porphyrin π-cation radical state.[10] On the other hand, ^{1}H NMR shift of the pyrrole proton for the meso-sunstituted porphyrin complex suggested r = 0.013 on the pyrrole β-position for the a_{2u} porphyrin π-cation radical state.[7] Thus, the A^H value of the pyrrole β-methyl proton is expected to be less than 4 MHz for compound I with the a_{2u} porphyrin π-cation radical state. The hyperfine coupling constants of the pyrrole β-methyl groups for compound I of HRP and *Ml*-CAT are in the range of the a_{1u} porphyrin π-cation radical states, but larger than that of the a_{2u} porphyrin π-cation radical state. Therefore, this study clearly indicates that the compound I of both HRP and *Ml*-CAT are consistent with the a_{1u} porphyrin π-cation radical state, but not the a_{2u} porphyrin π-cation radical state.

References

(1) H. B. Dunford, *Heme Peroxidases*, Wiley-VCH, New York, 1999.

(2) Y. Watanabe, Y.; J. T. Groves, in *The Enzymes*, ed by D. Sigman, Academic Press, New York, **1992**, Vol. 20, pp 405-452.

(3) J. E. Roberts, B. M. Hoffman, R. Rutter, L. P. Hager, *J. Biol. Chem.* **1981**, 256, 2118.

(4) J. E. Roberts, B. M. Hoffman, R. Rutter, L. P. Hager, *J. Am. Chem. Soc.* **1981**, *103*, 7654.

(5) M. J. Benecky, J. E. Frew, N. Scowen, P. Jones, B. M. Hoffman, *Biochemsitry* **1993**, *32*, 11929.

(6) S. H. Kim, R. Perera, L. P. Hager, J. H. Dawson, B. M. Hoffman, *J. Am. Chem. Soc.* **2006**, *128*, 5598.

(7) a) H. Fujii, *J. Am. Chem. Soc.* **1993**, *115*, 4641. b) H. Fujii, T. Yoshimura, H. Kamada, *Inorg. Chem.* **1996**, *35*, 2373. c) H. Fujii, *Coord. Chem. Rev.* **2002**, *226*, 51.

(8) a) W. Patterson, T. L. Polous, D. B. Goodin, *Biochemistry* **1995**, *34*, 4342. b) A. Ivancich, H. M. Jouve, B. Sartor, J. Gaillard, *Biochemistry* **1997**, 36, 9356-9364.

(9) $A^{H} = A^{//}_{aniso} + a_{iso}(B_1 + B_2\cos^2 q)/(B_1 + B_2\cos^2 45)$. When $B_1 = 0$, $A^{H} = A^{//}_{aniso} + a_{iso}(2\cos^2 q)$. From the slope (1.39) and y intercept (-2.1) of the correlation line, the q and A_{aniso} were found to be 33.5° and –2.1 MHz, respectively.

(10) The maximum A_{aniso} component was assumed to be +2 MHz. The maximum a_{iso} for the a_{1u} and a_{2u} radicals were found to be 8.3 and 1.8 MHz, respectively, from $a_{iso} = 140$ x r for $q = 0$.

(11) a) Y. Sawaki, C.S. Foote, *J. Am. Chem. Soc.* **1979**, *101*, 6292. b) W.R Wangner, E.H. Rastetter, *J. Org. Chem.* **1983**, *48*, 402

(12) R.G.F. Giles, M.V. Sargent, *J. Chem. Soc. Perkin Trans. I.* **1974**, 2447.

C.A. Reed, T, Mashiko, S.P. Bentley, M.E. Kastner, W.R. Scheidt, K. Spartalian G.J. Lang, *J. Am. Chem. Soc.* **1979**, *101*, 2948.

PART IV.

SUMMARY AND CONCLUSIONS

In the present thesis, the author investigated the effect of an axial ligand on the electronic structure and reactivity of compound I using synthetic model complexes of compound I.

Part II describes the effects of the axial ligand on the reactivity of $O=Fe^{IV}por^{+\bullet}$. In chapter 1, to investigate the effect of axial ligands on the electronic structure and reactivity of compound I in peroxidases and catalases, $O=Fe^{IV}por^{+\bullet}$ complexes bearing a series of imidazole and 3-fluoro-4-nitrophenolate ligands were prepared by ozone oxidation of iron(III) porphyrins. Consequently, these axial ligands did not change the electronic state either the porphyrin π-radical or the iron(IV)-oxo center. On the other hand, the oxidation reactivity of $O=Fe^{IV}por^{+\bullet}$ complexes was drastically increased by the imidazole and phenolate axial ligands. The reaction rate for cyclooctene epoxidation with $O=Fe^{IV}por^{+\bullet}$ complexes was increased 100 ~ 400-fold with axial coordination of phenolate and imidazoles. A similar increment was observed for hydrogen abstraction from 1,4-cyclohexadiene and for electron transfer from *N,N*-dimethyl-*p*-nitroaniline. These results underscore the significance of histidine and tyrosinate ligands in the oxidation activity of compound I in peroxidases and catalases.

In chapter 2, the author has investigated a key factor in regulating the reactivity of $O=Fe^{IV}(TMP^{+\bullet})(L)$ complexes bearing different axial anion ligands, where TMP = tetra-mesitylporphyrin, and L = F^-, Cl^-, BnO^-, AcO^-, HcO^-, TFA^-, and NO_3^-. The reactivity of $O=Fe^{IV}(TMP^{+\bullet})(L)$ complexes was significantly affected by the nature of the axial ligand, and the reactivity order of $F^- > BnO^- > HcO^- > Cl^- > AcO^- > TFA^- > NO_3^-$ was invariable for various reactions (oxo transfer to cyclooctene, hydrogen abstraction from 1,4-cyclohexadiene, and electron transfer from *N,N*-dimethyl-*p*-nirtoaniline). The author found a linear correlation between the reactivity of $O=Fe^{IV}(TMP^{+\bullet})(L)$ complexes and the redox potentials ($E_{1/2}$) for $Fe^{III/II}$ couple of $Fe^{III}(TMP)(L)$ complexes.

Spectroscopic titration showed that the axial ligand regulated the reactivity order of $O=Fe^{IV}(TMP^{+\bullet})(L)$ complexes by tuning the thermodynamic stabilities of the reactant, $O=Fe^{IV}(TMP^{+\bullet})(L)$, and the product, $Fe^{III}(TMP)(L)$. Notably, the axial ligand modulated the stability of $Fe^{III}(TMP)(L)$ complexes more drastically than that of $O=Fe^{IV}(TMP^{+\bullet})(L)$ complexes. The fact that the reactivity of $O=Fe^{IV}(TMP^{+\bullet})(L)$ complexes is regulated primarily by the stability of the final product, $Fe^{III}(TMP)(L)$ complexes, is a novel concept.

To further investigate the effect of axial ligands, chapter 3 deals with the axial ligand effects of biomimetic axial ligands, such as imidazole and phenolate, which were characterized in chapter 1. Phenolate ligand rendered high oxidation reactivity to the $O=Fe^{IV}por^{+\bullet}$ complex by stabilization of the Fe^{III}por complex. By contrast, neutral ligands such as imidazole elicit a high oxidation power with $O=Fe^{IV}por^{+\bullet}$ complexes by causing a remarkable reduction in the energy of *transition states*, like compound II. These results indicate that the axial ligand tunes the reactivity of $O=Fe^{IV}por^{+\bullet}$ by controlling not only the energy states of the reactant ($O=Fe^{IV}por^{+\bullet}$) and the product (Fe^{III}por), but also the energy of the transition state.

Part III is devoted to understaning the chemoselectivity (chapter 1) and the electronic structure (chapter 2) of oxoiron(IV) porphyrin π-cation radical complexes. On the chemoselectivity of cyclohexene epoxidation versus hydroxylation by synthetic $O=Fe^{IV}por^{+\bullet}$ complexes, the author has shown that the C=C epoxidation reaction is enthalpically controlled, whereas the allylic C-H hydroxylation is entropically controlled. In chapter 2, hyperfine coupling constants (A^H) of $O=Fe^{IV}por^{+\bullet}$ complexes were investigated using electron nuclear double resonance (ENDOR) spectroscopy. By consequence, the author has proposed that the compound I for peroxidases and catalases are consistent in the a_{1u} radical state, but not in the a_{2u} radical state.

Finally, the author would like to comment on the functional roles of the axial ligands in heme enzymes, based on the results demonstrated in this thesis. The proximal histidine in peroxidases and the tyrosine residues in catalases would drastically increase the reactivity of compound I, resulting in much more reactivity compound I in peroxidases and catalases than in the synthetic model. A very reactive compound I would greatly increase the catalytic activity of these heme enzymes. Although this study can not show the effect of the thiolate axial ligand, the cysteine proximal ligands in cytochrome P450 may also work to the enhancement the oxo-transfer reactivity. The extremely high reactivity of compound I results from stabilization of the resting (ferric) state of these heme enzymes and the transition state of the heme enzyme by the axial ligands. The hydrogen bonding interactions between peptide backbone and the axial ligands, which are different and highly conserved, in these heme enzymes is another important factor in increasing the catalytic activity of these heme enzymes, as the hydrogen bond would weaken the anionic character of the proximal ligand. In the oxidation reactions of cyclooctene, 1,4-cyclohexadiene, *N*,*N*-dimethyl-*p*-nitroaniline, and hydrogen peroxide, the author could find no significant difference between the imidazole and phenolate axial ligands. While the axial ligand activates compound I in a heme enzyme, it would not be an essential factor in discriminating the enzyme function.

LIST OF PUBLICATIONS

1. Activation Parameters for Cyclohexene Oxygenation by an Oxoiron(IV) Porphyrin π-Cation Radical Complex: Entropy Control of an Allylic Hydroxylation Reaction.
   Akihiro Takahashi, Takuya Kurahashi, and Hiroshi Fujii
   Inorg. Chem. **2007**, *46*, 6227-6229.

2. ENDOR Study of Oxoiron(IV) Porphyrin π-Cation Radical Complexes as Models for Compound I of Heme Enzymes.
   Akihiro Takahashi, Yasunori Ohba, Seigi Yamauchi, and Hiroshi Fujii
   Chem. Lett. **2009,** *38*, 68-69.

3. Effect of Imidazole and Phenolate Axial Ligands on the Electronic Structure and Reactivity of Oxoiron(IV) Porphyrin π-Cation Radical Complexes: Drastic Increase in Oxo-Transfer and Hydrogen Abstraction Reactivities
   Akihiro Takahashi, Takuya Kurahashi, and Hiroshi Fujii
   Inorg. Chem. in press

OTHER PUBLICATIONS

1. Magnetic and Infrared Properties of the Azide Complex of (2,7,12,17-Tetrapropyl-porphycenato)iron(III): A Novel Admixing Mechanism of S = 5/2 and S = 3/2 States.

   Saburo Neya, Akihiro Takahashi, Hirotaka Ode, Tyuji Hoshino, Masayuki Hata, Akira Ikezaki, Yoshiki Ohgo, Masashi Takahashi, Hirotsugu Hiramatsu, Teizo Kitagawa, Yuji Furutani, Hideki Kandori, Noriaki Funasaki, and Mikio Nakamura

   Eur. J. Inorg. Chem. **2007,** 3188-3194.

2. Electronic Properties in a Five-Coordinate Azido Complex of Nonplanar Iron(III) Porphyrin: Revisting to Quantum Mechanical Spin Admixing.

   Saburo Neya, Akihiro Takahashi, Hirotaka Ode, Tyuji Hoshino, Akira Ikezaki, Yoshiki Ohgo, Masashi Takahashi, Hirotsugu Hiramatsu, Teizo Kitagawa, Yuji Furutani, Víctor A. Lórenz-Fronfría, Hideki Kandori, Noriaki Funasaki, and Mikio Nakamura

   Bull. Chem. Soc. Jpn. **2008,** *81*, 136-141.

ACKNOWLEDGMENT

The present thesis is summary of the author's studies from 2006 to 2009 at Department of Functional Molecular Science, the Graduate University for Advanced Studies. This work is generously supported by Institute for Molecular Science and carried out under the supervision of Associate Professor Hiroshi Fujii. The author wishes to express his cordial gratitude to Associate Professor Hiroshi Fujii for his continual direction, stimulating discussion, and hearty encouragement.

The author is really grateful to Professor Takashi Ogura and Mr. Kenichiro Ikemura (University of Hyogo) for resonance Raman measurements, and Professor Seigi Yamauchi and Associate Professor Yasunori Ohba (Tohoku University) for electron nuclear double resonance measurements.

This work would not have been possible without help of the members and coworkers in the Associate Professor Hiroshi Fujii's laboratory. The Author is deeply indebted to Drs. Takuya Kurahashi, Masato Kujime、Daisuke Nonaka for valuable suggestions and unfailing encouragement. Acknowledgments are also due to Mrs. Misako Tanizawa for their office work and heartfelt kindness.

Finally, the author expresses his sincere gratitude to his parents for their supports, generous understanding, and affectionate encouragement.

Okazaki, January 2009

Akihiro Takahashi